ORNL/Sub--85-55904/0

DE90 006722

DEVELOPMENT OF A DESIGN METHODOLOGY FOR HIGH TEMPERATURE CYCLIC APPLICATION OF MATERIALS WHICH EXPERIENCE CYCLIC SOFTENING

Final Technical Report
for the Period
May 1 1985 to September 30 1988

by

Douglas L. Marriott
and
James F. Stubbins

December 1988

Work performed under Subcontract 19X-559904C
WBS Element UI-2
of the
Department of Energy
AR&TD Fossil Energy Materials Program

College of Engineering
University of Illinois at Urbana-Champaign
Urbana, IL 61801

DISCLAIMER

TABLE OF CONTENTS

1. INTRODUCTION

This is the final report on work carried out as part of the Department of Energy AR&TD Fossil Energy Materials Program under Subcontract 19X-55904C WBS Element UI-2 during the period May 1, 1985, through September 30, 1988.

The project has as its original focus the high temperature behavior of 2.25 Cr-1 Mo steel, heat treated to produce a predominantly bainitic microstructure and the load carrying response of components made of this material. The purpose was to determine the essential characteristics of the material in question under combinations of sustained and cyclic loading. To this end, experiments were carried out on uniform and notched specimens under both steady and cyclic loading using specially acquired electro-mechanical test machines.

It emerged that a very important feature of mechanical behavior under the conditions of interest was the strong tendency of this material to cyclically soften, particularly at high temperature in the creep range, giving the illusion of a severe creep/fatigue interaction under certain conditions. This finding led to a significant component of the project being devoted to investigation of the effects of local, as opposed to generalized, cyclic softening, and the implications this phenomenon might have on the setting of allowable design stress limits.

The cyclic softening phenomenon has implications for the potential use, or otherwise, of heat treated steels for pressure vessel manufacture. Primary design stress limits in pressure vessel design are invariably based on static strength. For example, according to the requirements of the ASME Boiler and Pressure Vessel Design Code, Section VIII, Div. 2, the allowable value is the minimum of one-third of the UTS or two-thirds of the yield strength at temperature, or one-third of the ambient temperature yield strength.

Heat treated low alloy steels in general, and this includes martensitic, 9 to 12% Cr/Mo steels as well as the bainitic 2.25 Cr I Mo steel examined in this study, suffer cyclic softening of up to 40 percent compared with their initial monotonic strength. If it is necessary to compute allowable design limits on the softened state therefore, virtually all benefit gained by the heat treatment in the first place will be lost.

There are situations where it would be needlessly conservative to use the softened state to define the material strength. An obvious case is when the component in question clearly does not experience any cyclic loading. This is not a common situation but there are more complex situations in which cyclic softening is localized and therefore does not reduce the overall load carrying capacity of the component. One of the main thrusts developed in the course of this project was to discriminate between situations where cyclic softening is, or is not, a significant factor in setting allowable design stresses.

In addition to deformation studies, work has also been done on fatigue and fatigue crack propagation. There is a significant frequency effect. The effect of environment has been investigated and it has found that while oxidation influences fatigue life, it is not possible to explain all frequency effects as environmental in origin.

During the project period interest of the research sponsors changed from the specific problems associated with the grades of 2.25Cr 1 Mo steel originally being studied in this project toward the more general problems of time-dependent modification of material strength, either by cyclic loading or by time-at-temperature through the process of thermal aging. This change in emphasis was motivated by the development of a class of advanced austenitic steels with enhanced creep and oxidation properties potentially capable of operating at up to 700°C. These materials are being considered as candidates for replacement reheater- and superheater-tubing in fossil fired plants and for new plants design for supercritical operation.

Due to the complex microstructure which provides these materials with their high temperature strength, there is reason so believe that they may subject to aging effects including the cyclic softening observed in the bainitic low alloy steel at lower temperature but also loss of strength cause by thermal overaging.

In response to this change in interest on the part of the research sponsors, the project was broadened in scope durings its last year to begin to examine service-dependent changes in material strength in a more general way with cyclic softening being considered as one special case.

The experimental work of the final year of this program has been devoted almost exclusively to studies of 17 Cr 14 Ni Cu stainless steel, similar in composition to the tubing material used in the

Eddystone power plant. This is an established material with properties similar to the advanced austenitics of primary interest. It is being used in preliminary studies because it is more readily available than the advanced austenitics.

The object of this work is to investigate the potential for cyclic softening, following essentially the work already carried out on the bainitic low alloy steel, extend it to include the effects of time-at-temperature and then to see what interactive effects there might be if any between thermal aging combined with cyclic mechanical loading. Tests performed so far suggest that the austenitic material is cyclically stable under rapid cyclic loading but the creep curves indicate a strong thermal softening effect. It has yet to be determined whether there is any synergetic interaction between cyclic and thermal effects.

Some work has been carried out, toward the end of the project period, to develop practical tools for evaluating components in which significant aging or other softening effects are likely to be experienced. This work has resulted in a practical methodology for dealing with time-dependent cyclic softening and it appears that the procedure can be extended with relatively little work to include the effects of thermal softening.

The format of this report is as follows: The second chapter is a review of the work carried out in approximately chronological order under the headings of

1. 2.25 Cr 1 Mo Steel--Elevated Temperature Fatigue and Environmental Effects
2. Preliminary Studies of Advanced Austenitics
3. A Uniaxial Constitutive Model for Cyclic Softening
4. The Iso-Cyclic Stress-Strain Approach to Evaluation of Components in Cyclic Softening Materials
5. Testing of High Temperature Austenitic Alloys
6. Design Methodology for Aging Materials--Application to Cyclic Softening

This review chapter is followed by chapters which describe the individual areas in more detail.

Finally, the last chapter reviews the main conclusions and prospects for future work.

2. REVIEW OF WORK DONE

Most of the work carried out up to August 1987 has been reported in Interim Report ORNL/SUB/85-55904/01 [2.1].

This report described the materials, specimens, test facilities, and test programs in detail.

Work on the influence of temperature, hold time, and oxidation on fatigue of bainitic 21/4 Cr 1 Mo steel was also reported. This work included plain and EDM notched specimens in air and vacuum.

A theoretical model for cyclic softening was given. This model assumes that softening is a simple function of the accumulated plastic deformation.

A simplified method of component analysis for dealing with the cyclic softening problem in complex geometries was outlined and results given for the Bridgman notch specimen used in the experimental program. This method postulates the concept of a "relaxation locus" as the stress-strain path followed at points of severe strain in a component during the transition from elastic to inelastic material behavior., It was concluded from studying some simple finite element models that the "relaxation locus" is primarily a function of the component geometry and not strongly dependent on the material constitutive relationship. This concept was used to propose a simple method of determining stability under conditions of local material softening.

At the time of the previous report, no testing had been done on the austenitic material but a supply had been procured and specimens had been ordered.

The following sections describe progress made since the previous report with review of earlier work included where appropriate to maintain continuity.

2.1 2.25 C I MO STEEL--ELEVATED TEMPERATURE FATIGUE AND ENVIRONMENTAL EFFECTS

This work was essentially completed at the time of the previous report. The only more recent development was the publication of the results of this part of the study in detail in a thesis by Kschinka. The main results of this study are contained in Chapter 3 of this report.

A significant influence of hold time in compression and tension was observed with fatigue life reduced by about a factor of 2 by a six minute tensile hold and a factor of 4 by three minutes in both tension and compression. No explanation has been found so far for this reduction in life.

2.2 PRELIMINARY STUDIES OF ADVANCED AUSTENITICS

An eight inch diameter forging of 17 Cr 14 Ni Cu Mo austenitic steel was obtained from ORNL late in 1987. This is the material used for the tubing for the Eddystone power plant and is similar to the advanced austenitics developed at ORNL by Maziaz, et al.

Much of the experimental work up to the time of writing of this report has been taken up with upgrading peripherals such as extensometry in order to resist the sustained testing at 700°C in a reliable manner. Some serious testing has begum however and the results obtained so far are reported in Chapter 4. These include monotonic tensile tests, steady stress creep tests, strain controlled, low-cycle fatigue testing under different strain rates, and steady cyclic load crack growth.

The results so far sought that the material in the "as-received" condition is stable under rapid cyclic loading but shows some tendency to cyclic softening at slow strain rates.

Creep tests indicate a strong tendency toward thermal softening with a rapid onset of tertiary creep leading rapidly to failure following an extended period of relatively slow creep strain.

2.3 A UNIAXIAL CONSTITUTIVE MODEL FOR CYCLIC SOFTENING

Like the work on environmental effects on fatigue, this part of the study was completed and reported in full in the interim report and presented at the ASME PVP Conference in San Diego in 1987. A detailed account of both the experimental and theoretical work is contained in Handrock's thesis.

The model is one of limited scope which does not attempt to provide a full constitutive description of the cyclic softening phenomenon. Instead, it treats the problem as a perturbation on the conventional Manson-coffin fatigue relation. The material parameters of the cyclic stress-strain curve, instead of being considered to be constants are assumed to be functions of the accumulated plastic deformation and modified in a loop-by-loop basis.

According to this approximately theory, the relationship between the stress range and strain range is given by

$$\Delta\sigma^* = h\,(\Sigma\Delta\varepsilon_p)^n\,(\Delta\varepsilon_p)^m \qquad (2.1)$$

where $\Delta\varepsilon_p$ denotes inelastic cyclic strain range and $\Sigma\Delta\varepsilon_p$ denotes cumulative cyclic strain magnitude.

For the 2.25 Cr 1 Mo steel, the constants in this equation at 565°C are h = 843 MPa, n = -0.0661, and m = 0.0905.

Excellent correlation was found between this model and experiment both for time-independent and time-dependent cyclic loading.

2.4 THE ISO-CYCLIC STRESS-STRAIN APPROACH TO EVALUATION OF COMPONENTS IN CYCLIC SOFTENING MATERIALS

The objective of this theoretical study was to develop a practical method for predicting the behavior of components of complex geometry made of cyclic softening material.

The problem is related to the question of primary design stress limits. For example, according to the requirements of the ASME Boiler and Pressure Vessel Design Code, Section VIII, Div. 2, the allowable value is the minimum of one-third or the UTS or two-thirds of the yield strength at temperature of one-third of h ambient temperature yield strength. If softening occurs generally throughout the component under cyclic conditions, then the softened state is appropriate for determining design allowables. If this is assumed as a universal rule however, it is unlikely that the cost of heat treatment could ever be justified.

In practice, there are many circumstances where the degree of cyclic deformation required to produce significant softening is localized and does not, therefor, degrade the overall load carrying capacity of the component. Two examples are constrained plastic deformation at the root of a notchlike feature and surface strains induced by thermal transients. In these cases, if it can be firmly established that cyclic deformation is local, then considerable savings in material can be gained by using the initial monotonic strength of the material.

The purpose of this theoretical study was to develop a method for determining when cyclic deformation could be judged "local."

The exact approach to this problem would be to use a precise constitutive model including cyclic softening, e.g. Miller's MATMOD and carry out a detailed cycle-by-cycle finite element analysis of the component in question. So far it has not been possible to integrate all the constituents of such an ambitious simulation.

An alternate approximate method was developed by Handrock based on the concept of "isocyclic" stress/strain curves, analogous to the isochronous curves commonly used in creep analysis. The procedure is detailed in Chapter 6 of this report. These isocyclic curves represent the approximate relationship between stress and strain following a specified number of stress reversals. A single elastic-plastic stress analysis of the component is required for each number of cycles of interest. Cyclic plasticity is judged to be localized for the number of cycles of interest if the plastic zone calculate by this procedure is localized.

Handrock's method is clearly conservative compared with the real situation. This is because the isocyclic stress/strain curve assumes softening to occur at the maximum rate for the entire life whereas the strain range at a generic point will increase with cycles due to the progressive softening process. Since softening is a relatively insensitive function of cycles, however (see Eq,. (2.1)), the degree of conservatism is expected to be small.

Even Handrock's analysis is too complex to be used in many true design situations however since it still requires an inelastic analysis to be carried out. This approach is viewed more as the basis for simpler methods which will be described later than as a design method in it shown right.

2.5 DESIGN METHODOLOGY FOR AGING MATERIALS--APPLICATION TO CYCLIC SOFTENING

Although the approximate method proposed by Handrock is probably too complex for most design applications, it nevertheless provides a useful conceptual basis for a more practical approach.

A method has been developed for dealing with cyclic softening which si believed to be consistent with the practices of the ASME Code. This method was first presented at the AR&TD Fossil Energy

Materials Program Conference held in Oak Ridge, September 1988. Details are given in Chapter 7 of this report.

The approach is based on the observation that the stress/strain conditions at a point of local inelastic deformation in a complex component follow a "relaxation locus" which appears to be independent or at least insensitive to the detailed constitutive material behavior and is primarily a function of the component geometry. Furthermore, it has been demonstrated that this locus can be determined by multiple linear elastic finite element stress analyses by perturbing the elastic stiffness of individual elements.

The isocyclic stress/strain relation and the "relaxation locus" can both be plotted on common axes and their intersection define an equilibrium state. It is a matter of judgment as to whether the change of strain between the initial elastic state and the final softened state is considered "local" or generalized plastic deformation. More work needs to be done to define an objective criterion of "localized plastic deformation." An interim definition adopted in this study is whether he relaxation locus is steeper than the Neuber hyperbola defined as the line on which the product of stress and strain remains constant.

The proposed design procedure does not require the constitutive behavior of cyclic softening to be considered explicitly for the purposes of primary design. If on the basis of preliminary analysis it can be shown that cyclic softening effects will be localized, then the initial monotonic material properties can be used in setting the primary design limits. If this criterion is not satisfied, the fully softened state must be used. This proposed design procedure is a departure from the conventional approach used in the ASME Design Code because instead of using fixed design limits these are a function of the expected transient service conditions.

So far the only softening phenomenon to be dealt with explicitly by this approximate approach is time-independent cyclic softening. However, it appears that the same approach can be extended to deal with more complex, time-dependent softening effects such as thermal aging and combined thermo-mechanical interactions. Before this extension can be made whoever, it is necessary to determine the character of thermal softening in materials such as the advanced austenitics in which such effects are expected. This is the subject of work which was started in the past year to examine the mechanical behavior or 17 Cr 14 Ni Cu austenitic steel.

2.6 REFERENCES

2.1 Leckie, F. A., D. L. Marriott, J. F. Stubbins, J. L. Handrock, and B. Kschinka, "Development of a Design Methodology for High Temperature Application of Materials which Experience Cyclic Softening," ORNL/SUB/85-55904/01, UILU WNG 88-4011, August 1987.

3. ELEVATED TEMPERATURE FATIGUE AND ENVIRONMENTAL EFFECTS

3.1 INTRODUCTION

2.25Cr-1Mo steel has compiled an impressive service record in the petroleum, chemical process, and power generation industries as an elevated temperature structural material used in pressure vessels and piping systems. Although conventionally used in the annealed condition (ASME SA387-22 Class 1) which has a predominantly proeutectoid ferrite microstructure, there has recently been more interest in heat treated conditions of this alloy (ASME SA387-22 Class 2 and SA542) which produce bainitic microstructures and enhance mechanical properties.

Bainitic 2.25Cr-1Mo steel is currently the reference pressure vessel material for coal liquefaction and gasification applications. This process requires massive vessels to operate continuously at temperatures up to 482°C (900°F) and pressures up to 27.6 MPa (4000 psi), requiring wall thicknesses of at least 300 mm (12 in) and possibly in excess of 400 mm (16 in) [3.1]. These proposed design criteria extend considerably beyond present experience; hence there is a pressing need for an adequate understanding of the performance of this alloy.

Of particular concern is the little-understood and potentially dangerous creep-fatigue damage interaction. Containment vessels typically undergo thermally and mechanically induced strain cycles associated with start-up, shut-down, and fluctuations in operating conditions. Such cycles usually produce small mechanical strains, normally less than about 0.5% with hold periods ranging from perhaps 10 to 1000 hours throughout the design lifetime of 30 or 40 years [3.2]. These transients lead to a combination of creep and fatigue damage which is potentially more deleterious than either mechanism acting independently. Hence a component may fail in a relatively low number of such cycles, particularly in the presence of a hostile environment. The possibility of premature failure therefore must be considered at temperatures where creep is likely to influence low cycle fatigue behavior. Accordingly, appropriate elevated temperature, strain-controlled fatigue data must be generated in the laboratory and extrapolated to anticipated service conditions.

Currently the creep-fatigue data base for bainitic 2.25Cr-1Mo is very limited. This is a serious deficiency in that creep-fatigue is recognized to be a major design criterion for the conventional annealed alloy [3.3]. Furthermore, environment plays an important, perhaps even dominant, role in long term creep-fatigue behavior of annealed material [3.4]. The present work is undertaken to assess the sensitivity of bainitic 2.25Cr-1Mo steel to creep-fatigue-environment interactions for the purpose of high temperature structural design.

3.2 EXPERIMENTAL PROCEDURE

3.2.1 Material

The test material is a 2.25Cr-1Mo steel forging with low residuals manufactured by Kawasaki Steel (Heat 646363) and supplied by Oak Ridge National Laboratory. The composition is given in Table 3.1; note the low concentrations of P, S, As, Sn, and Sb impurities. The alloy was quenched and tempered in the form of 400 mm ring forging as follows: austenitize at 1070°C (1960°F) for 18 hours, water quench; temperature at 650°C (1200°F) for 17 hours; air cool. This was followed with a simulated post-weld heat treatment of 695°C (1283°F) for 19 hours. This processing produced a microstructure consisting of essentially 100% bainite, as confirmed by microscopic analysis. Room temperature strengths fell within ASME SA336 Class F22 specifications. Complete tensile properties at room temperature and 565°C (1050°F) are given in Table 3.2.

3.2.2 Specimen Preparation

Uniform gage length fatigue specimens as depicted in Fig. 3.1 were prepared from the virgin plate material. The unique double shoulder geometry was design specifically for purposes of vacuum testing. The inner shoulders were provided to mount type 321 stainless steel flexible tubing which acted as a miniature retort encapsulating the gage section of the specimen in vacuum. The tubing was fastened to the specimen shoulders using an electron-beam brazing process. The entire brazing procedure was performed in a vacuum of about 1.3 MPa (10 microtorr). In this way the gage section of the specimen was encapsulated in a reasonable vacuum without resorting to a costly retort system. This technique also

eliminated misalignment problems prevalent in complex retort arrangements. A vacuum-encapsulated specimen prepared in this manner is shown in Fig. 3.2. Complete details of this innovative technique are presented elsewhere [3.5].

The only drawback to this method was the necessity to place the extensometry on the same shoulders used to mount the flexible tubing. Hence correlations had to be made between strain in the gage section and strain between the shoulders. This was accomplished by using two extensometers simultaneously, one on the gage section and one on the shoulders. Strain was controlled in the gage section and monitored between the shoulders. While the correlation is straightforward in the case of pure fatigue, it is somewhat more complex in hold time tests as stress relaxation effects accrue. However, in three separate correlation tests, the displacement range between the shoulders was nearly identifiable in every case and was constant throughout the majority of fatigue life. This displacement was then used as the controlling parameter in the vacuum tests.

Finally, in an effort to separate the relative amounts of crack initiation and crack growth, tiny notches were manufactured in selected specimens by the process of electro-discharge machining (EDM). Each notched specimen has four separate notches as depicted in Fig. 3.3. Notch dimensions were about 60 microns deep and 75 microns wide, with a notch root radius of roughly 40 microns to yield an elastic stress concentration factor of approximately 2.5. Two sets of notches were provided so that one set was available for microscopic analysis after failure occurred at the other set.

3.2.3 Mechanical Testing

Uniaxial strain controlled fatigue tests were performed on a commercial closed-loop electrohydraulic test machine equipped with a resistance furnace. A standard high temperature axial extensometer was employed to maintain strain control. Hysteresis loops were periodically recorded; the cyclic load imposed on the specimens was monitored on a strip chart recorder.

All tests were conducted at 565°C (1050°F). This temperature, while above the anticipated service temperature of 482°C (900°F), was chosen to enhance creep without altering the original carbide structure. A fully reversed strain range of 0.50% was used exclusively, except for other tests required to

generate a strain-life curve. This strain range was selected for three reasons. Firstly, it is a reasonable estimate of anticipated service conditions. Secondly, there are currently fewer data at such strain levels than exist at 1.0% and above. Finally, previous research of annealed 2.25Cr-1Mo [4.4, 4.6] found hold periods at low strain ranges to be more damaging than at higher strains (>1%) relative to pure fatigue in each instance, suggesting a more severe creep-fatigue interaction effect.

Four basic strain histories were examined: pure fatigue (no hold periods), fatigue with tensile hold periods, fatigue with compressive hold periods, and fatigue with both tensile and compressive hold periods. All hold periods were introduced at maximum absolute strain amplitude. Hold period duration was varied from 6 to 3 to 1.5 to 0.75 to 0.6 minutes. Strain rate during the ramp portions of the waveforms was 0.004 per second.

All specimens were used in the as-machined condition with no subsequent grinding or polishing. Failure was defined as a 50% reduction in tensile stress level from the initial (maximum) value.

3.3 RESULTS AND DISCUSSION

The strain-life data are shown in Fig. 3.4, where they are compared with the best fit curve for bainitic 2.25Cr-1Mo data gathered by Sanderson et al. [3.7] from a variety of international sources, all obtained in the temperature range of 550 to 600°C (1020 to 1110°F). The data presented in this study lie well within the scatter band, very near the best fit line of Sanderson et al.

Since the basic strain-life behavior for the material used here appears consistent with that of other bainitic 2.25Cr-1Mo alloys, it was decided to concentrate the bulk of the research program at one strain range. One half percent fully reversed total strain range (±0.25%) was selected for the reasons outlined earlier. Individual tests and their results are summarized in Table 3.3.

3.3.1 Material Response

Basic material response was the same for both smooth and pre-notched specimens and in both air and vacuum environments. In all tests the material exhibited rapid cyclic softening during approximately the first twenty percent of life. Thereafter the softening rate decreased as the hysteresis loop stabilized.

This response is illustrated in the stress range versus fraction of fatigue life graph of Fig. 3.5. The rapid decrease in stress range after about 70% of cyclic life is due to formation of long cracks. After this point stress decreased quickly up to failure. This overall behavior is in good agreement with other studies of bainitic 2.25Cr-1Mo steel [3.8, 3.9, 3.10, 3.11].

During constant strain hold period tests, the material relaxed considerably with a corresponding gain in creep strain. As seen in Fig. 3.6, stress relaxed in an exponential-like manner, decreasing very quickly the first several seconds but only slowly thereafter. Relaxation rates in tension and compression were essentially identical, and the amount of relaxation decreased throughout the duration of the test (see Fig. 3.7). Similar relaxation behavior of bainitic 2.25Cr-1Mo was reported by Brueur et al. [3.11].

The failure mode most commonly associated with "creep-fatigue interaction," one where fatigue loading accelerates either the growth of grain boundary cavities or wedges [3.12], was not evident in this material. Instead, the creep-fatigue interaction exhibited itself as enhanced softening. This mode of response is probably due both to the nature of the bainitic microstructure and to the low concentration of residual elements in the material composition. The elements S, P, As, Sn, and Sb have been associated with failure of steels along prior austenite grain boundaries [3.13]. The low levels of these elements may preclude this mode of fracture in the present alloy, or alternately, accentuate it in other heats or heat treatments of this material. Even creep failure of the alloy in the present study at 565°C is not associated with void formation and growth. The failure mode is similar in form to that of tensile failure where plastic instability, not creep-induced cavitation, controls the response [3.14]. Thus the accelerated failure under combined creep and fatigue loading seems to be more closely associated with time dependent dislocation restructuring in the bainitic laths than with fatigue-enhanced cavity growth.

3.3.2 Effect of Hold Periods

The introduction of a hold period into the hysteresis loop caused a significant reduction in fatigue life compared to the continuously cycled case (no hold period), as seen in Fig. 3.7. This was true regardless of the type of hold period (tensile, compressive, or combined tensile/compressive) or its duration.

In air, tensile holds were generally somewhat more damaging than compressive holds, but the combined tensile/compressive waveform was considerably more damaging than either of the previous cases. Hold periods also caused the stress range to be considerably reduced from the continuously cycled case, as shown in Figs. 3.5 and 3.7. It is seen that this effect occurs immediately upon the onset of loading. In general, there was little difference in the amount of stress range reduction between the various types of hold time waveforms.

The effect of hold period duration was not marked. With only two exceptions, the six minute tensile hold test and the 0.6 minute compressive hold test, hold periods of shorter duration for a given waveform yielded higher lives. However, this trend was not strong and hold period duration had only minor influence on fatigue life. This is seen in Fig. 3.8, which compares stress range versus cycles for various hold time durations for the combined tensile/compressive hold waveform. Such behavior could indicate a saturation effect (i.e., after a certain point, the hold period duration has no effect) which has been proposed by Carden et al. [3.15], or may suggest that the hold periods were not long enough for a time dependent effects to become significant.

The constant strain hold waveform and temperature, however, were such that considerable stress relaxation occurred during each hold period throughout the entire test (see Fig. 3.9). Of course, this results in an increase in plastic (i.e., creep) strain and a corresponding decrease in elastic strain since the total strain remains constant. This increase in creep strain is almost certainly deleterious to fatigue resistance. Thus the most reasonable explanation for the only marginal effect of hold period duration is the kinetics of the stress relaxation. As mentioned before, stress relaxes in an exponential-like fashion during a dwell period, decreasing very rapidly the first few seconds but only slowly thereafter. Therefore most creep strain occurs quickly, with little difference in total creep strain for the hold period durations studied here. This behavior is illustrated in the relaxation curves of Fig. 3.6, expressed as percent of peak stress versus time (at half the failure life) for various tensile hold period durations. Even though hold time duration varies by an order of magnitude, there is only marginal difference in the ultimate percentage of peak stress. Again, this behavior agrees well with other relaxation data of bainitic 2.25Cr-1Mo steel [3.11].

The hold period data in air are summarized in Fig. 3.10, which plots log time to failure versus log cycles to failure. The figure indicates the overall effect of hold periods, including the trends of the three different hold period waveforms for various hold time durations. It is seen that the symmetrical tensile/compressive hold waveform is most damaging, followed by the tensile only hold and then the compressive only hold waveforms. The relatively minor influence of hold period duration is illustrated by the nearly vertical slope of the dashed lines. Note also that the dashed lines all roughly intersect the pure fatigue datum point. All the data are quite consistent with the exception of the six minute tensile hold point (life greater than expected) and the 0.6 minute compressive hold point (life less than expected).

3.3.3 Effect of EDM Notches

In air, electro-discharge-machined (EDM) notches reduced cyclic life by an average of 22% compared to analogous tests of smooth specimens. The largest decrease was observed in the pure fatigue case; there was little effect on the combined tensile/compressive hold period test. Both the six minute tensile hold and six minute compressive hold tests experienced approximately a 25% reduction in life. EDM results in air are summarized in Fig. 3.11. In every case the specimen failed at one of the notch pairs.

The deleterious influence of hold periods on fatigue resistance, regardless of their location in the hysteresis or their duration, immediately suggests the presence of a strong creep interaction. If creep was the sole damage mechanism, however, the results of tension only holds period tests and compression only hold period tests should be similar since creep rates are equal in tension and compression. In every case, however, tensile hold tests yielded lower lives than analogous compressive hold tests. The EDM notch data offer an explanation for this behavior. If the EDM notch is taken to be a nucleated fatigue crack, the results verify that the majority of useful life is consumed by crack propagation. This is a reasonable conclusion in that the material is quite ductile and testing is in the low-cycle fatigue regime; hence substantial plastic deformation is expected and cracks should initiate early in life.

Since tensile holds are more damaging than compressive holds, and the major portion of fatigue life is spent in crack growth, it follows that tensile holds promote crack propagation. This makes sense

intuitively in that the crack tip is subjected to a greater stress intensity factor. Furthermore, the ingress of aggressive environment to the crack tip is facilitated while the crack is held open. Compressive holds, on the other hand, do not induce tensile stresses at the crack tip except for possible oxide "wedging" action, and therefore do not enhance propagation rates. Compressive holds reduce life from the continuously cycled case primarily through the acceleration of softening. This damage becomes significant for exposure in air where crack surface oxidation stabilizes crack growth. In vacuum, while accelerated softening takes place, the development of major cracks is much slower. Both tensile and compressive hold period waveforms are more harmful than pure fatigue due to the stress relaxation induced creep strain, but it is the additional factor of increased crack growth rate that makes tensile holds more damaging than analogous compressive holds, and exposure in air more damaging than in vacuum.

It follows that the combined tensile/compressive waveform, since it amasses practically twice as much creep strain, has a yet greater fatigue reduction factor than either of the above cases. Again, this is due to the exponential-like stress relaxation during the hold periods. Two hold periods per cycle result in nearly double the creep damage as does a single hold period, in either tension or compression, despite the same overall cyclic frequency. This is due to the fact that the stress must relax from the peak value twice per cycle in the combined hold case versus once per cycle for the single hold case. Figure 3.6 indicates that most of the stress relaxation occurs very rapidly, and not much additional damage accrues after the initial relaxation period. In addition, the tensile hold portion of the waveform aids crack propagation.

3.3.4 Interrupted Fatigue Tests

The EDM notch data suggest that engineering sized cracks (>100 microns in length) form quite early in cyclic life. If crack growth is indeed the controlling fatigue mechanism, one would anticipate several initiation sites, one of which grows into a large failure-causing crack. In an effort to determine more precisely when these cracks form, a series of interrupted fatigue experiments was conducted, terminating the tests at 25%, 15%, 10%, and 5%, respectively, of normal cyclic life for smooth specimens. As before, a fully reversed strain range of 0.50% was employed at 565°C (1050°F), but only the pure fatigue

waveform was utilized for this portion of the test program. After completion of mechanical testing, the specimen gage section was removed for surface analysis in a scanning electron microscope (SEM). No surface preparation was administered other than simple ultrasonic cleaning.

The SEM photomicrographs (see Fig. 3.12) clearly show the presence of small fatigue cracks in the base metal, even after only 5% of failure life. Naturally, the cracks at 25% of cyclic life are longer, deeper, and tend to branch more than the cracks observed earlier in life. In addition, several cracks at 25% are step-like in nature, as if two or more parallel cracks (perpendicular to loading axis) were intersected by cracks aligned at right angles to them (i.e., parallel to the loading axis). This phenomenon is illustrated in Fig. 3.12a.

From the evidence obtained from the interrupted tests it is tempting to state, for practical purposes, that cracks nucleate almost immediately upon the onset of cyclic straining and fatigue life is entirely controlled by crack propagation. It must be noted, however, that the oxide scale, although cracked, frequently concealed the actual condition of underlying metallic substrate. In occasional locations where the oxide partially or completely spalled, revealing relatively nascent metal, there usually was no crack visible in the substrate. This was particularly true in the briefest tests, i.e., at 5% and 10% of life. Thus removal of the oxide film by chemical means, as described by Brooks and Lundin [3.16], is probably desirable but was not yet undertaken as of this writing.

There is also some evidence of repeated film rupture and subsequent chemical attack at regions of localized strain, as indicated by the multiple scale layers in Fig. 3.12b; note at least two layers of thick oxide scale. Of course, this redundant fracture and oxidation action may very well be a prominent mechanism for fatigue crack initiation in the metallic substrate.

Interrupted tests were also performed on EDM notch specimen at 15% and 25% of cyclic life. These did not reveal a great deal, but confirmed that EDM notches provide preferred initiation sites for the primary crack. Every EDM notch examined (four per specimen) had a large crack at its tip, across the entire notch length, as seen in Fig. 3.13a. Small secondary oxide cracks were observed from the notches in both specimens.

Finally, two analogous tests were conducted in vacuum. Both tests were stopped at 25% of fatigue life; one specimen was smooth and the other EDM notched. These exhibited very different cracking behavior than the specimens exposed to an oxidizing environment. In both cases the gage section was completely free of any cracks. There were, however, a number of slop bands observed, oriented at roughly 45 degrees to loading axis. Only in the EDM notches were cracks present, and again all four notches nucleated cracks (Fig. 3.13b). These interrupted tests in vacuum underline the important role of the oxide in fatigue crack initiation.

3.3.5 Effect of Vacuum

The kinetics of oxidation are extremely rapid at elevated temperature, and environmental degradation can affect the results of even very short duration tests. Of course, the influence of oxidation increases with time, and as seen in Table 3.3 and Fig. 3.10, even very brief hold periods of 0.6 minute cause time to failure to increase by seven-fold over the pure fatigue case. Naturally, for longer hold periods the gain in testing time is even more dramatic, with some tests lasting over 200 hours. At the 565°C (1050°F) test temperature, such lengthy tests permit severe oxidation. Hence the possibility was considered that environmental degradation may be the primary damage mechanism in high temperature time dependent fatigue. Therefore selected tests were conducted in vacuum to better ascertain the influence of oxidation on fatigue life. These tests are among the very first investigations of the creep-fatigue behavior of bainitic 2.25Cr-1Mo steel in an inert environment.

Figure 3.14 shows the stress amplitude as a function of loading cycle for vacuum tests on smooth specimens. It is again apparent that the hold time wave forms accelerate material softening. When compared to results in air, testing in vacuum resulted in a significant increase in fatigue resistance for all waveforms characterized. Life data for smooth specimens in both air and vacuum are compared in Fig. 3.15; the average gain in life for the four different waveforms is 410%. As expected, the increase was most dramatic for the hold period tests due to their lengthy duration and consequent severe oxidation in air at 565°C (1050°F). In fact, in vacuum the three minute compressive hold period test had a greater life than its pure fatigue counterpart. This was true for both smooth and EDM notch specimens (see

Fig. 3.16) and may result in part from the "welding" of the crack surfaces during the compressive hold, an effect that would be impossible in air due to formation of corrosion products in the crack. The rewelding phenomenon has been offered in other studies of 2.25Cr-1Mo steel [3.17.3.18] as explanation for negligible crack growth rates during compressive dwells in vacuum.

Conversely, any waveform with a tensile hold was very detrimental, reducing cyclic lifes to roughly half of pure fatigue and compressive hold results. It is interesting to note the combined tensile/compressive hold period waveform (1.5 minute each), despite rewelding during the compressive dwell, was slightly more deleterious than the three minute tensile-only hold waveform. This held true for both smooth and pre-flawed specimens (Fig. 3.16), indicating that rewelding could almost, but not quite, overcome the additional damage imparted by two hold times per cycle. (As in air, the combined tensile/compressive waveform results in twice the creep strain as a single hold period, since stress relaxation behavior is independent of environment.)

As seen by comparing Figs. 3.11 and 3.16, EDM notches have a larger fatigue reduction factor in vacuum (41%) than they do in air (22%). This implies that a greater portion of cyclic life is spent in crack initiation (again considering the EDM notch as a nucleated fatigue crack). Alternatively, one may state that oxidation aids in crack initiation. This conclusion lends credence to other theories of premature oxide induced fatigue crack nucleation [3.19, 3.20, 3.21] in the annealed version of this material. However, one should not be mislead by the smaller percentage of life consumed by crack propagation in vacuum (59%) as opposed to air (78%). Keep in mind that in terms of absolute fatigue cycles, 59% of vacuum life still considerably exceeds 78% of cyclic life in air. Therefore, another possible conclusion is that crack propagation is retarded in inert atmosphere as compared to results in air. This too is in agreement with previous investigations of ferritic 2.25Cr-1Mo steel [3.22, 3.23].

The combined effects of EDM notches and vacuum are illustrated in Fig. 3.17. This graph plots stress range versus cycles for specimens tested in pure fatigue under four different conditions: with and without EDM notches in both air and vacuum. The two trends discussed earlier are apparent. The graph shows both the enhancement of fatigue life due to vacuum and also the more severe effect of EDM notches in the inert environment.

Almost all of the vacuum test specimens exhibited unique surface markings on the gage section. Small areas has an "orange peal" type surface roughness and texture. Most of these regions contained at least one small crack, strongly suggesting that these zones are due to excess localized plastic deformation (see Fig. 3.18); they may be densely clustered slip bands, which were observed in the interrupted vacuum tests at 25% of failure life. Most vacuum specimens had one or two such areas, the effect being especially palpable in specimens subjected to hold period loadings. No evidence of this phenomenon was observed in the tests conducted in air, although the surface discoloration and heavy oxide scale may have partially hidden its presence. Still, such markings were so unmistakable on vacuum specimens it is believed they would be noticeable on air specimens if present.

In marked contrast to the vacuum test specimens, which normally were very clean and shiny, specimens tested in air were frequently severely oxidized. Hold period test specimens, due to the lengthy test duration, were particularly encrusted with scale. As found in previous research of 2.25Cr-1Mo steel [3.19, 3.20, 3.24], the oxide scale behavior varied depending on the type of hold period. The oxide on specimens subjected to tensile-only holds spalled considerably, whereas the oxide on specimens subjected to compressive-only holds was much more adherent. This is illustrated in Fig. 3.19. In the other investigations, however, the oxide behavior was cited as the reason for compressive dwells being more damaging than corresponding tensile dwells; here that situation is reversed and is explained by increased crack growth rate during tensile holds, recalling that crack propagation is the dominant fatigue mechanism in air for these test conditions.

Oxide scale on combined tensile/compressive waveform specimens acted similarly to that of the compressive-only hold specimens, tending to crack rather than spall.

3.6 MODELING OF DATA

Efforts were made to incorporate the data into existing creep-fatigue interaction models. Among the most common are linear damage summation, strain range partitioning, frequency separation, and damage rate. All of these models have drawbacks, however, and none adequately describes the data generated in this study.

The familiar linear damage summation model is the simplest to apply, requiring only fatigue and constant stress creep data, but is grossly inaccurate so frequently that any agreement appears strictly fortuitous. Furthermore, the approach is entirely phenomenological, with no mechanistic basis, and makes no distinction between tensile and compressive hold periods. The other creep-fatigue models mentioned are more sophisticated and usually more accurate, but are limited by other difficulties. The major drawbacks are the large number of numerical coefficients required and the complex tests necessary to generate them. In addition, these models are empirical or semi-empirical in nature, making it difficult to predict their general applicability.

In contrast, the oxide interaction model of Challenger, et al. [3.22] has several features that initially make it very appealing for the present work. Firstly, it is based on the same alloy system, 2.25Cr-1Mo steel. Secondly, it is a purely mechanistic approach. Thirdly, and most uniquely, it considers environmental effects as the primary damage mechanism, i.e., the formation and cracking (not exfoliation) of surface oxide scales, which subsequently act as stress concentrators to induce premature crack initiation in the metal substrate. As described previously, oxidation appears to be the major influence on fatigue behavior in this investigation.

On closer inspection, however, this model also proves to be inadequate. Although based on an environmental interaction, the correlation relies on assumptions which are not valid for the material examined here. For instance, to simplify the effect of oxide induced crack initiation, the model assumes fatigue cracks nucleate in the metallic substrate immediately following cracking of the oxide layer. This is obviously an oversimplification, perhaps a severe one. Figure 3.12b anc c clearly shows an oxide crack, but no noticeable damage of any kind in the underlying metal.

This conservative assumption may be offset somewhat by the model's determination of cyclic to crack initiation. For the conditions explored here, 0.50% strain range and 565·C (1050°F), the model predicts crack nucleation at roughly 50% of cyclic life. As evidenced by the results of the EDM notch and interrupted tests, this estimation is much too high. The disagreement may not be surprising since the correlation relies on crack initiation data of type 304 stainless steel, an entirely different alloy system lacking even the same crystal structure as 2.25Cr-1Mo steel.

The model also predicts more severe damage for compressive holds than for tensile holds. It is argued that an oxide scale grown while the material is in compression is more likely to crack open during the loading ramp from full compression to full tension, than a similar scale grown while the material is in tension and ramped into compression. In the present study, however, the tensile hold is always found to be more damaging. Finally, and perhaps most significantly, the founders of the model acknowledge that acceleration of crack growth rates by hold periods has a strong influence on fatigue behavior. Ths is particularly true for tensile dwells, which encourage the ingress of aggressive environment to the crack tip. However, this parameter is not incorporated into the correlation due a lack of experimental data. Consequently, any error introduced by the omission of hold time effects on crack growth is compounded when cracks initiate early in life, as found in the present investigation.

The intent of this argument is not to prove the model of Challenger et al. is completely without value, for it quite accurately predicted their observed results. Furthermore, the approach is based on behavior of ferritic 2.25Cr-1Mo and may not be appropriate for the bainitic version of the material used here. Still, some of its simplifying assumptions are quite tenuous and, unfortunately, it is based on mechanisms that do not occur in the material and conditions utilized in this study.

3.4 SUMMARY AND CONCLUSIONS

Uniaxial strain controlled fatigue and creep-fatigue tests of a bainitic 2.25Cr-1Mo steel forging were performed at 565°C (1050°F) in both air and vacuum environments; the bulk of experiments were carried out at 0.50% fully reversed strain range. Tests were conducted with tension only hold periods, compression only hold periods, combined tension and compression hold periods, and without any holds (continuously cycled). Hold period duration was varied between 6.0 and 0.6 minutes. Selected tests were performed with pre-flawed specimens, and limited interrupted fatigue tests were also executed.

This research was conducted to understand the effects of waveform and environment on the elevated temperature fatigue behavior of this material for possible application in thick walled pressure vessels. The principal observations and conclusions of this study are as follows:

1. Regardless of waveform and environment, much of the initial strength advantage of the bainitic microstructure, gained by quenching, is lost via cyclic softening.
2. In air, the introduction of a hold period into the cyclic waveform, regardless of its location or duration, significantly reduces fatigue life due to additional plastic (creep) strain from stress relaxation.
3. In air, combined tensile/compressive hold periods are most damaging, compressive-only holds are least damaging, and tensile-only holds are intermediate. This behavior is attributed to accumulated creep strain during all dwells and increased crack growth rate during tensile dwells.
4. Regardless of environment, hold period duration has only martinal influence on fatigue life due to the kinetics of stress relaxation (most creep strain occurs rapidly).
5. EDM notches reduce cyclic life by an average of 22% in air, indicating that the majority of useful life is consumed by crack propagation. This is confirmed by surface analysis of smooth specimen interrupted tests at 5% to 25% of fatigue life, which exhibit fairly extensive crack systems.
6. Vacuum enhances life roughly four-fold compared to results obtained in air. Compressive holds yield the best results, even better than pure fatigue, while any waveforms with a tensile hold is much more damaging. This is attributed to crack tip rewelding during compressive dwells.
7. EDM notches have a larger effect in vacuum than in air, strongly suggesting that oxidation aids in fatigue crack initiation. Oxidation also appears to increase crack propagation rates as opposed to vacuum.
8. The data are not adequately described by any mechanistic creep-fatigue model. Even the environmental damage approach of Challenger et al. is based on different mechanisms than occur here and hence is inappropriate.

3.5 REFERENCES

3.1. Swindeman, R. W., M. K. Booker, and W. J. McAfee, "A Plan to Develop the Design Methodology and Associated Materials Data for the Fatigue Analysis of SRC Dissolver Vessels," Oak Ridge National Laboratory, TN, 1982.

3.2. Swindeman, R. W., "Cyclic Stress-Strain-Time Response of a 9Cr-1Mo-V-Nb Pressure Vessel Steel at High Temperature," Pressure Vessel and Piping Conference, TX, 1984.

3.3. Swindeman, R. W., "Response of Ferritic Steels to Nonsteady Loading at Elevated Temperatures," Research on Chrome-Moly Steels (ed., Swift, R. A.), MPC-21, American Society of Mechanical Engineers, NY, 1984, pp. 31-42.

3.4. Marriott, D. L., J. F. Stubbins, F. A. Leckie, J. L. Handrock, and B. Kschinka, "Development of a Design Methodology for High-Temperature Cyclic Applications of Materials Which Experience Cyclic Softening," AR&TD Fossil Energy Program Contract Meeting Conference, to be published by Oak Ridge National Laboratory for DOE/AR&TD, May, 1987.

3.5. Rawlins, C. E., et al., "Report to the American Petroleum Institute on the Program to Study Materials for Pressure Vessel Service with Hydrogen at High Temperatures and Pressures," Metal Properties Council, NY, 1982.

3.6. Ishiguro, T., Y. Murakami, K. Ohnishi, and J. Watanabe, "A 2 1/4 Cr - 1 Mo Pressure Vessel Steel with Improved Creep Rupture Strength," Application of 2 1/4 Cr-1 Mo Steel for Thick-Wall Pressure Vessels, ASTM STP 755, American Society for Testing and Materials, 1982, pp. 383-417.

3.7. Wada, T., and T. B. Cox, "A New 3Cr-1.5Mo Steel for Pressure Vessel Applications," Research on Chrome-Moly Steels, MPC-21, American Society of Mechanical Engineers, 1984, pp. 77-93.

3.8. Swindeman, R. W., "Isochronous Relaxation Curves for Type 304 Stainless Steel after Monotonic and Cyclic Strain," Journal of Testing and Evaluation, Vol. 7, 1979, pp. 192-198.

3.9. Orr, J., F. F. Beckitt and G. D. Fawkes, "The Physical Metallurgy of Chromium-Molybdenum Steels for Fast Reactor Boilers," International Conference on Ferritic Steels for Fast Reactor Steam Generators, Paper 16, British Nuclear Society, London, 1977.

3.10. Copeland, J. F., and G. J. Licina, "A Review of 2 1/4 Cr - 1 Mo Steel for LMFBR Steam Generator Applications," Structural Materials for Service at Elevated Temperatures in Nuclear Power Generation (ed., Schaefer, A. O.), MPC-1, American Society of Mechanical Engineers, NY, 1975, pp. 55-84.

3.11. Klueh, R. L., "Heat-to-Heat Variations in Creep-Rupture Properties of Annealed 2 1/4 Cr - 1 Mo Steel," Journal of Pressure Vessel Technology, Transactions of the ASME, Vol. 105, 1983, pp. 320-328.

3.12. Swindeman, R. W., and R. L. Klueh, "Constant- and Variable-Stress Creep Tests on 2 1/4 Cr - 1 Mo Steel at 538•C," Res Mechanica, Vol. 3, 1981, pp. 245-270.

3.13. Corwin, W. R., M. K. Booker, B. L. P. Booker, and C. R. Brinkman, "Characterizing Fatigue Crack Propagation in 2 1/4 Cr - 1 Mo Steel for Steam Generator Applications", Trans. of the 5th International Conf. on Structural Mechanics in Reactor Technology, Vol. F, Paper No F5/12, 1979.

3.14. Handrock, J. L., and D. L. Marriott, "Cyclic Softening Effects on Creep Resistance of Bainitic Low Alloy Steel Plain and Notched Bars," Properties of High-Strength Steels for High-Pressure Containments (ed., Nisbett, E. G.), MPC-27, American Society of Mechanical Engineers, NY, 1986, pp. 93-102.

3.15. Handrock, J. L., D. L. Marriott, and J. F. Stubbins, "Development of a Uniaxial Constitutive Model for a Strain Induced Softening Material," Thermal Stress, Material Deformation, and Thermo-Mechanical Fatigue (eds., Sehitoglu, H., and S. Y. Zamrik), PVP Vol. 123, American Society of Mechanical Engineers, NY, 1987, pp. 83-89.

3.16. Tuppeny, W. H. Jr., "Criteria for Pressure Vessel Design in the U.S.A.," Design Criteria of Boilers and Pressure Vessels, American Society of Mechanical Engineers, NY, 1969, pp. 37-52.

3.17. Ronay, M., "Fatigue of High-Strength Materials", Fracture, An Advanced Treatise, Vol. III (ed., Liebowitz, H.), Academic Press, NY, 1971, pp. 431-482.

3.18. Drucker, D. C. Plasticity in Structural Mechanics (eds., Goodier, J. N., and N. J. Hoff), Pergamon Press, 1960, pp. 407-455.

3.19. Prager, W., An Introduction to Plasticity, Addison-Wesley, MA, 1959.

3.20. Hodge, P. G. Jr., Plastic Analysis of Structures, McGraw-Hill, NY, 1959.

3.21. Masur, E. F., "On Tensor Rates in Continuum Mechanics 'ZAMP'," Vol. 16, 1965, pp. 191-201.

3.22. Onat, E. T., and D. C. Drucker, "On the Concept of Stability of Inelastic Systems," Journal of Aeronautical Sciences, Vol. 21, 1954, pp. 543-548.

3.23. Palmer, A. C., G. Maier, and D. C. Drucker, "Convexity of Yield Surfaces and Normality Relations for Unstable Materials or Structural Elements," Brown University Report Nonr 562(20) to appear.

3.24. Maier, G., and D. C. Drucker, "Elastic-Plastic Continua Containing Unstable Elements Obeying Normality and Convexity Relations," Schwiezerischen Bauzeitung, Vol. 23, No. 9, June, 1966.

Table 3.1 Composition of Kawasaki 2.25Cr-1Mo Steel

C	0.13
Mn	0.53
P	0.003
S	0.003
Si	0.25
Cr	2.33
Ni	0.15
Mo	0.96
V	0.01
Cu	0.16
Al	0.011
As	0.002
Sn	0.001
Sb	0.0005
Fe	balance

Table 3.2 Tensile Properties of Kawasaki 2.25Cr-1Mo Steel

strain rate = 0.004 per second

	25°C	565°C
Elastic Modulus (GPa)	208	159
0.2% Yield Strength (MPa)	474	348
Ultimate Strength (MPa)	590	380
True Fracture Stress (MPa)	1280	838
corrected to (MPa)*	1090	699
True Fracture Ductility	1.53	1.94
% Reduction of Area	78.4	85.6
True Strain @ Ultimate Load	.076	.019
Strain Hardening Exponent	0.11	0.06
Strength Coefficient (MPa)	855	510

* Corrected for necking with Bridgman's Correction Factor

Table 3.3 Results of Fatigue Tests at 565°C and 0.50% Strain Range

At Half the Failure Life

Test No.	Specimen	Environment	Smooth or EDM	Hold Period (min.)	Stress Range (MPa)	Stress Amplitudes (MPa) Tensile Peak	Tensile Relaxed	Compressive Peak	Compressive Relaxed	Cycles to Failure	Time to Failure (hr.)
1	6B	Air	S	0	472	238	—	234	—	3783	2.6
2	DS-1	Air	S	6 T	406	190	132	216	—	2000	201
3	DS-4	Air	S	6 C	413	218	—	195	133	2050	206
4	A4A	Air	S	6 T+C	411	202	134	209	138	895	180
5	DS-2A	Air	S	3 T	431	201	145	230	—	1465	74
6	DS-11	Air	S	3 C	409	216	—	193	142	2245	114
7	DS-10	Air	S	3 T+C	402	201	138	201	138	905	91
8	A10A	Air	S	1.5 T	438	207	157	231	—	1648	42
9	DS-14	Air	S	1.5 C	402	209	—	193	148	2340	60
10	A7	Air	S	1.5 T+C	433	213	156	220	162	1042	53
11	DS-5F	Air	S	.75 T+C	436	218	167	218	165	1278	33
12	DS-BR2	Air	S	0.6 T	432	206	158	226	—	1662	18
13	DS-ER1	Air	S	0.6 C	435	226	—	209	160	1821	19
14	DS-16	Air	EDM	0	452	226	—	226	—	2664	1.9
15	DS-5	Air	EDM	6 T	419	197	139	222	—	1536	155
16	DS-17	Air	EDM	6 C	413	220	—	193	136	1550	156
17	DS-A	Vac	EDM	3 T+C	419	213	148	206	141	803	81
18	DS-1A	Vac	S	0	450	227	—	223	—	9750	6.8
19	DS-E	Vac	S	3 T	419	196	150	223	—	5447	276
20	DS-6F	Vac	S	3 C	410	224	—	186	139	11903	603
21	DS-BR9	Vac	S	1.5 T+C	382	192	144	190	138	5001	254
22	DS-D	Vac	EDM	0	464	234	—	230	—	5276	3.7
23	DS-1F	Vac	EDM	3 T	406	189	146	217	—	3789	192
24	DS-2F*	Vac	EDM	3 C	410	215	—	195	128	5550	293
25	DS-BR4	Vac	EDM	1.5 T+C	395	198	157	197	144	3275	166

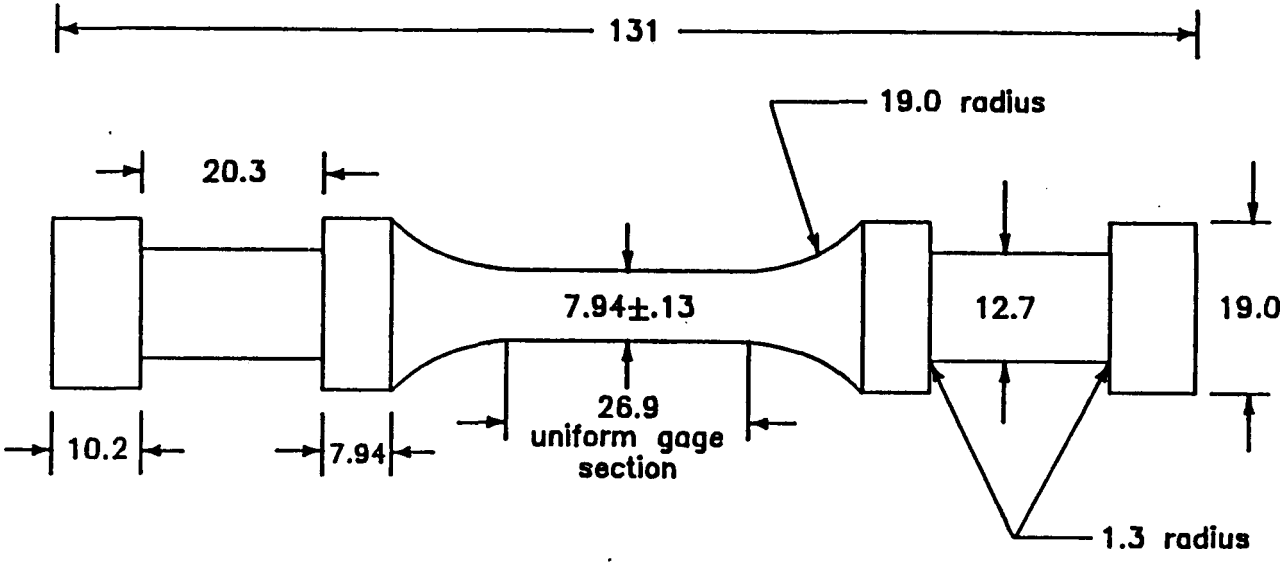

Figure 3.1 Schematic of 2.25Cr-1Mo fatigue specimen. Special double geometry is designed for purposes of bellows tubing encapsulation. All dimensions given in mm.

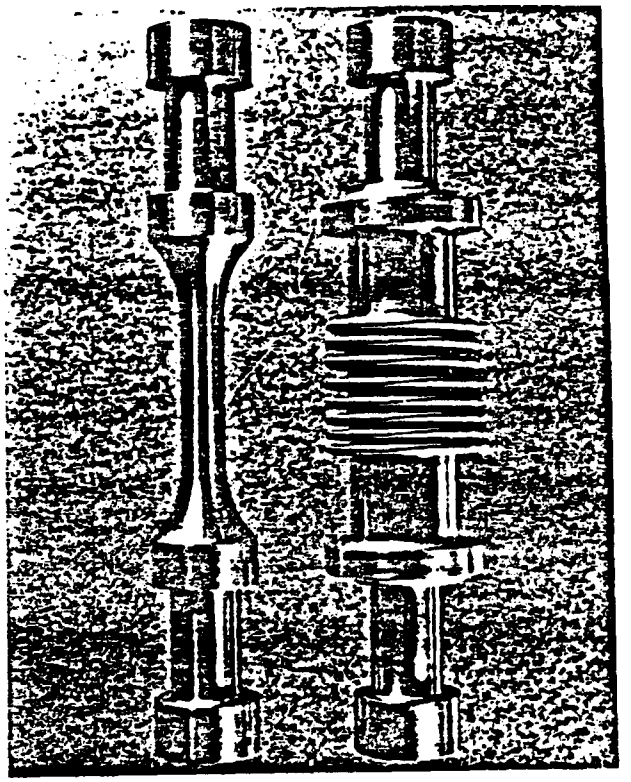

Figure 3.2 Kawasaki 2.25Cr-1Mo fatigue specimen before (left) and after (right) bellows tubing vacuum encapsulation. The mil steel rings at the ends of the bellows tubing serve as brazing surfaces and also provide secure mounting surfaces for the axial extensometer.

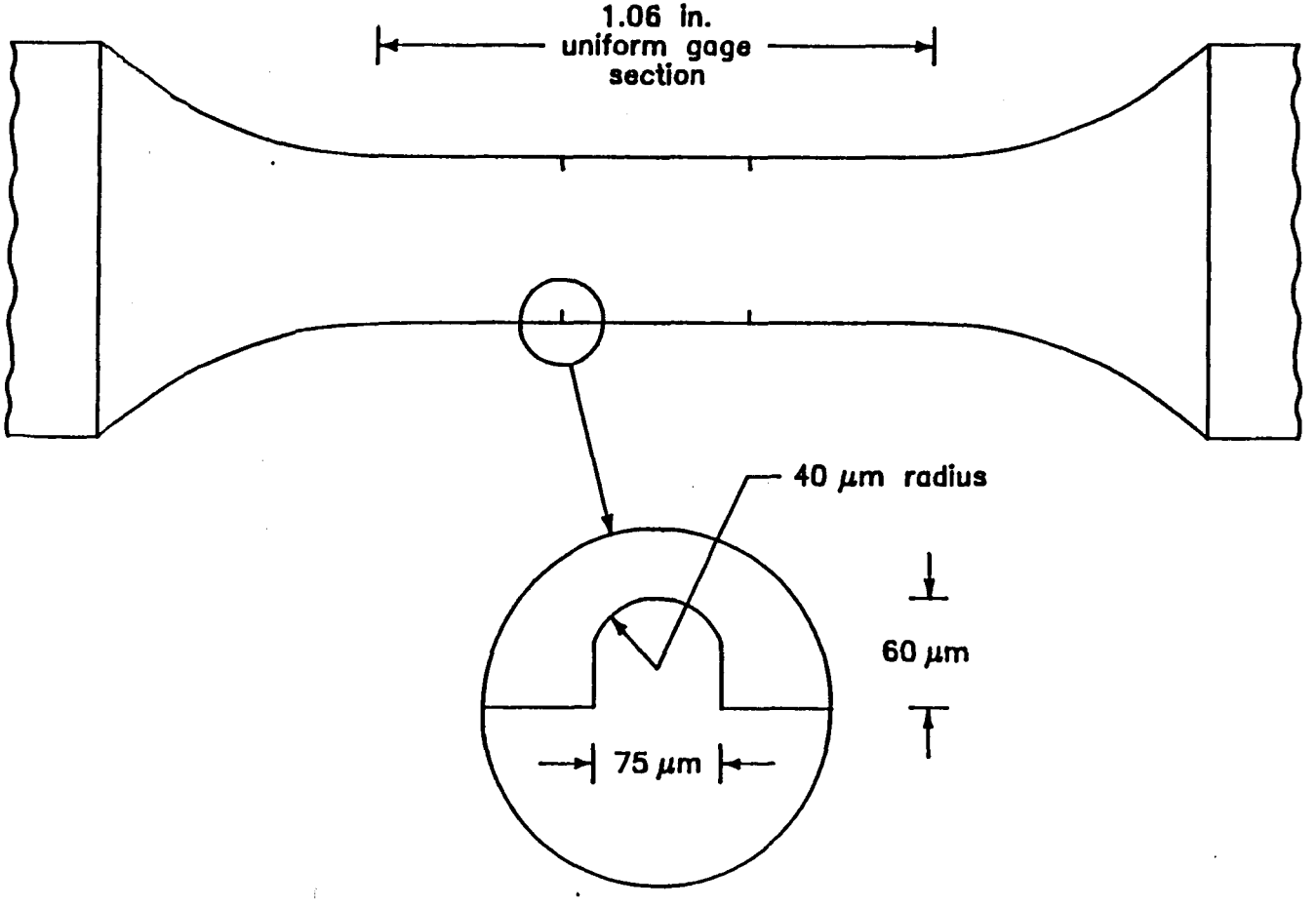

Figure 3.3 Schematic diagram of electro-discharge machined (EDM) notch.

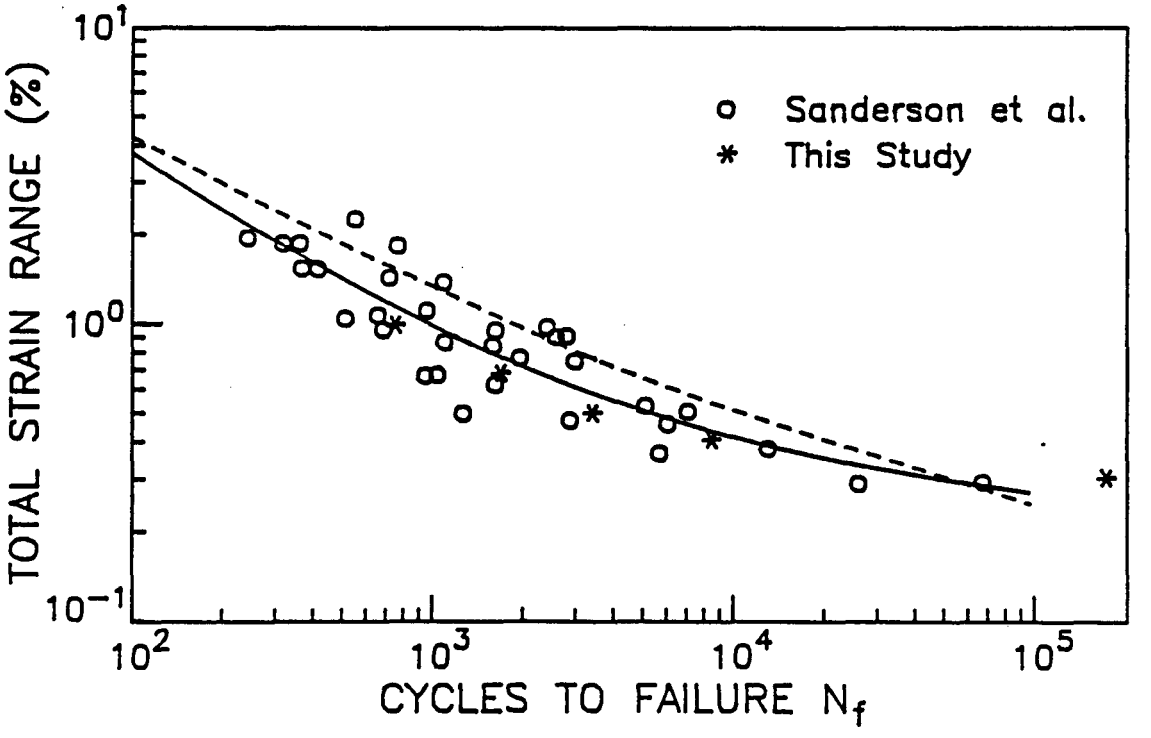

Figure 3.4 Strain life plot for bainitic 2.25Cr-1Mo steel in the temperature range 550 to 600°C (1020 to 1110°F). Solid line represents the best fit the data gathered by Sanderson et al. [7]. Dashed line is analogous, but for ferritic (annealed) material.

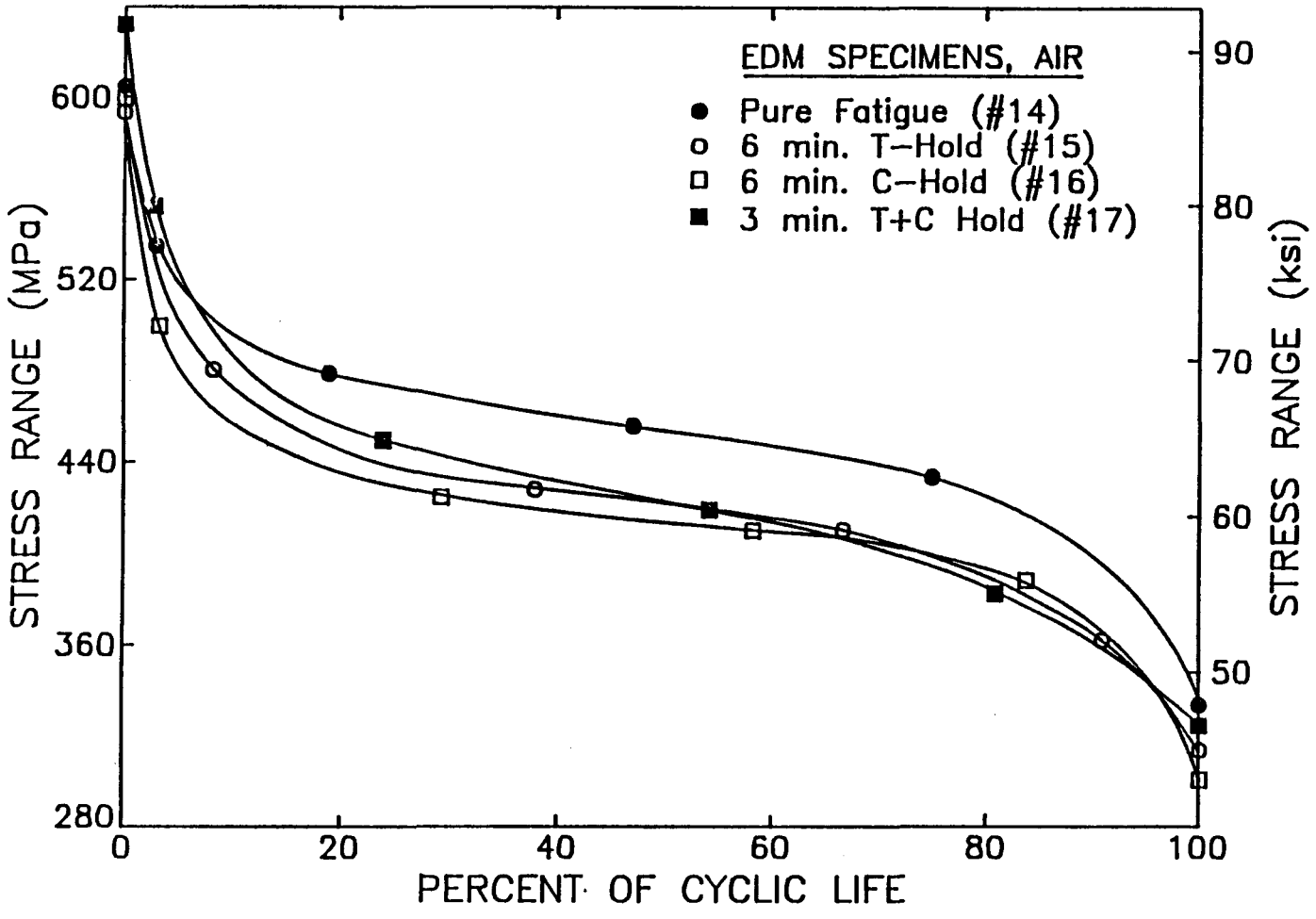

Figure 3.5 Stress range versus percent of cyclic life for the four different waveshapes. Note both the immediate softening response and the decreased stress range due to the hold period waveforms. This behavior was essentially identical for all specimens, regardless of geometry (smooth or EDM) or environment (air or vacuum). Parenthesis indicate test number as given in Table 3.

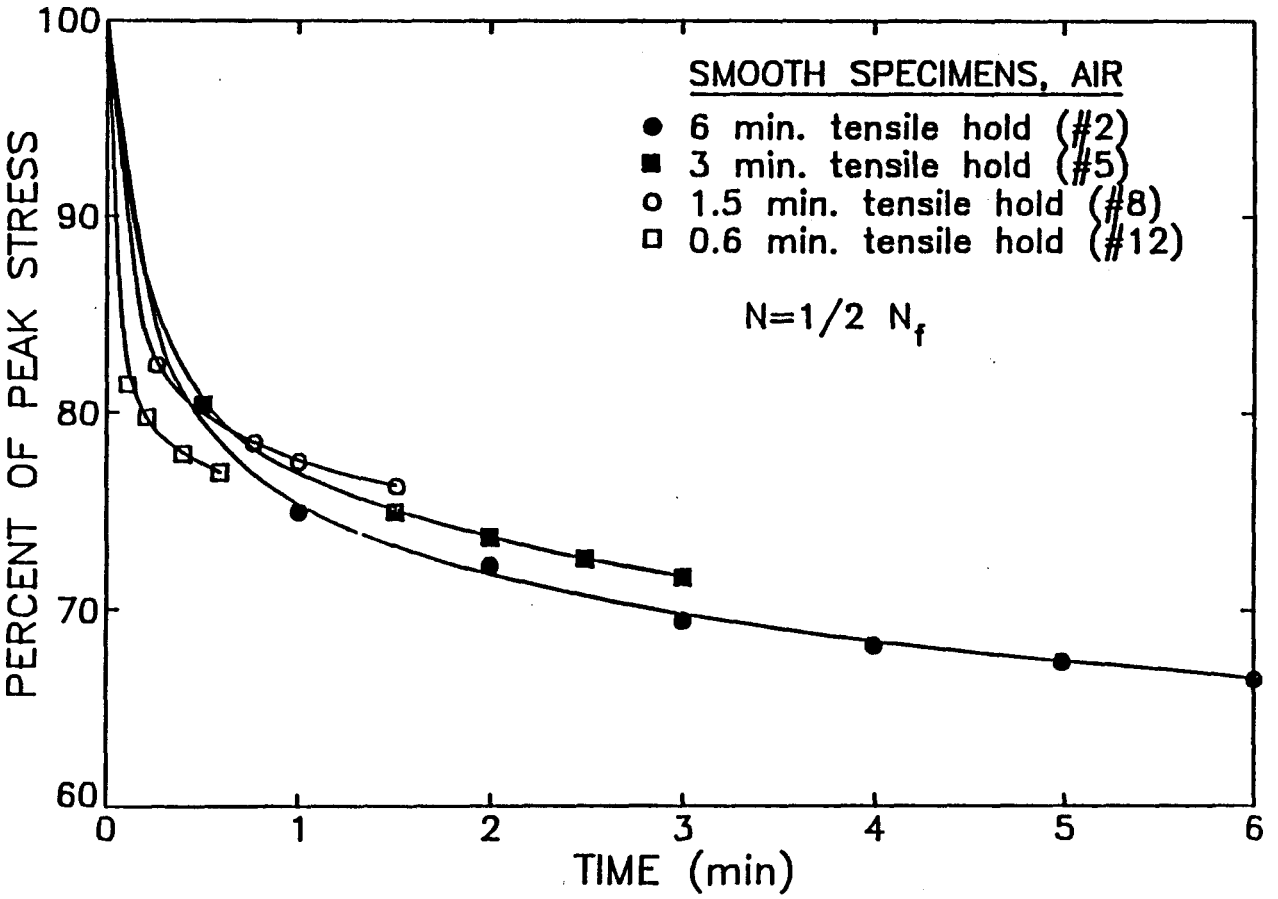

Figure 3.6 Percent of peak stress versus time (at 0.5 Nf) for tensile hold period waveforms. Note the similarity in the amount of stress relaxation in each case, despite the wide variance in hold period duration.

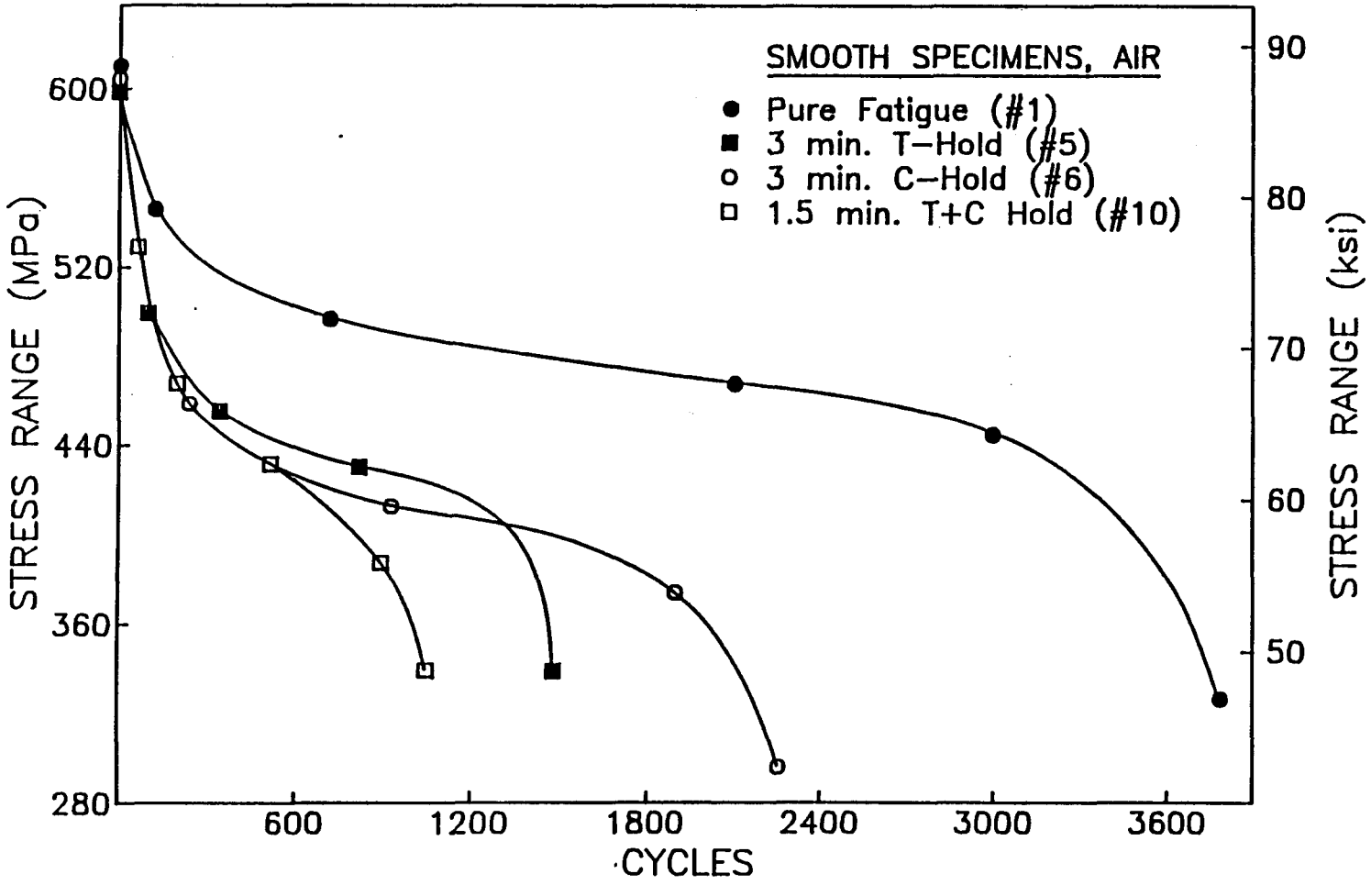

Figure 3.7 Stress range versus cycles for the four different waveforms, indicating the deleterious effect of hold periods on fatigue resistance.

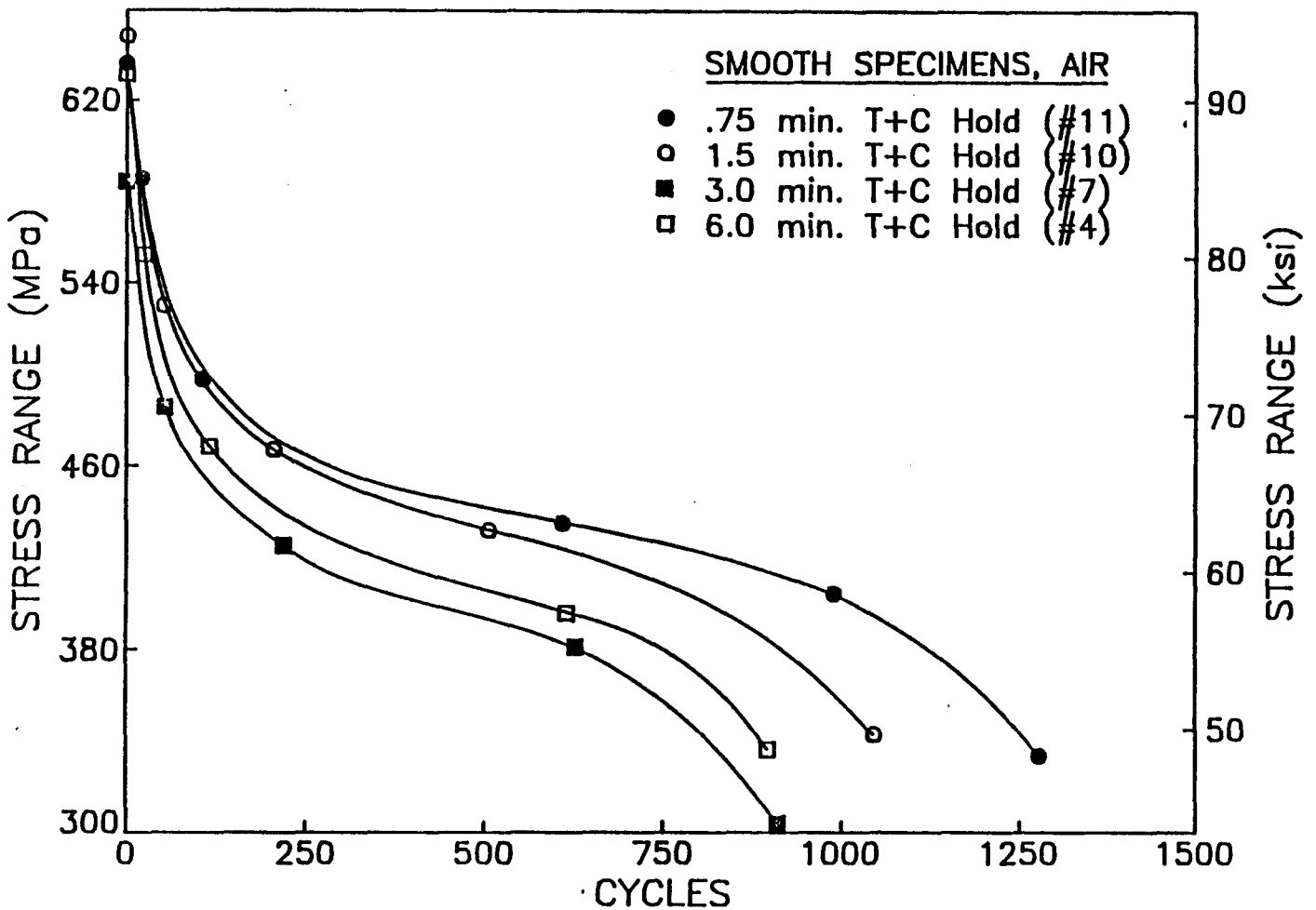

Figure 3.8 Stress range versus fatigue cycles for the combined tensile/compressive hold waveform, illustrating the only minor effect of hold period duration on fatigue life.

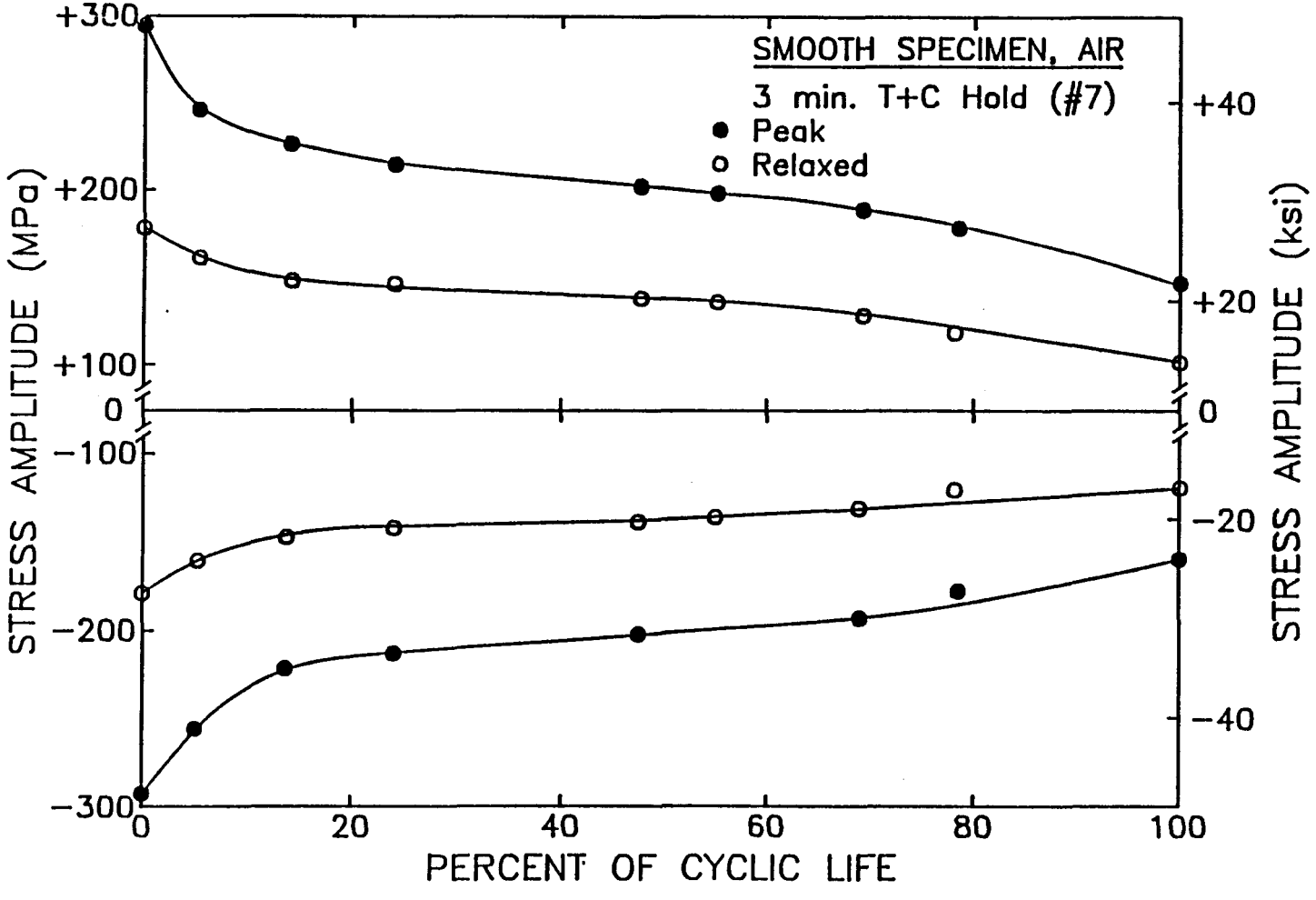

Figure 3.9 Peak and relaxed stress versus percent of cyclic life, showing the amount of stress relaxation throughout an entire test. Test conducted on a smooth (unnotched) specimen in air.

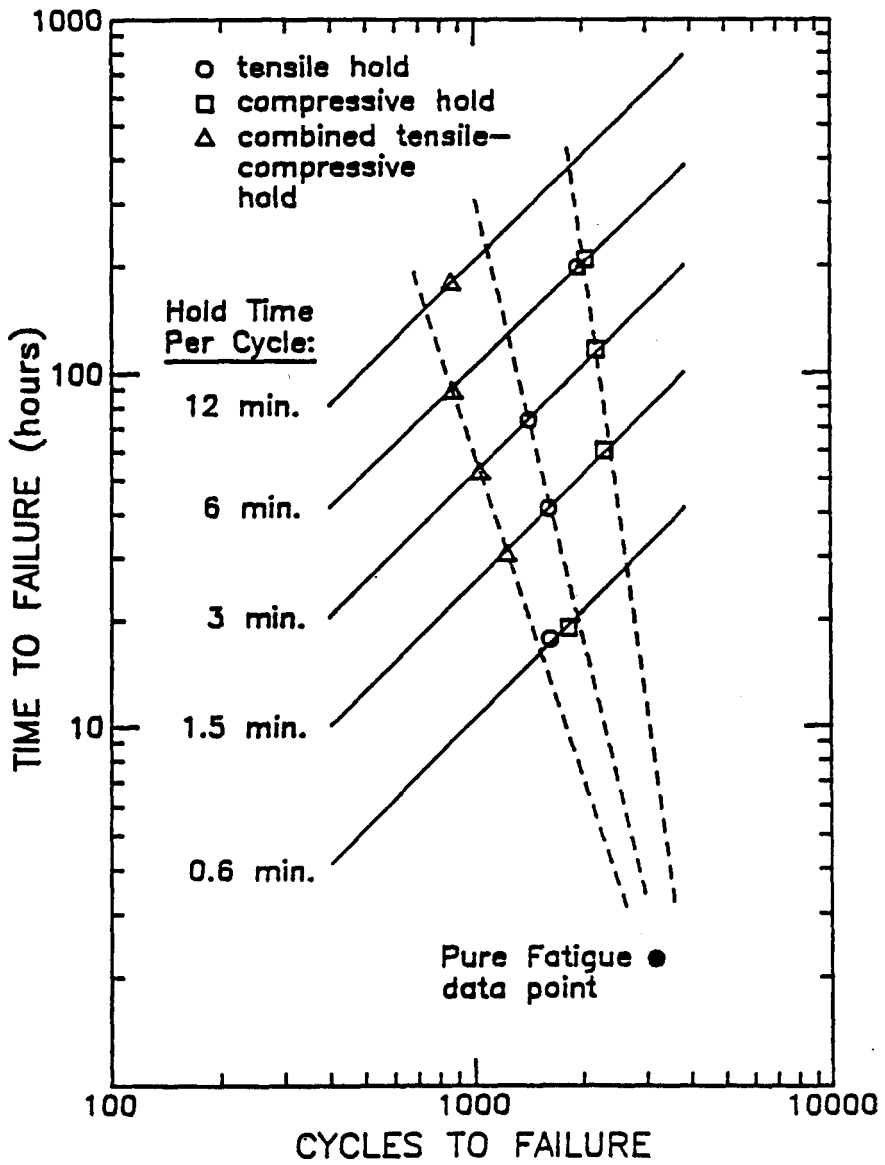

Figure 3.10 Time to failure versus cycles to failure diagram, showning the overall effects of hold periods at 565°C and 0.50% fully reversed strain range. Data is for smooth specimens tested in air.

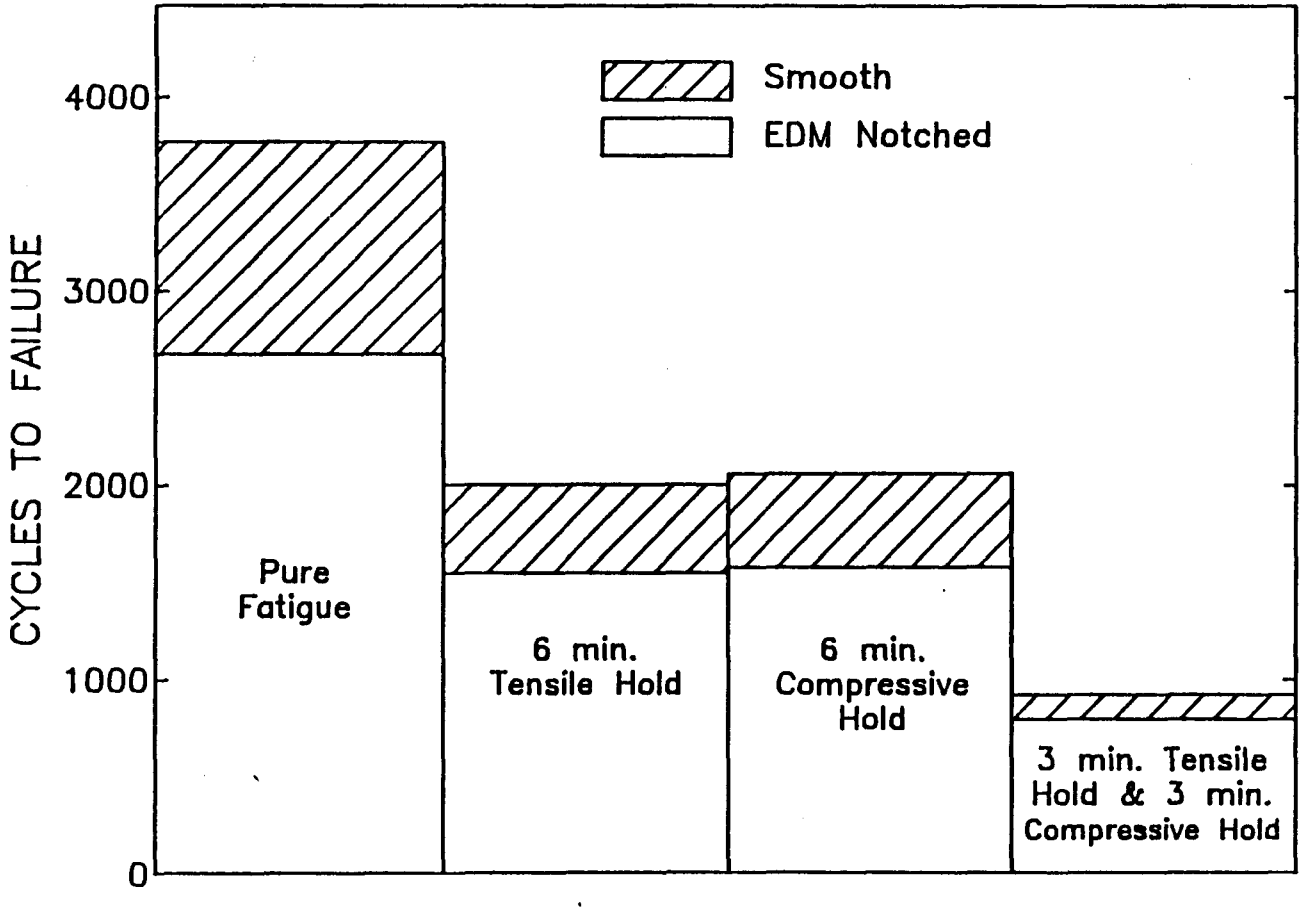

Figure 3.11 Comparison of fatigue life data in air for smooth and EDM notch specimens. Averaging reduction in life due to EDM notches for the above waveforms is 22%.

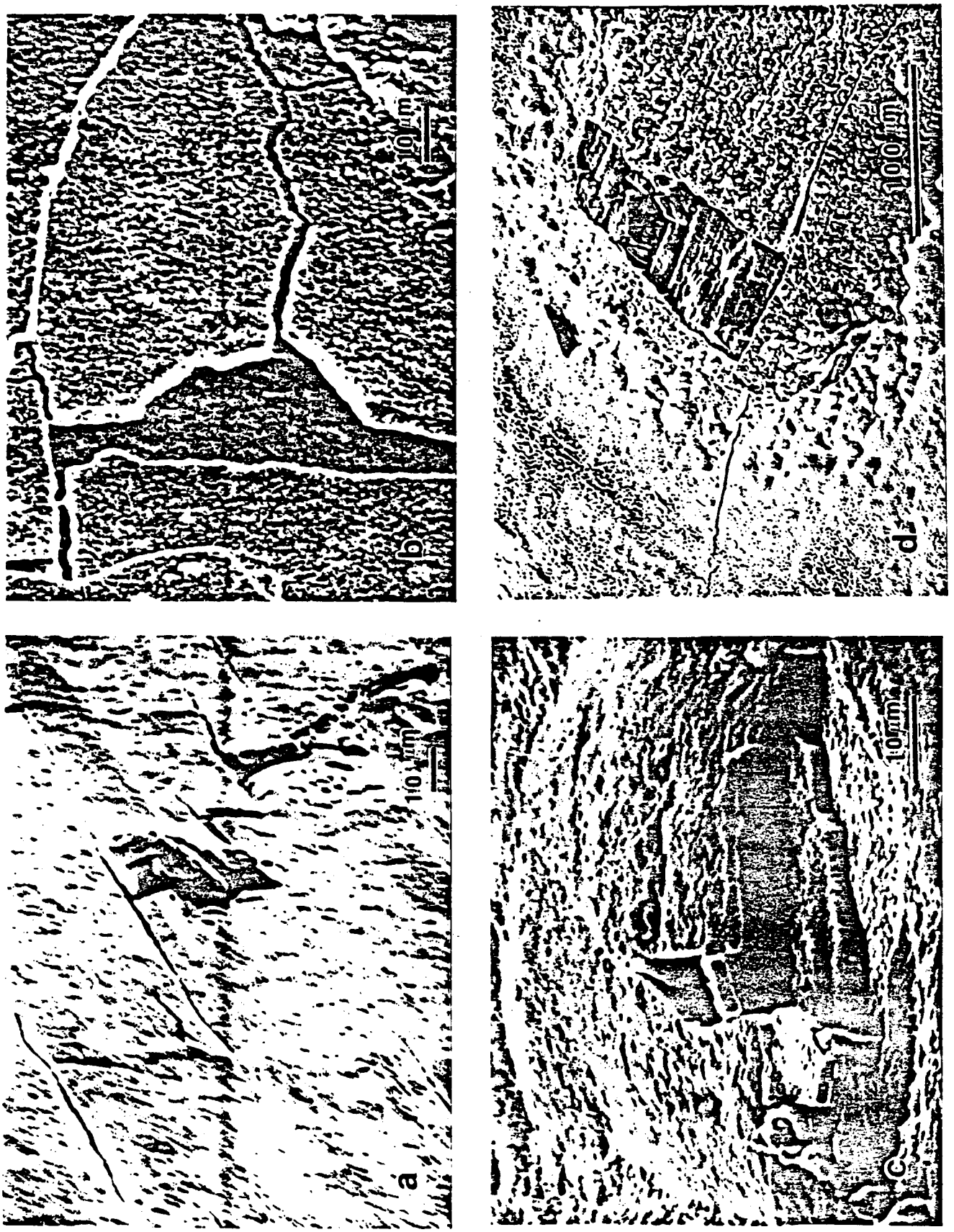

Figure 3.12 Scanning electron micrographs showing surfaces of specimens subjected to: (a) 25%, (b) 10%, (c) 10% and (d) 5% of normal cyclic life for smooth specimens in air.

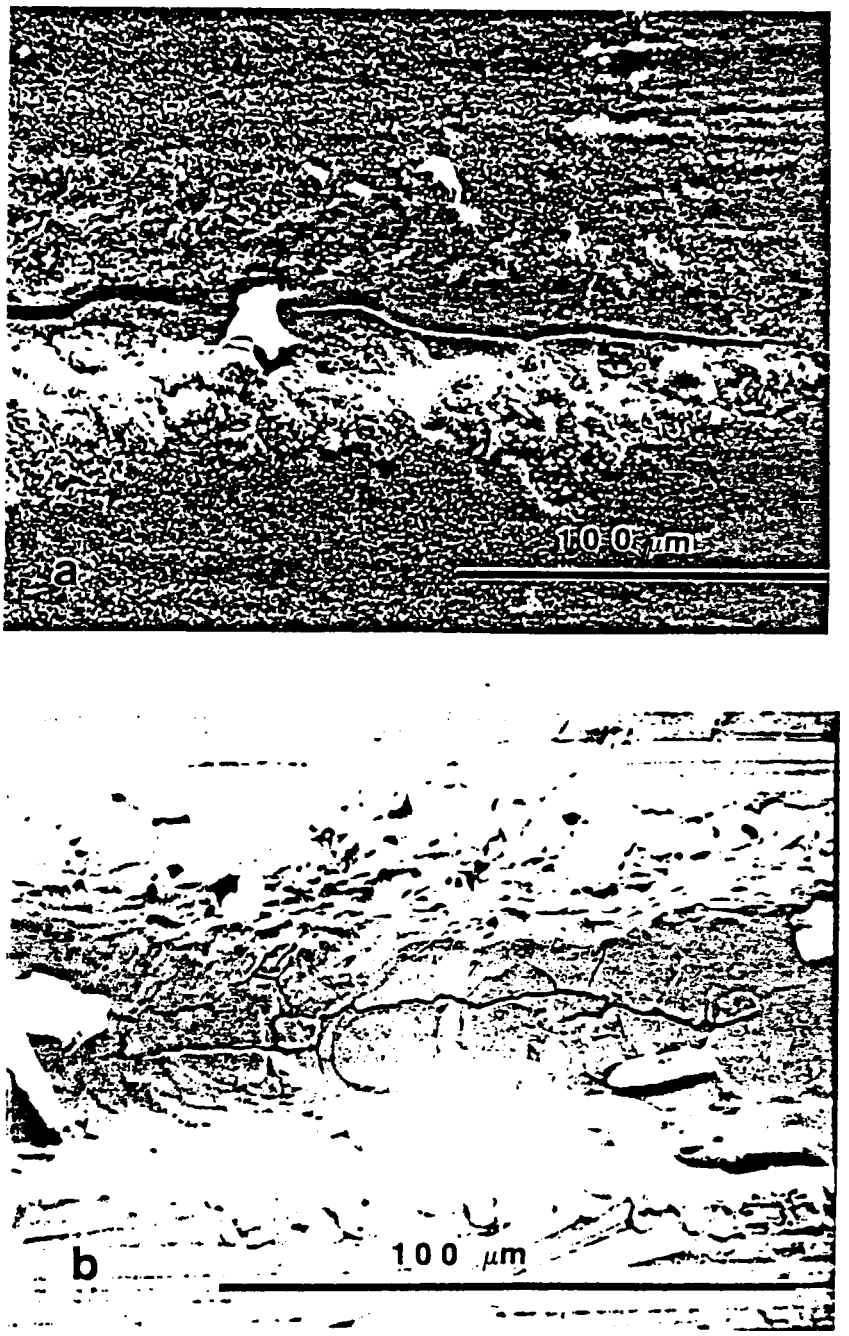

Figure 3.13 Scanning electron micrographs of EDM notches tested to 25% of normal pure fatigue life in (a) air and (b) vacuum. Cracks were also observed away from the notch in the air specimen but not in the vacuum specimen.

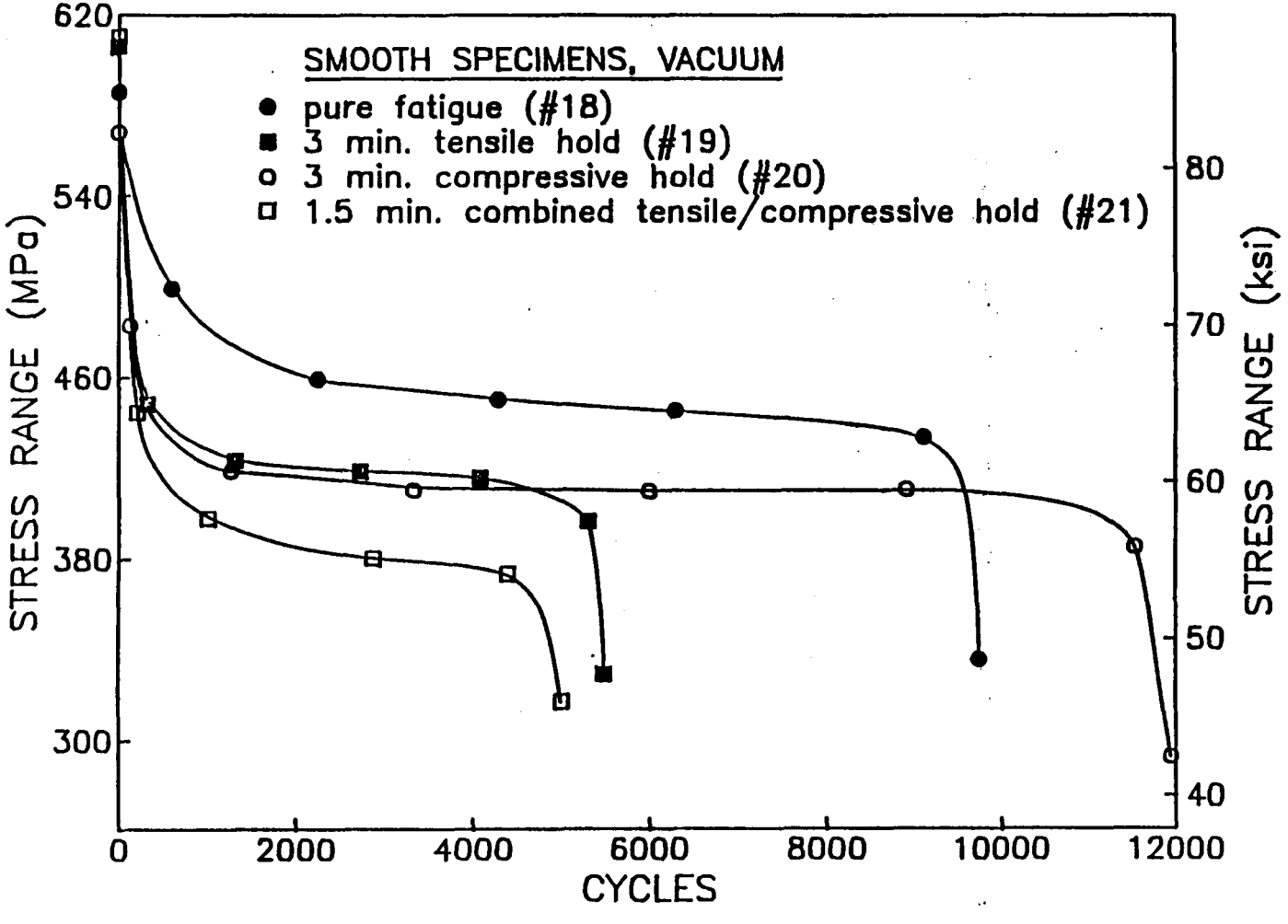

Figure 3.14 Stress range versus cycle for four different wave forms appied to smooth specimens in vacuum.

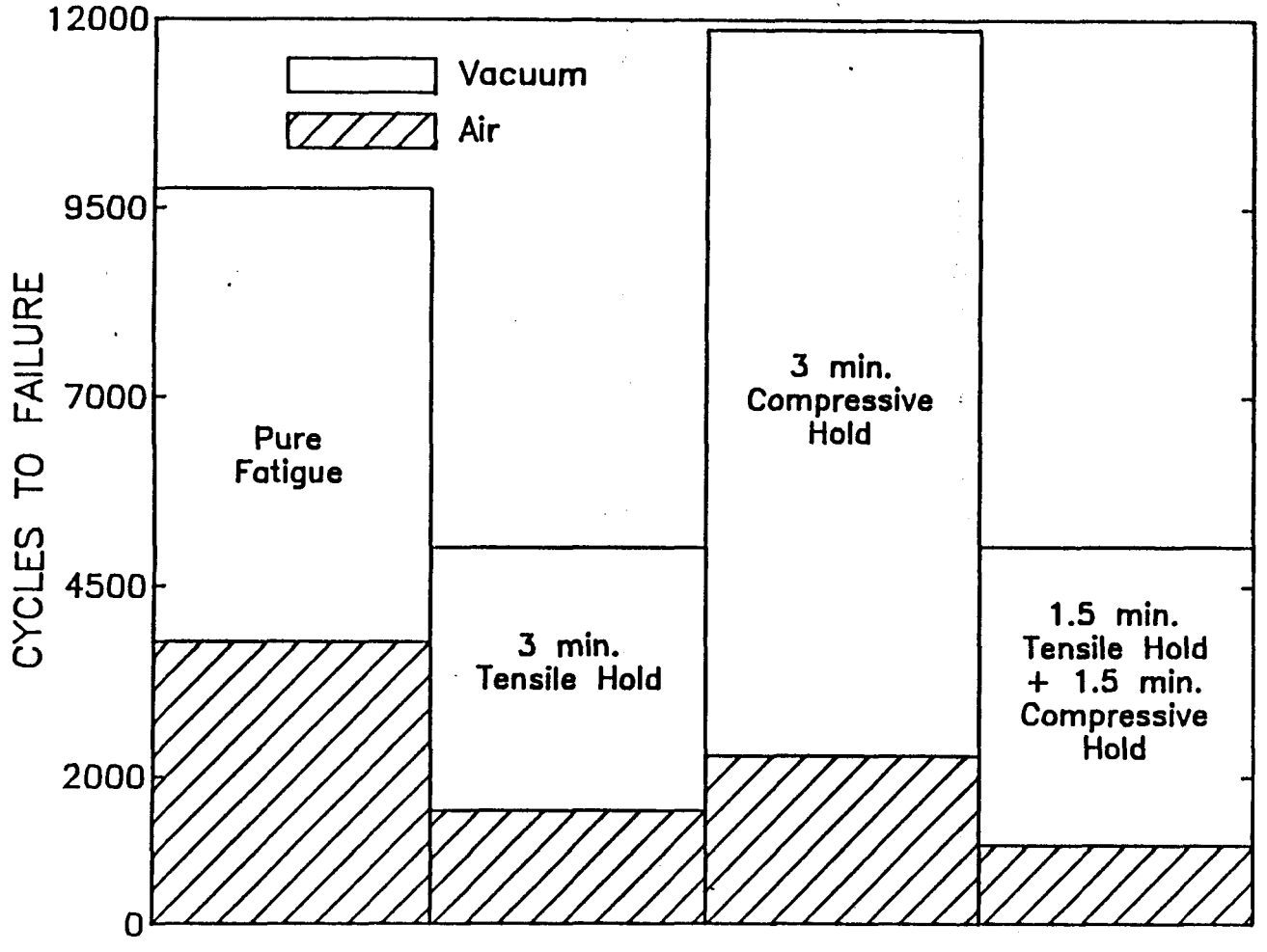

Figure 3.15 Comparison of fatigue life data for smooth specimens tested in both air and vacuum. Average increase in life due to vacuum for the above waveforms is 410%.

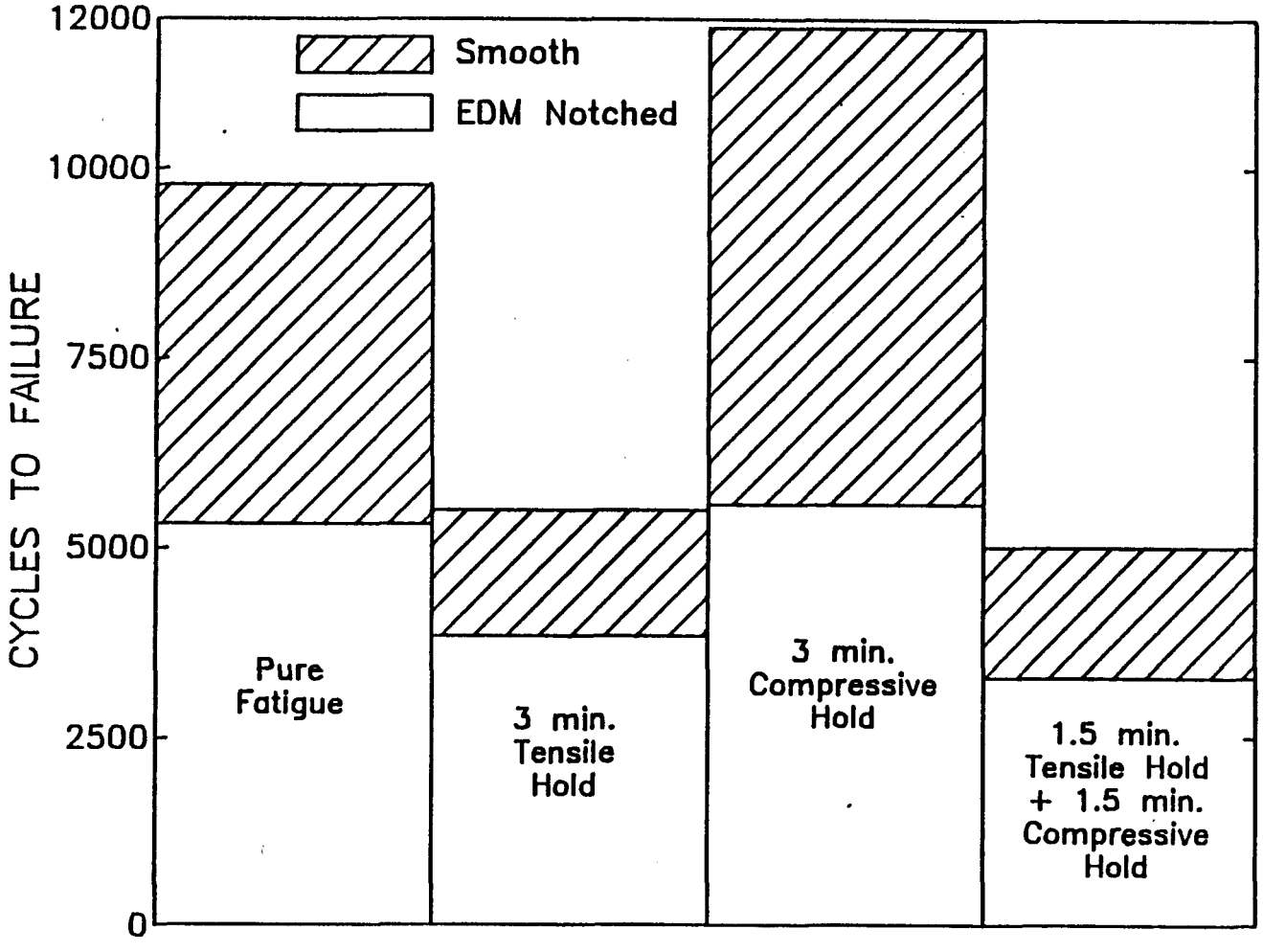

Figure 3.16 Comparison of cyclic data in vacuum for both smooth and EDM notch specimens. The average reduction in cyclic life due to EDM notches was 41% in vacuum opposed to 22% in air.

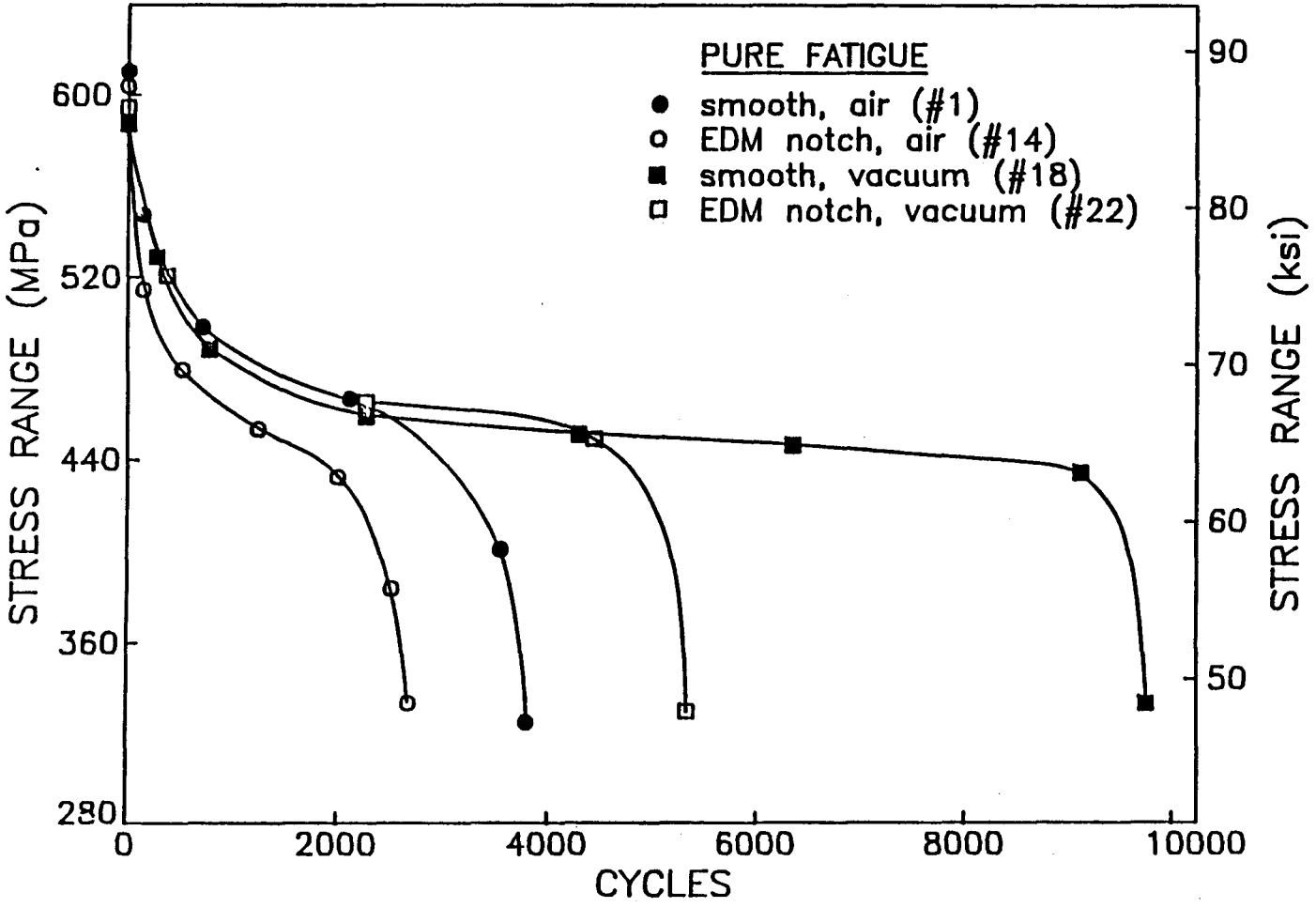

Figure 3.17 Stress range as a function of cycles for pure fatigue waveforms, showing the relative effects of smooth versus EDM notch specimen geometry and air versus vacuum enfironment.

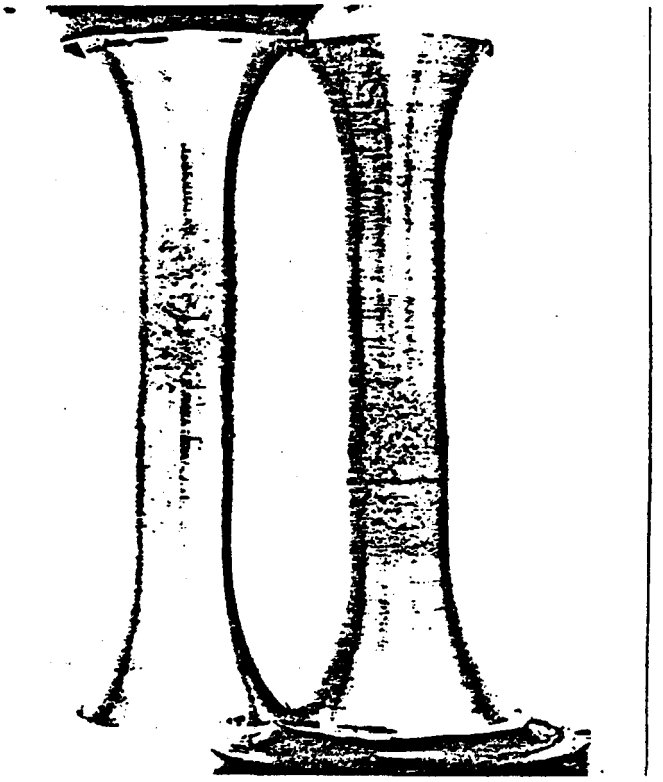

Figure 3.18 Photograph of two vacuum test specimens, illustrating the characteristics "orange peel" regions of extensive localized plastic deformation. Note EDM notches in the specimen at right.

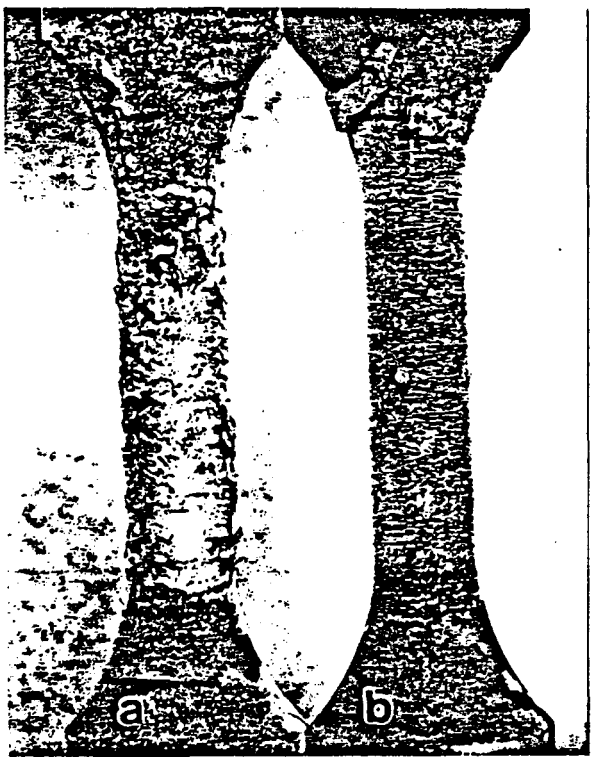

Figure 3.19 Comparison of oxide scale behavior on specimens subjected to:
(a) a six minute tensile hold period (DS-1)
(b) a six minute compressive hold period (DS-4)
Oxide on (a) spalled considerably, while oxide on (b) was much more adherent.

4. PRELIMINARY STUDIES OF ADVANCED AUSTENITICS

The material used in these preliminary studies is Alloy 17-14 Cu Mo. This is not one of the alloys developed at ORNL by Maziaz, et al., but it is similar in composition and performance and has the advantage of being readily available. It is also the material which was used in the Eddystone power plant and testing of this material therefore has a secondary value in providing data for residual life assessment of that particular plant.

Work so far on this material has been limited to exploratory studies for setting test priorities in a future, more extensive, program.

The following four basic tests have been carried out: strain controlled LCF tests, steady load creep tests, fatigue crack growth rate tests, and creep crack tests.

In anticipation of the likely impact of thermo-mechanical treatment during manufacture on in-situ material properties, tests have been performed on the material with different pre-test treatments. These include solution annealed, mill annealed (i.e. as-received), and cold-worked, solution annealed and aged.

4.1 STRAIN CONTROLLED LCF TESTS

Nine strain controlled fatigue tests have been performed on mill annealed material. The specimen geometry and the test machine are identical to those used in the studies of 2.25 Cr 1 Mo steel described earlier. The test temperature in this case was 700°C.

Tests were run under fully reversed saw-toothed waveform at two strain rates of 0.004/sec and I.4 E-5/sec.

Figure 4.1 shows the results on a strain-life plot. There is an eight-fold reduction in cyclic life in going from the higher to the lower strain rate. This change was accompanied by a transition from trans-granular to intergranular fracture. In this respect, the material shows typical behavior for austenitic steel as elevated temperate.

Hold time tests are in progress.

4.2 STEADY LOAD CREEP TESTS

Five steady load creep tests have been performed 700°C at the same nominal stress of 200 MPa. Three of these went to rupture and two were interrupted during secondary stage creep.

The results for the tests to rupture are shown in Fig. 4.2. These consist of two specimens in the mill annealed condition and one which was solution annealed.

The solution annealed material showed shorter lives (100 to 112 hours) and lower ductility than the mill annealed material.

One creep sample solution was solution annealed, cold-worked, and aged to simulate the taupe of treatment suggested by Maziaz, et al. This specimen showed very low creep rates and the test was terminated after 890 hours because it was progressing so slowly. This is a very significant encore in life compared with the as-received condition.

In all instances, metallography performed on the failed specimens showed wedge cracking at grain boundary triple points. So far the interrupted specimens have not been examined.

4.3 FATIGUE CRACK GROWTH RATE TESTS

Three fatigue crack growth rate tests have been conducted at 700°C. These test were performed on 1 inch wide by 1/8 inch thick center cracked plates under a maximum tensile load of 1000 lbs and an R-ratio of 0.05. Crack growth was monitored by dc potential drop.

The results of tests at three frequencies are shown in Fig. 4.3. The effect of frequency is typical of materials of this type. At all frequencies, the crack growth rate is correlated well by the elastic stress intensity K.

Examination of the fracture surfaces shows transgranular crack propagation in the majority of instances with about 5 percent intergranular surface observed in the 0.1 Hz test. Lower frequency tests are in progress.

4.4 CREEP CRACK TESTS

Two steady stress creep tests have been performed on the center cracked specimen. Crack propagation was monitored by dc potential drop using the same technique as for the fatigue crack experiments.

The results are shown in Fig. 4.4 showing the correlation of crack growth with C* net section stress and stress intensity range. There is considerable scatter in the results which may be a function of inaccuracies in the potential drop method or it could signify inadequacies in the methods of correction. Whether the reason is one or the other has yet to be determined. In either event the amount of scatter is not atypical of results published in the open literature.

Both tests were interrupted when the crack growth reached 0.1 inch. The crack opening angle at this point was close to 80°C which is indicative of very creep ductile material.

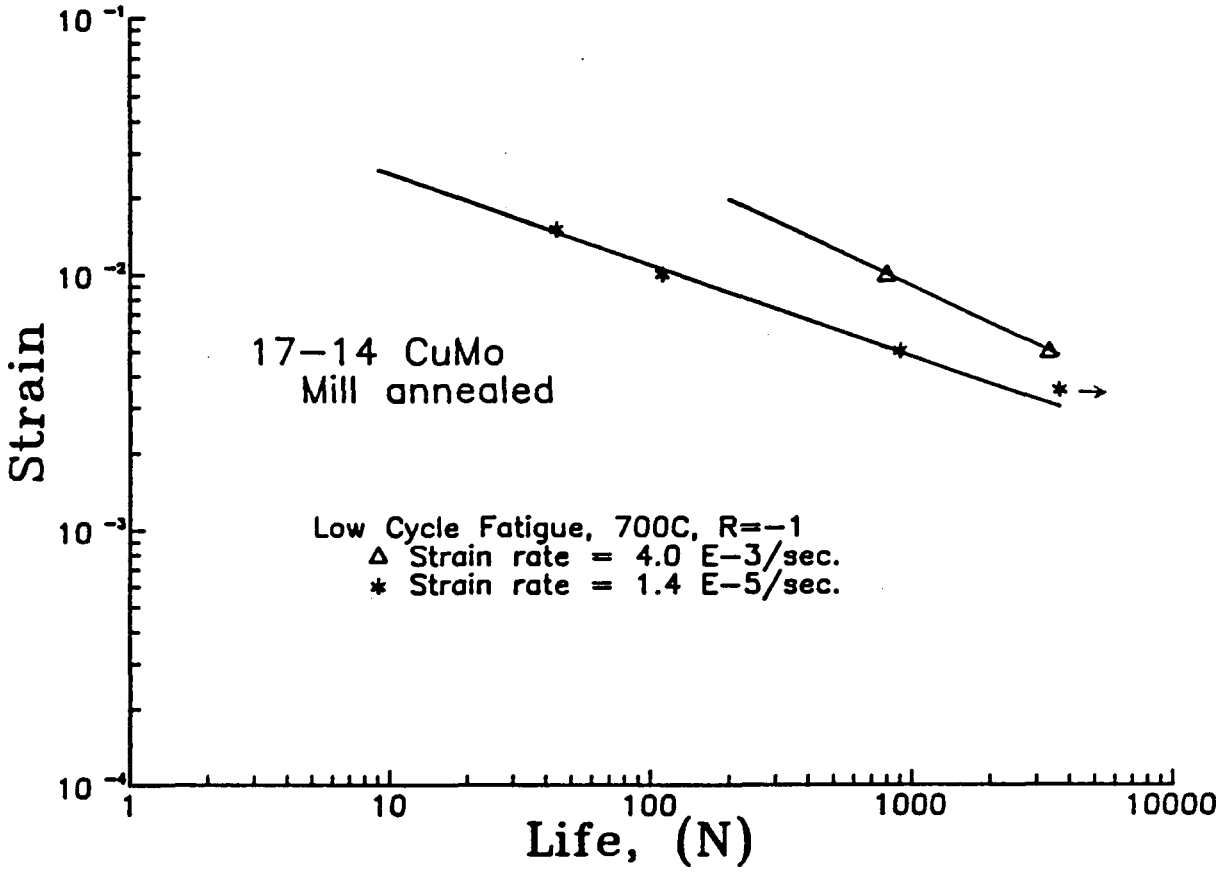

Figure 4.1 17-24 Cu Mo Mill Annealed - Strain/life fatigue data at high and low strain rates

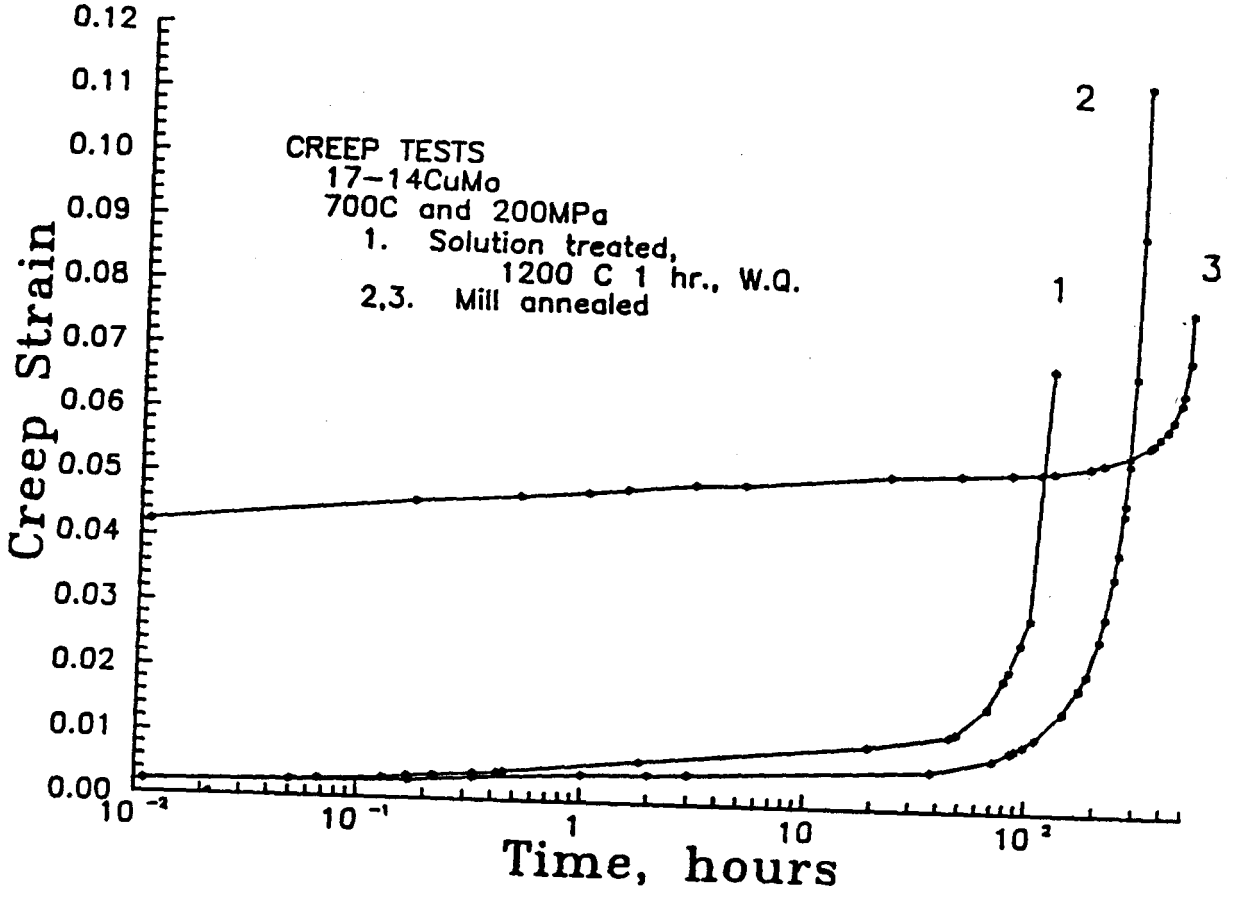

Figure 4.2 17-24 Cu Mo - Steady load creep data

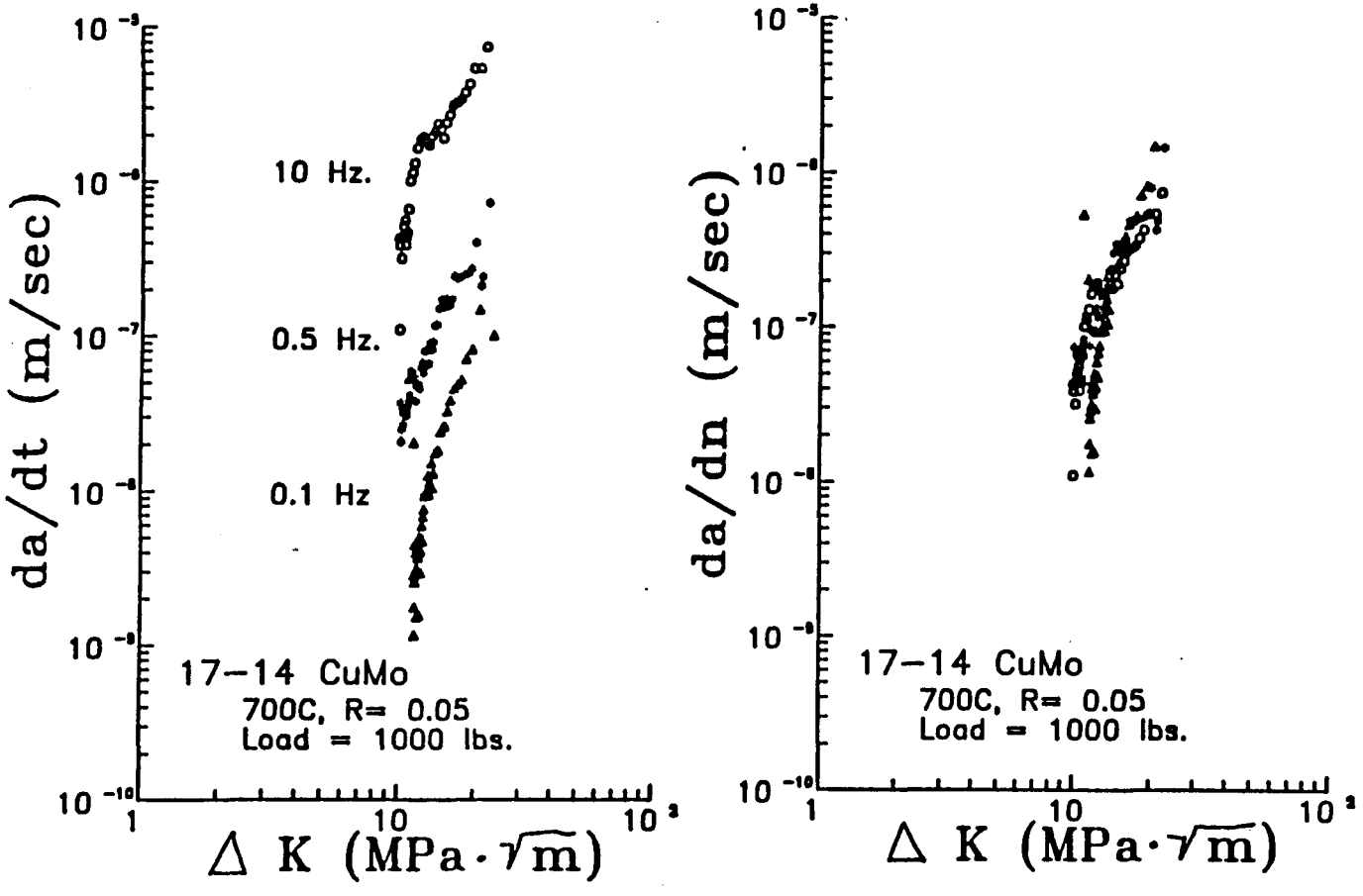

Figure 4.3 17-24 Cu Mo - Fatigue crack growth data

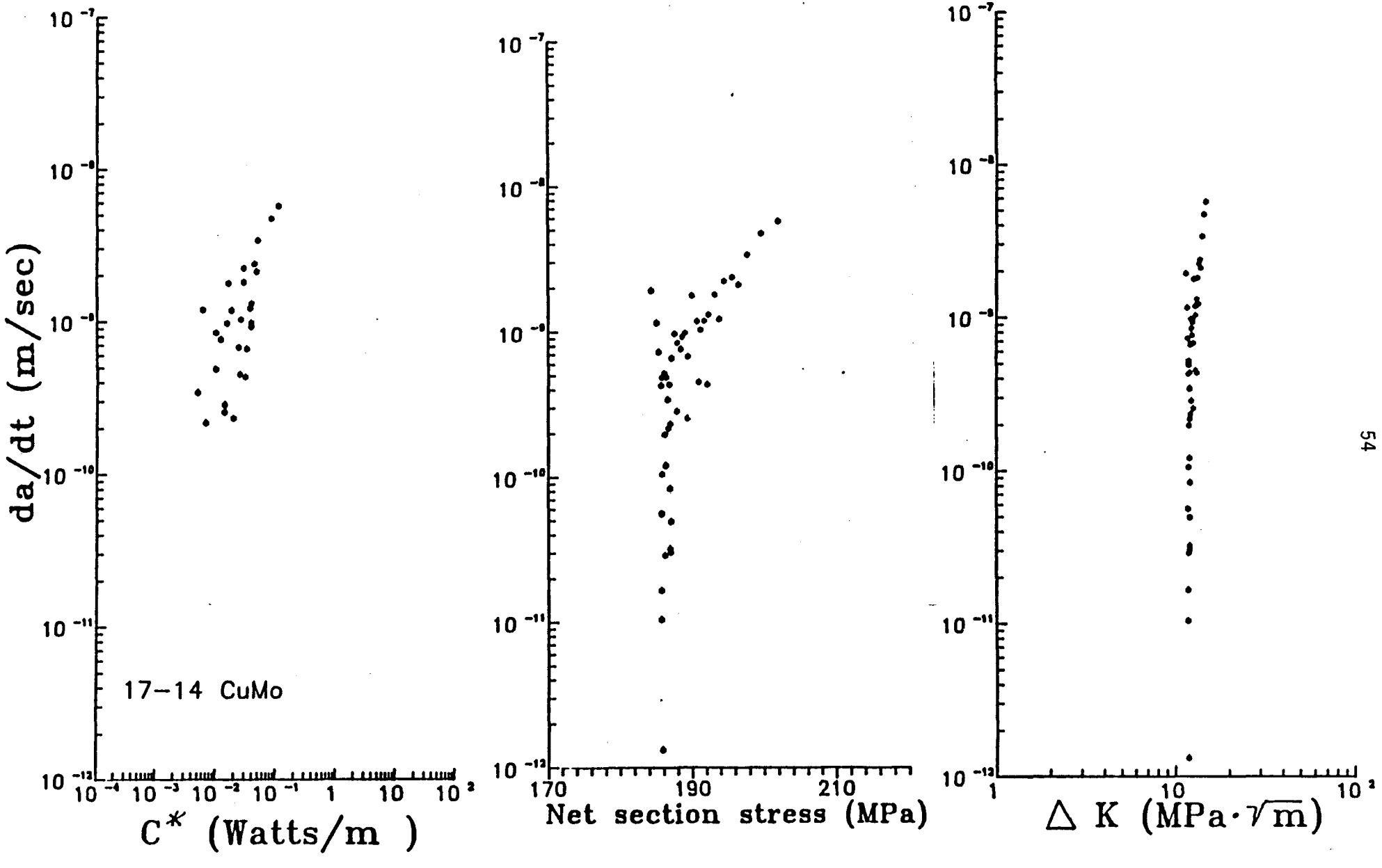

Figure 4.4 17-24 Cu Mo - Steady load creep crack growth data

5. MATERIAL CHARACTERIZATION

5.1 INTRODUCTION

To investigate the effects of a material's behavior on the response of a component it is necessary to have an understanding of how the material responds under various loading conditions. Once this has been determined some means of characterizing the behavior of the material is needed. In this chapter characterizations of the time independent and time dependent behavior of this material are presented. The purpose of these representations was not to obtain a precise model of the material behavior, but to capture the essential characteristics of the softening phenomenon. For this reason the time independent and time dependent material behavior was investigated separately.

A model for time independent cyclic behavior was developed which was an extension of the Ramberg-Osgood model of stable cyclic inelastic behavior. In this model cyclic softening was postulated as being a function of accumulated plastic strain. This dependency on accumulated plastic strain was implemented through the material constants of the Ramberg-Osgood relation.

In examining time dependent material behavior steady load creep test results were used to predict material response under stress relaxation conditions. In these predictions total strain, strain hardening and time hardening creep theories were utilized.

Finally, isochronous creep curves were used to examine the interaction between creep deformation and material softening under cyclic loading conditions. These studies treated the effects of creep deformation as a perturbation of time independent behavior.

5.2 MODELING OF TIME INDEPENDENT CYCLIC BEHAVIOR

5.2.1 Introduction

Several unified constitutive models have been developed which claim to model some form or another of cyclic softening. Unfortunately, none of these models have been found appropriate for the modeling of cyclic softening behavior when a significant, continuous, decrease in strength occurs, such as is the case with the current material. For this reason a time independent uniaxial constitutive model of strain induced cyclic softening has been developed. In this model softening was postulated to be a function of accumulated plastic strain. For convenience all nomenclature pertaining to the development and use of this model is contained in Table 5.1.

5.2.2 Experimental Data

The data utilized in this study was obtained from smooth specimen strain controlled fully reversed fatigue tests performed by Pejsa [5.1]. Two strain ranges, 0.5% and 1.0%, were used. Both tests were performed at the relatively high strain rate of 0.004/sec in order to minimize the effects of time dependent processes. Tests were conducted on material in the as-received condition at a temperature of 565°C.

During mechanical testing stress-strain hysteresis loops were recorded at regular intervals throughout the life of the specimen. This data provided a record of the progression of material softening in terms of changes in cyclic stress-strain material response. The model was developed from data obtained from the fully reversed 1.0% strain range cyclic test. The predictive capability of the model was examined by comparing predictions and experimental results of the 0.5% strain range test.

5.2.3 Description of Simplified Softening Model

The model described here was developed as an extension of an existing model of stable cyclic inelastic behavior which has been used extensively and found to represent material behavior with reasonable fidelity. The model assumes that the loading and unloading regions of the stress-strain hysteresis loop may be represented by a Ramberg-Osgood form [5.2]. For the uniaxial case

Total Strain $$\Delta\varepsilon^* = \Delta\varepsilon_e^* + \Delta\varepsilon_p^* \quad (5.1)$$

Elastic Strain $$\Delta\varepsilon_e^* = \frac{\Delta\sigma^*}{E} \quad (5.2)$$

Inelastic Strain $$\Delta\varepsilon_p^* = \left(\frac{\Delta\sigma^*}{C}\right)^{1/m} \quad (5.3)$$

An asterisk (*) superscript is used to indicate specific stress and strain values in individual hysteresis loops. The use of this notation will be discussed in further detail later. It should be noted that the use of a nonconventional notation for the constants in Eq. (5.3) was done deliberately so as to emphasize the difference between these values and those commonly used to describe a materials cyclic stress-strain curve.

To include strain induced softening it was assumed that C and m are functions of the cumulative plastic strain only. This was an intuitive assumption based on empirical observations of softening behavior in a number of diverse situations [5.1, 5.3, 5.4]. This means that

$$\Delta\sigma^* = C(\Sigma\Delta\varepsilon p) \cdot (\Sigma e_p^*)^{m(\Sigma\Delta\varepsilon_p)^n} \quad (5.4)$$

As will be discussed later, experimental evidence showed that $C(\Sigma\Delta\varepsilon_p)$ has an n-power form,

$$C(\Sigma\Delta\varepsilon p) = h \cdot (\Sigma\Delta\varepsilon_p)^n \quad (5.5)$$

where $\Sigma\Delta\varepsilon_p >$ critical strain, and $n < 0$ necessarily, to model softening behavior.

To avoid a singularity at zero accumulated plastic strain, in this model it was assumed that C was constant for $\Sigma\Delta\varepsilon_p^* < 2.8$ percent. This was chosen as a reasonable reflection of observed material behavior.

No attempt has been made here to represent multiaxial stress states. As far as deformation under multiaxial stress is understood at the present time, this is a routine operation. The material appeared to

soften isotropically in uniaxial tests. Due to this, and from what can be understood of the underlying mechanisms, it seems reasonable to assume that the parameters governing softening should be scalars [5.5]. In-phase multiaxial behavior can therefore be modeled by replacing the cumulative plastic strain in the uniaxial case with the cumulative Mises plastic strain $\Sigma(|\Delta\varepsilon_{eff}|)$.

5.2.4 Development of Model

During the mechanical testing of this material stress-strain hysteresis loops were recorded at regular intervals throughout the life of the specimen. These data provided a history of the progression of softening on the cyclic stress-strain response of the material. Figure 5.1 shows a semi-log plot of stress range versus number of cycles for a fully reversed 1.0% strain range cyclic test. The material is observed to soften continuously throughout the duration of the test. This plot also shows a significant increase in loss of strength towards the end of the test. This acceleration of strength loss marks the onset of significant cracking in the specimen. Such a behavior is commonly observed in the strain control fatigue testing of all but very brittle materials.

Individual hysteresis loops were assumed to be antisymmetric and to close upon the completion of each cycle. The tension loading (and likewise compression loading) portion of the hysteresis loop was represented using a form of the Ramberg-Osgood stress-strain relation [5.2]. In the uniaxial case this relation is given in Eqs. (5.1) through (5.5).

Figure 5.2 provides a graphical representation of these terms. As shown, the origin of the stress-strain axis is located at the beginning of the reversal. An asterisk (*) superscript is used to differentiate between relative stress/strain values (such as $\Delta\sigma^*$ and $\Delta\varepsilon_e^*$) and absolute stress/strain ranges (such as $\Delta\sigma$ and $\Delta\varepsilon_e$).

The values of the material constants C and m used above are cycle dependent. This cycle dependency was evaluated by plotting log relative stress ($\Delta\sigma^*$) versus log relative plastic strain (Δe_p^*)for a number of cycles throughout the life of the specimen. Such a plot is shown in Fig. 5.3 for a few representative cycles. This figure shows that relative stress and plastic strain are adequately modeled by a Ramberg-Osgood relation, particularly when significant relative plastic strain has developed in the cycle.

The exponent, m, of the power law relation (representing the slope of the log $\Delta\sigma^*$ versus log Δe_p^* plot in Fig. 5.3) showed no cyclic dependency and was therefore taken as a constant (m = 0.0905). At lower plastic strain levels a slight non-linearity is observed in the log relative stress versus log relative plastic strain plot. For the current analysis this discrepancy was treated as a second order effect, and therefore neglected.

The coefficient, C, in the power law relation showed a definite cyclic dependency. Figure 5.4 shows a log-log plot of the coefficient C versus number of cycles, N. Due to the observed linearity of this plot, this relationship was represented through the use of an n-power law. The coefficient C was then determined as

$$C = 1190 \cdot (N)^{-0.0687} \text{ MPa} \tag{5.6}$$

By combining Eqs. (5.3) and (5.6) the relative stress-plastic strain relation becomes

$$\Delta\sigma^* = 1190 \cdot (N)^{-0.0687} \cdot (\Delta\varepsilon_p^*)^{0.0905} \text{ MPa} \tag{5.7}$$

Until now, relative stress and plastic strain have been related by a cycle dependency. It is ultimately desired to relate these terms through an accumulation of plastic strain. Recall that in Fig. 5.1 absolute stress range was presented as a function of cycle number. From this figure the following numerical fit was obtained

$$\Delta\sigma = -86.9 \cdot \log(N) + 724 \text{ MPa} \tag{5.8}$$

Since testing was performed by cycling between specified total strain limits (±0.5% for the 1.0% strain range test) the plastic strain range developed during any given cycle may be determined. For the imposed test conditions

$$\Delta\varepsilon = 0.01 = \Delta\varepsilon_e + \Delta\varepsilon_p \tag{5.9}$$

Using Hooke's law ($\Delta\varepsilon_e = \Delta\sigma/E$) the plastic strain range is

$$\Delta\varepsilon_p = 0.01 - \frac{\Delta\sigma}{E} \tag{5.10}$$

Substituting Eq. (5.8) and the appropriate value of Young's modulus, E, into Eq. (5.10) gives

$$\Delta\varepsilon_p = 5.47 \times 10^{-4} \cdot \log(N) + 5.45 \times 10^{-3} \tag{5.11}$$

From Eq. (5.11) accumulated plastic strain was obtained as a function of number of cycles by summing the increment of plastic strain developed in each given cycle. Figure 5.5 shows a plot of this relationship. This figure shows that a power law relation provides a good fit to the calculated results. The resulting power law relation is

$$\Sigma\Delta\varepsilon_p = 10^{-2.27} \cdot (N)^{1.04} \tag{5.12}$$

Combining Eqs. (5.7) and (5.12) it is now possible to relate relative stress and plastic strain as a function of accumulated plastic strain. Doing this, the resulting relative stress-plastic strain relation is

$$\Delta\sigma^* = h \cdot (\Sigma\Delta\varepsilon_p)^n \cdot (\Delta\varepsilon_p^*)^m \tag{5.13}$$

where, h = 843 MPa, n = -0.0661, and m = 0.0905.

The previous relation provides a model of the stress-strain response of this material subjected to cyclic loading.

5.2.5 Model Predictions

This model was developed from data obtained from a fully reversed 1.0% strain range cyclic test. The predictive capability of this model was evaluated by comparing predictions with the experimental results of a fully reversed 0.5% strain range cyclic test. In predicting material response a forward solution method was used to estimate the accumulated plastic strain at a variety of cycle numbers. This solution process involved determining, through an iterative procedure, the absolute stress and plastic strain ranges at each of the cycle numbers of interest.

Due to the functional form used in the data curve fitting process a slight modification to the proposed model was necessary. To avoid a singularity at zero accumulated plastic strain a cutoff C_o was imposed for the constant C in the relationship between stress range and plastic strain range. This modification specifies that the cyclic stress-strain response of the material remains unchanged until a critical amount of plastic strain has been accumulated. In this analysis a critical accumulated plastic strain of 2.8%, corresponding to a cutoff value, C_o, equal to 1068 MPa, was used. This value is representative of the amount of plastic strain accumulated experimentally in the initial softening stage of the 0.5% strain range test.

Figure 5.6 shows a semi-log plot of experimental and predicted results of stress range versus numbers of cycles for the 0.5% strain range test. The predicted results are shown to correspond very well with those obtained experimentally.

The proposed model also allowed the determination of individual stress-strain hysteresis loops. Figure 5.7a shows a plot of the experimental and predicted hysteresis loops at cycle number 50 for the 1.0% strain range test. As expected the predicted results agree quite well with the experimental results. (Recall that the model as developed from data obtained from the 1.0% strain range test.)

Figures 5.7b and 5.7c show predicted and experimental hysteresis loops at cycle numbers 50 and 2500, respectively. Once again the predicted results correspond well with those obtained experimentally.

5.2.6 Discussion of Results

Considering the objectives of the work reported here, the approximate constitutive relation appears to work very well indeed. As shown by Fig. 5.6, the cyclic stress range for a 0.5% strain range was predicted very closely from an equation which was derived entirely from 1.0% strain range data.

The analytical formulation of the constitutive relation, in the form of power relations, produces results which are satisfactory for practical purposes. The only modification which was considered necessary in this study, was to impose a cutoff, C_o, for the constant C in the relationship between stress range and plastic strain range. This was necessary to avoid a singularity at zero accumulated plastic strain. This was not considered to be a fundamental problem, but was merely a consequence of the restricted functional form used in the curve fitting process. No doubt a more complex analytical form could be used to fit the C-curve over its entire range, if necessary.

The current model has been developed for strain cycling with zero mean stress. It is believed that the existing model can be extended to include variable stress ratio (R) effects in a similar manner as has been used frequently in the past in constructing variable stress range hysteresis loops for fatigue analysis [5.6-5.9].

More refined representations of strain induced softening, based for example on unified constitutive models, may be possible. The object of this study, however, was to examine the effects of softening on overall component equilibrium. In this regards the model presented here appears to be satisfactory for the purpose of simulation studies on more complex geometries, such as n-bar structures, tubes under thermal cycling, and beam sections in bending.

5.3 TIME DEPENDENT VARIABLE STRESS BEHAVIOR

5.3.1 Introduction

The constitutive model discussed in the previous section was developed by utilizing high strain rate cyclic test results. These test conditions minimized the effects of time dependent processes, such as creep. In this section the time dependent behavior of the material is discussed. The purpose of this work, as in the case of the cyclic material behavior, was not to develop refined constitutive models, but to develop a good understanding of the behavior of the material. In accomplishing this task results of steady load creep tests, described in [5.10], were used to predict the response of the material under stress relaxation conditions. Investigation of the effects of creep deformation on cyclic material behavior was also conducted. In this work isochronous creep curves were used to predict low frequency material response from high frequency test data. The predictions were then compared with actual test results.

5.3.2 Prediction of Stress Relaxation Test Results

In Chapter 3 results of stress relaxation tests were presented. These results provided an indication of the response of the material to variable stress conditions. Presently there are a variety of equation of state formulations which have the capability of modeling variable stress, time dependent, material behavior. Three of the most common methods, and those which will be discussed here, are the time hardening, strain hardening, and total strain formulations. These three models have been described in detail in the literature [5.11,5.12], and so a detailed discussion of the models themselves will not be presented here.

In [5.10] the Bailey-Norton law was used to model steady load creep behavior. This model stated that creep strain was related to stress and time by a power law relation. This relationship was given as

$$\varepsilon_c = k\,\sigma^n\,t^m \tag{5.14}$$

where, k, n, and m are material constants. (For convenience all nomenclature used in examining time dependent material behavior is contained in Table 5.2.)

From the Bailey-Norton law it is possible to derive the time hardening, strain hardening, and total strain formulations for modeling variable stress behavior. These derivations are straight forward and can easily be found in the open literature [5.11,5.12]. For this reason the mathematical development of the models will not be presented, but simply the final results. The time hardening, strain hardening and total creep formulations are

Time Hardening Model

$$\dot{\varepsilon}_c = k\, m\, \sigma^n\, t^{m-1} \tag{5.15a}$$

Strain Hardening Model

$$\dot{\varepsilon}_c = k^{1/m}\, m\, \sigma^{n/m}\, \varepsilon_c^{\left(\frac{m-1}{m}\right)} \tag{5.15b}$$

Total Strain Model

$$\varepsilon_c = k\, \sigma^n\, t^m \tag{5.15c}$$

It is pointed out that the time and strain hardening models are rate dependent relations, defining the creep behavior in terms of the creep strain rate ($\dot{\varepsilon}$). These models can be used to predict stress relaxation conditions by imposing compatibility requirements. In this case compatibility requires that the total strain remain constant.

$$\varepsilon = \text{constant} = \varepsilon_e + \varepsilon_p + \varepsilon_c \tag{5.16}$$

By taking the time derivative of this relation the additional requirement that the elastic and creep strain rates sum to zero is obtained.

$$\dot{\varepsilon} = 0 = \dot{\varepsilon}_e + \dot{\varepsilon}_c \qquad (\dot{\varepsilon} = 0) \qquad (5.17)$$

By application of the total strain and strain rate compatibility requirements the three variable stress relations were formulated to model stress relaxation conditions. These relaxation formulations are

Time Hardening Model of Relaxation Behavior

$$\sigma = [(n-1)\, k\, E\, t^m + \sigma_o^{1-n}]^{\frac{1}{n-1}} \qquad (5.18a)$$

where

σ_o = stress at time equal to zero

Strain Hardening Model of Relaxation Behavior

$$\Delta\sigma = -m\, E\, k^{1/m}\, \sigma^{n/m}\, ((\varepsilon-\varepsilon_p) - \frac{\sigma}{E}^{(\frac{m-1}{m})})\, \Delta t \qquad (5.18b)$$

where

$\Delta\sigma$ = stress increment

Δt = time increment

Total Strain Model of Relaxation Behavior

$$\sigma = E((\varepsilon - \varepsilon_p) - k\, \sigma^n\, t^m) \qquad (5.18c)$$

The resulting time hardening and total strain models provide closed form solutions relating stress to time. The strain hardening model, however, requires an incremental solution procedure. In addition, some assumption regarding the development of initial creep strains must be made in order to begin the solution procedure. In this analysis the Bailey-Norton law was used to calculate the amount of creep strain developed in the initial increment of time (δt). From this creep strain the stress drop, and therefore the absolute stress value, after the initial time increment could be determined. From this point on the model was used to calculate all future values of stress change ($\Delta\sigma$) and absolute stress (σ).

Predictions of relaxation behavior were made by using the primary and secondary creep constants of the Bailey-Norton law presented in [3.10]. Figures 5.8a and 5.8b show experimental and predicted stress relaxation results for an applied constant strain of 0.50%. Figure 5.8a shows that the primary creep constants provide good predictions of actual material response. The time hardening formulation in particular gave very good predictions, especially at times in excess of several hours.
Predictions using the secondary creep constants, shown in Fig. 5.8b, yielded results which consistently under predicted the amount of stress relaxation. This was true of each of the three models.

5.3.3 Effects of Creep Deformation on Cyclic Behavior

High frequency cycling has been shown to cause a significant reduction in the strength of this material. This strength reduction has been related to an accumulation of time independent plasticity. For elevated temperature use of this material it is important to determine the relationship between the development of time independent and time dependent plasticity, and the effects of this deformation on the strength of the material.

As a first approximation it was assumed that strength loss had an insignificant effect on the creep resistance of the material. If this hypothesis were true it should be possible to predict decreases in strength due to time dependent effects by treating creep deformation as a perturbation on time independent behavior. Figure 5.9a contains plots of the positive stress, tension-going portions of two hysteresis loops taken from fully reversed strain control cyclic tests. In each test a 0.50% total strain range

was used and the same cycle number (N=2) was selected for plotting. The first curve, however, was taken from a test conducted at a relatively high strain rate (4.0×10^{-3}/s), whereas the second curve was taken from a relatively low strain rate (1.4×10^{-5}/s) test. In this plot isochronous creep curves were used to represent creep strain as a time dependent perturbation on time independent behavior. Prediction of the low frequency time dependent stress-strain behavior was obtained by connecting points on the isochronous curves which corresponded to the amount of strain developed at the low frequency strain rate. This figure shows that the reduction in strength due to time dependent effects has been over estimated. This result is not surprising since in using the isochronous creep curves the predicted amount of creep deformation at any given stress level assumes that stress level to be maintained over the entire duration of the cycle.

Figure 5.9b shows stress-strain plots from the same tests used for the plots in Fig. 5.9a. In this case hysteresis curves were taken after a considerable number of cycles were accumulated. If the reduction in strength due to cyclic and creep deformation do in fact act independently it should again be possible to predict, with reasonable accuracy, the results of low frequency tests by adding creep deformations to the high strain rate test results. This figure clearly indicates that cyclic softening causes a reduction in the creep strength of this material. Figures 5.10a and 5.10b show plots similar to those presented in Figs, 5.9a and 5.9b, but for a 1.0% strain range cyclic test. These plots also lead to the conclusion that cyclic softening results in a degradation of the creep properties of this material. Early in the test, when essentially no cyclic softening had occurred, use of the isochronous curves to modify the time independent material behavior provided reasonable predictions of the low strain rate test results (see Fig. 5.10a). After a significant number of cycles had been accumulated, however, the method provided very poor predictions of time dependent behavior.

One possible means of relating reduction in creep resistance to decrease in strength is to assume that creep deformation is dependent upon the ratio of the applied stress to the current yield strength. From this assumption the Bailey-Norton creep law (Eq. (5.14)) becomes

$$\varepsilon_c = k \sigma_{y1}^{s} \left(\frac{\sigma}{\sigma_{yN}}\right)^{n} t^{m} \tag{5.19}$$

where

σ_{y_1} = initial strength

σ_{y_N} = yield strength at cycle number N

This modification has the effect of increasing the amount of predicted creep strain at a given stress level. This increase is equal to the ratio of the initial to final yield strengths raised to the power n, the stress exponent in the Bailey-Norton law. (In the current analysis the material yield strength was taken as the maximum stress level in the cycle.) This decrease in creep strength causes a shift in the isochronous creep curves shown in Figs. 5.9b and 5.10b. This resulted in a corresponding shift of the predicted time dependent stress-strain curve. These new time dependent curves, though still conservative, provided improved predictions of the time dependent behavior of the material. (For clarity sake the modified isochronous creep curves were not included in Figs. 5.9b and 5.10b.)

From this analysis cyclic softening has been shown to cause a reduction in creep resistance of this material. It appears as though this reduction can be related to a decrease in the yield strength of the material. At this point there is little to be gained from further refinement of the current model. For a more rigorous analysis secondary effects, such as differences in accumulated plastic strain between test cases and the method used for predicting creep strain under variable stress conditions, should be considered.

5.4 CONCLUSIONS

To investigate the effects of a material's behavior on component response it is necessary to have some means of characterizing the behavior of the material. In this study the purpose of this representation was to capture the essential characteristics of material softening.

A time independent uniaxial constitutive model representing strain induced cyclic softening was developed. This model assumed that softening was a function of accumulated plastic strain. Using this model good predictions were made of both overall strength loss (softening) and hysteresis behavior under controlled strain range conditions.

The time dependent behavior of the material was investigated by examining its response under stress relaxation conditions. This work showed that material behavior was predicted quite well by using primary creep constants derived under steady load creep conditions. Using these material constants the strain hardening creep formulation provided good predictions of material behavior in the first hour of the relaxation period. The time hardening formulation provided the best predictive capabilities at times in excess of several hours.

The response of this material to time dependent cyclic behavior was investigated by treating creep deformation as a time dependent perturbation on time independent behavior. These studies showed that cyclic softening reduces the creep resistance of this material. By assuming that the creep resistance was governed by the ratio of the applied stress level to the current yield strength reasonable first-order predictions of cyclic time dependent material behavior were made.

5.5 REFERENCES

5.1 Pejsa, P. N., "Elevated Temperature Low-Cycle Fatigue of Two Bainitic 2.25 Cr - 1 Mo Steels," M.S. Thesis, University of Illinois at Urbana-Champaign, Urbana, IL, 1983.

5.2 Ramberg, W., and W. R. Osgood, "Description of Stress-Strain Curves by Three Parameters," NACA Technical Note No. 902, July, 1943.

5.3. Handrock, J. L., and D. L. Marriott, "Cyclic Softening Effects on Creep Resistance of Bainitic Low Alloy Steel Plain and Notched Bars," Properties of High-Strength Steels for High-Pressure Containments (ed., Nisbett, E. G.), MPC-27, American Society of Mechanical Engineers, NY, 1986, pp. 93-102.

5.4. Kschinka, B. A., "Creep-Fatigue-Environment Interaction in Bainitic 2.25 Cr 1 Mo Steel," M.S. Thesis, University of Illinois at Urbana-Champaign, IL, 1986.

5.5. Cescotto, S., F. Leckie, and E. Abrahamson, "Unified Constitutive Models for Creep and Plasticity of Metals at High Temperature," University of Illinois at Urbana-Champaign, IL, 1982.

5.6 Socie, D. F., M. R. Mitchell, and E. M. Caulfield, Fundamentals of Modern Fatigue Analysis, Fracture Control Program Report No. 26, University of Illinois at Urbana-Champaign, IL, 1978.

5.7 Bannantine, J. A., J. J. Comer, and J. L. Handrock, Fundamentals of Metal Fatigue Analysis, Mechanical and Industrial Engineering Department, University of Illinois at Urbana-Champaign, IL, 1987.

5.8 Matsuishi, M., and T. Endo, "Fatigue of Metals Subjected to Varying Stress," paper presented to Japan Society of Mechanical Engineers, Fukuoka, Japan, 1968.

5.9 Annual Book of ASTM Standards, Section 3 - Metals Test Methods and Analytical Procedures, Vol. 03.01-Metals-Mechanical Testing; Elevated and Low-Temperature Tests, PA, 1986, pp. 836-848.

5.10 Handrock, J. L., "The Effects of Strain Induced Softening on the Load Carrying Capacity of Components," Ph.D. Thesis, University of Illinois at Urbana-Champaign, Urbana, IL, 1988.

5.11 Kraus, H., Creep Analysis, John Wiley and Sons, NY, 1980.

5.12 Penny, R. K., and D. L. Marriott, Design for Creep, McGraw-Hill, London, 1971.

Table 5.1 Time independent constitutive model nomenclature.

C	Hysteresis loop strength coefficient
C_o	Cutoff value of C for small values of accumulated plastic strain
E	Young's modulus
h	Strength coefficient material constant
log	Common logarithm (base 10)
m	Hysteresis loop strain hardening exponent
n	Strength exponent material constant
N	Cycle number
$\Delta\varepsilon$	Absolute total strain range
$\Delta\varepsilon^*$	Relative total strain range
$\Delta\varepsilon_e$	Absolute elastic strain range
$\Delta\varepsilon_e^*$	Relative elastic strain range
$\Delta\varepsilon_p$	Absolute plastic strain range
$\Delta\varepsilon_p^*$	Relative plastic strain range
$\Delta\sigma$	Absolute stress range
$\Delta\sigma^*$	Relative stress range
$\Sigma\Delta\varepsilon_p$	Accumulated plastic strain
$S(\lvert\Delta\varepsilon_{eff}\rvert)$	Accumulated Mises plastic strain

Material constant values used in analysis.

C_o = 1068 MPa

E = 159 GPa

h = 843 MPa

m = 0.0905

n = -0.0661

3039tables, 3

Table 5.2 Time dependent material behavior nomenclature.

E	Young's modulus
k	Bailey-Norton creep law coefficient
k_1	Bailey-Norton law primary creep coefficient
k_2	Bailey-Norton law secondary creep coefficient
m	Bailey-Norton creep law time exponent
m_1	Bailey-Norton law primary creep time exponent
n	Bailey-Norton creep law stress exponent
n_1	Bailey-Norton law primary creep stress exponent
n_2	Bailey-Norton law secondary creep stress exponent
N	Cycle number
t	Time
$\Delta\sigma$	Stress increment
$\Delta\tau$	Time increment
ε	Total strain
$\dot{\varepsilon}$	Total strain rate
ε_c	Time dependent plastic (creep) strain
$\dot{\varepsilon}_c$	Time dependent plastic (creep) strain rate
ε_e	Elastic strain (σ/E)
$\dot{\varepsilon}_e$	Elastic strain rate
ε_p	Time independent plastic strain
σ	Stress
σo	Stress at time equals zero
σy	Yield strength
σ_{y_1}	Initial yield strength
σ_{y_N}	Yield strength at cycle number N

Material constant values used in analysis.

E	= 159 GPa	m_1 = 0.524
k_1	= 4.67×10^{-11} σ(MPa)	n_1 = 4.12
	= 1.34×10^{-7} σ(ksi)	n_2 = 8.77
k_2	= 2.26×10^{-22} σ(MPa)	
	= 5.14×10^{-15} σ(ksi)	

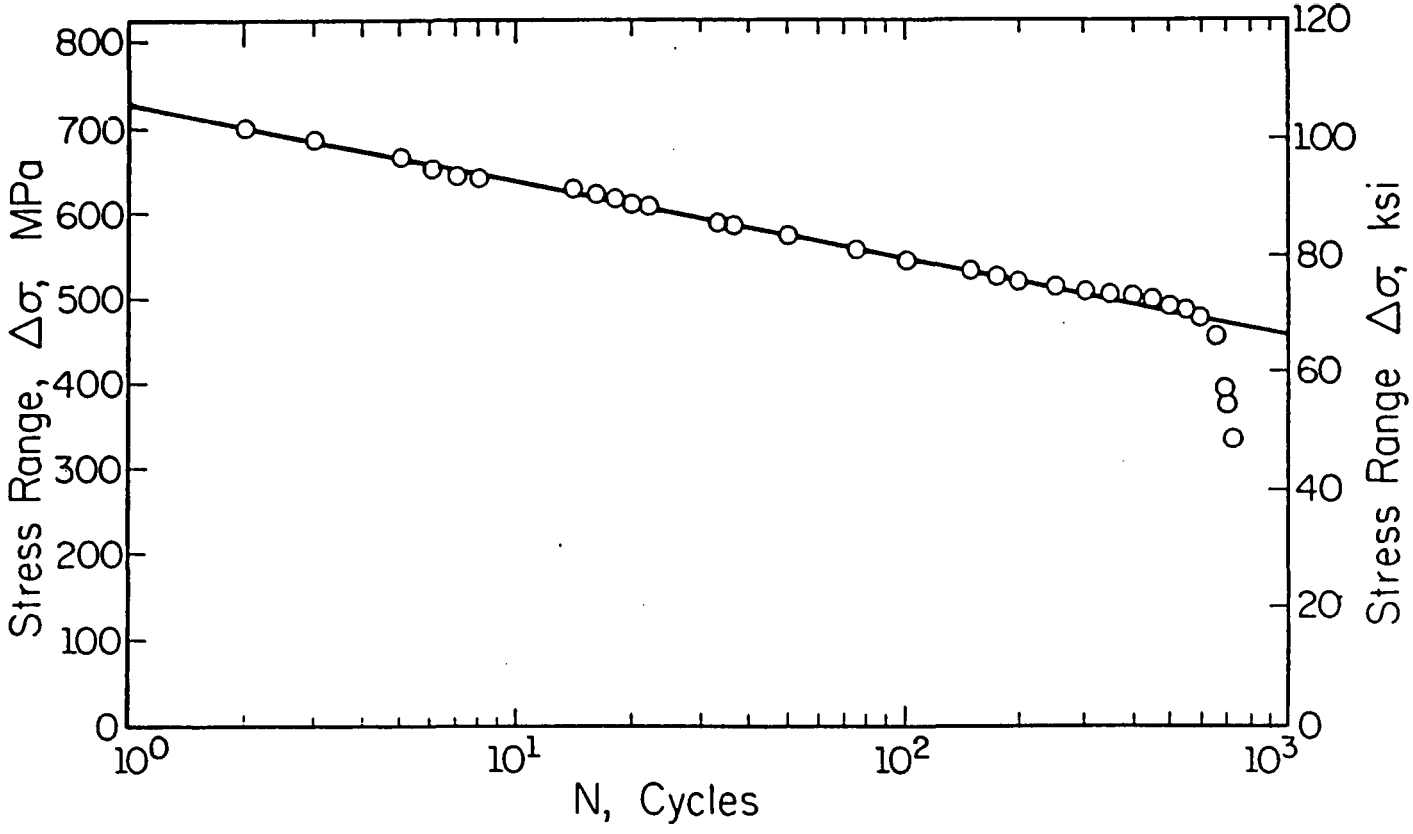

Figure 5.1 Stress range versus number of cycles for a fully reversed 1.0% strain range cyclic test

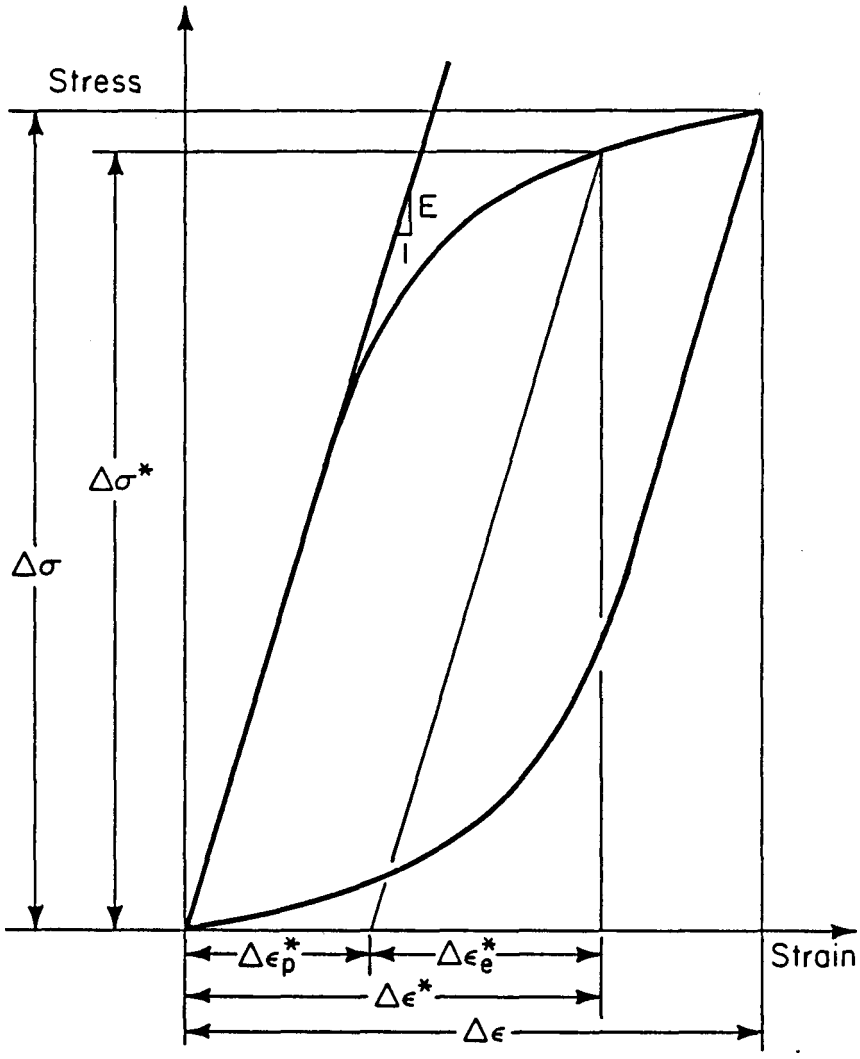

Figure 5.2 Definition of stress and strain ranges for a typical hysteresis loop.

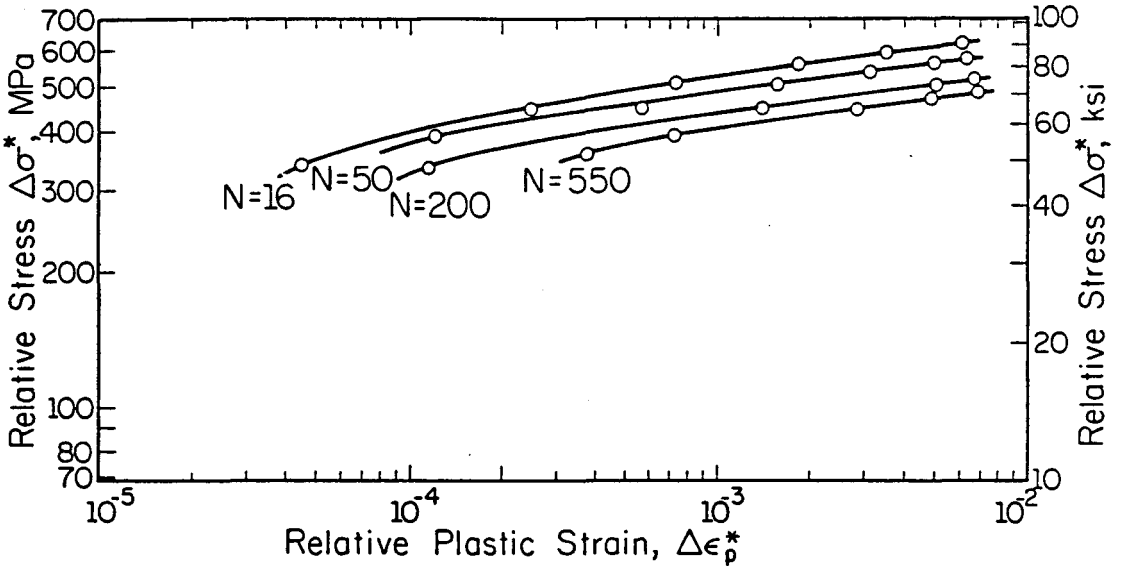

Figure 5.3 Relative stress ($\Delta\sigma^*$) versus relative plastic strain ($\Delta\varepsilon_p^*$) for a few representative cycles of a 1.0% strain range cyclic test.

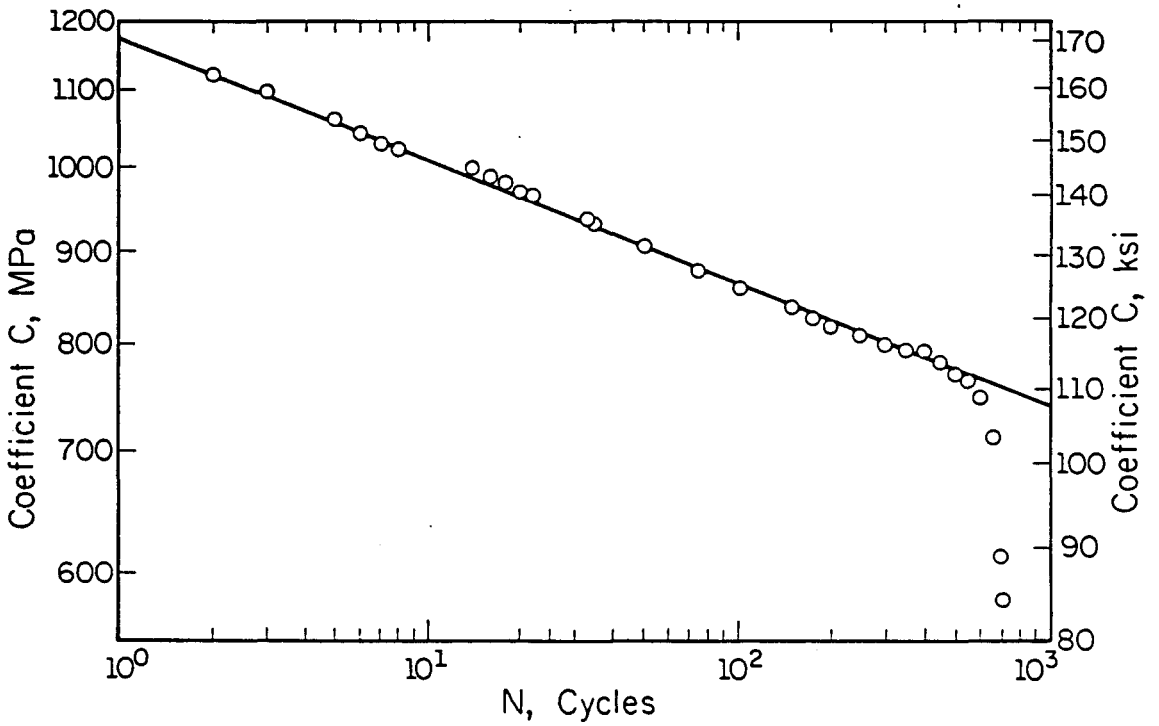

Figure 5.4 Coefficient C versus number of cycles for a 1.0% strain range cyclic test.

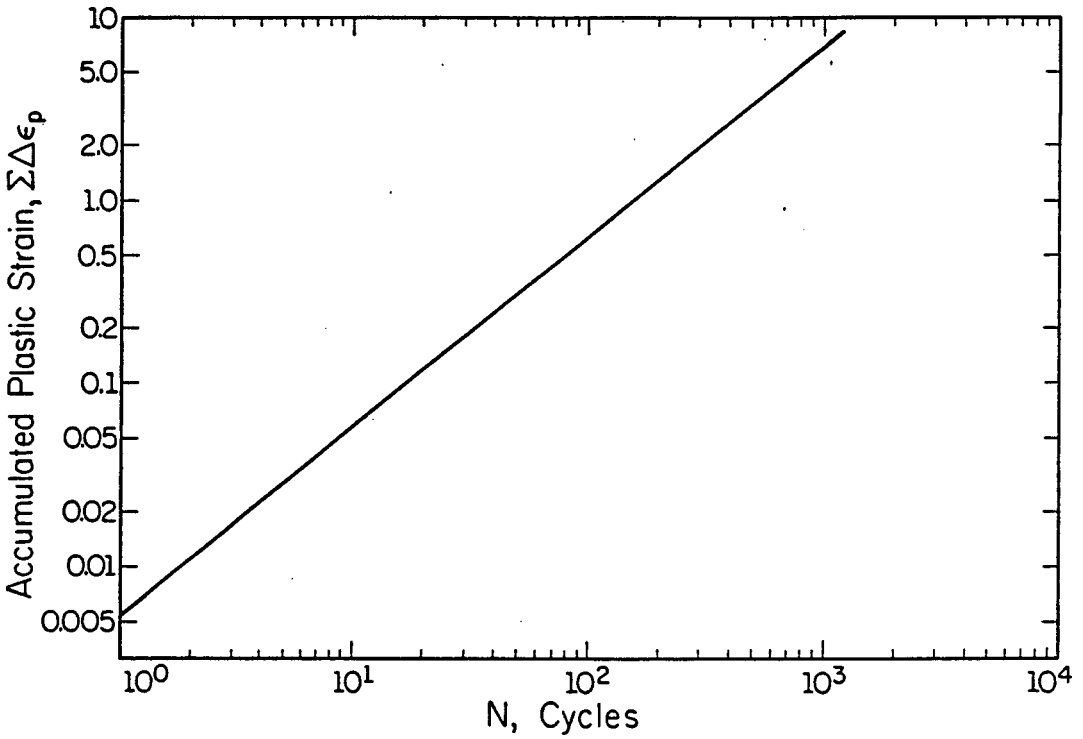

Figure 5.5 Accumulated plastic strain versus number of cycles for a 1.0% strain range cyclic test

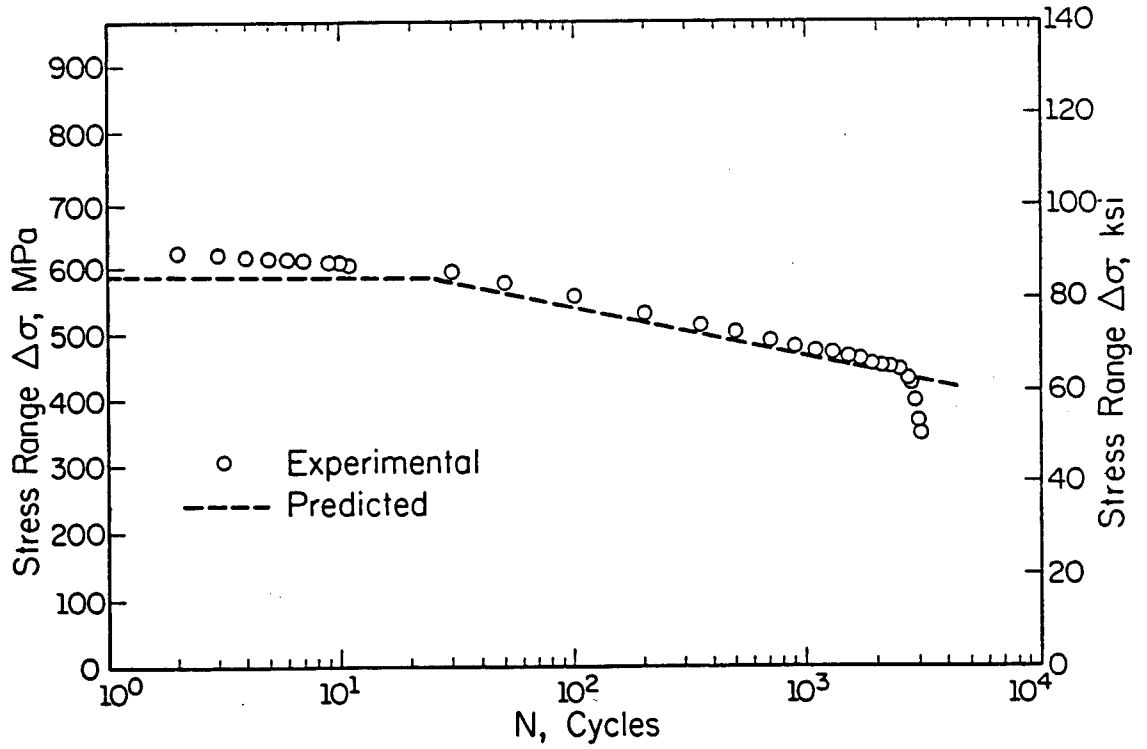

Figure 5.6 Experimental and predicted results of stress range versus number of cycles for a 0.5% strain range cyclic test.

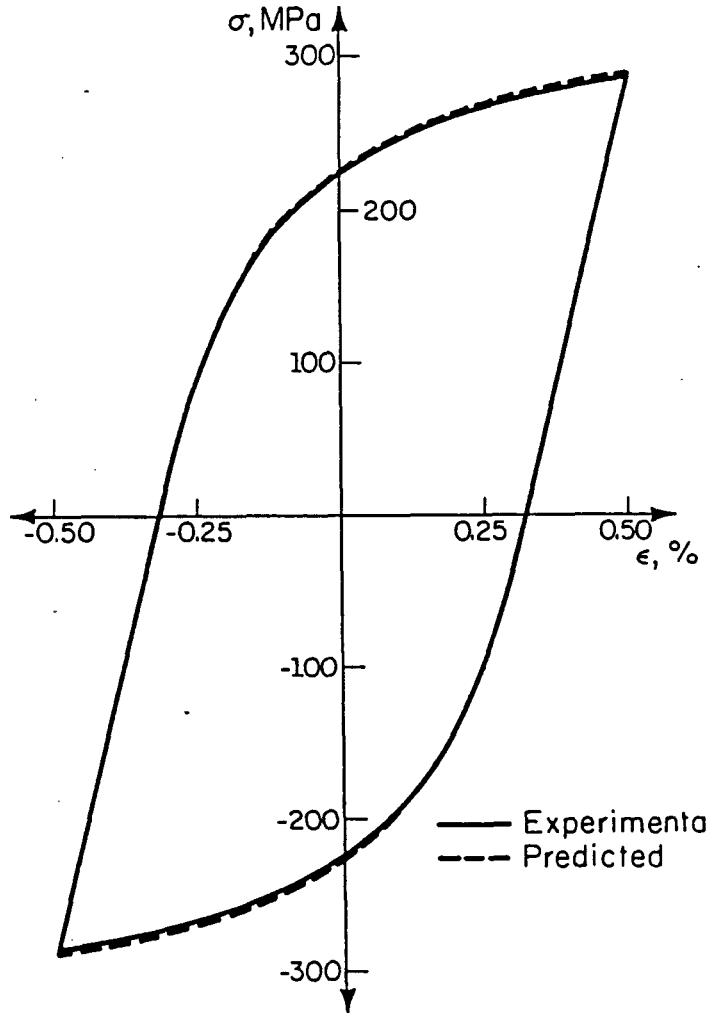

Figure 5.7a Experimental versus predicted hysteresis loops at cycle No. 50 for a 1.0% strain range cyclic test.

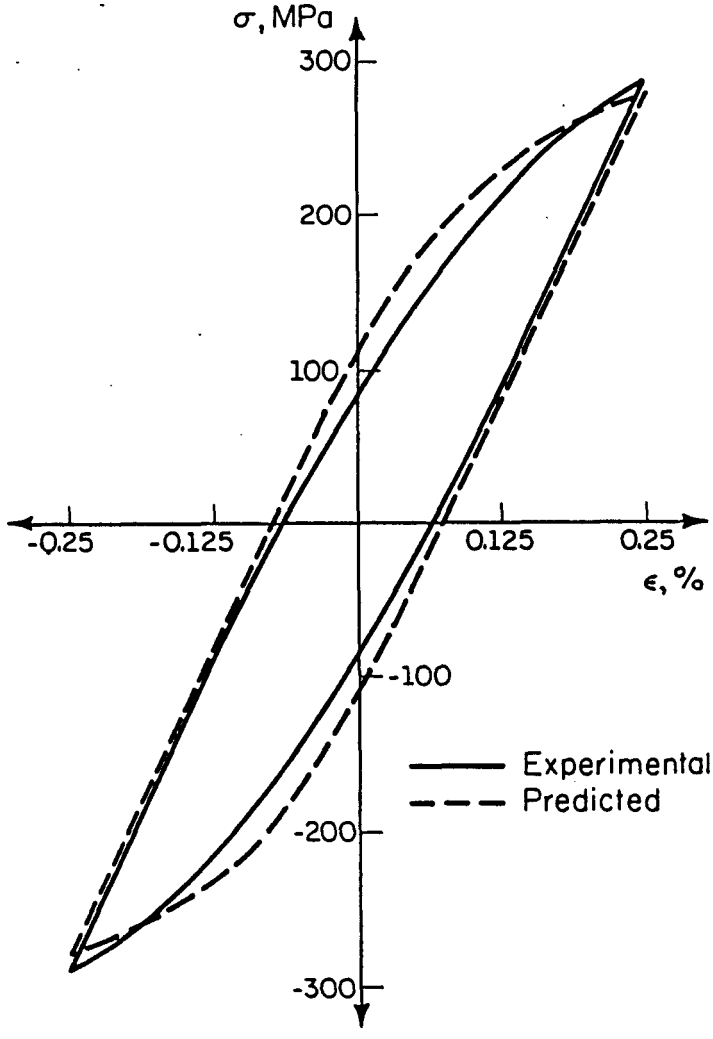

Figure 5.7b Experimental versus predicted hysteresis loops at cycle No. 50 for a 0.5% strain range cyclic test.

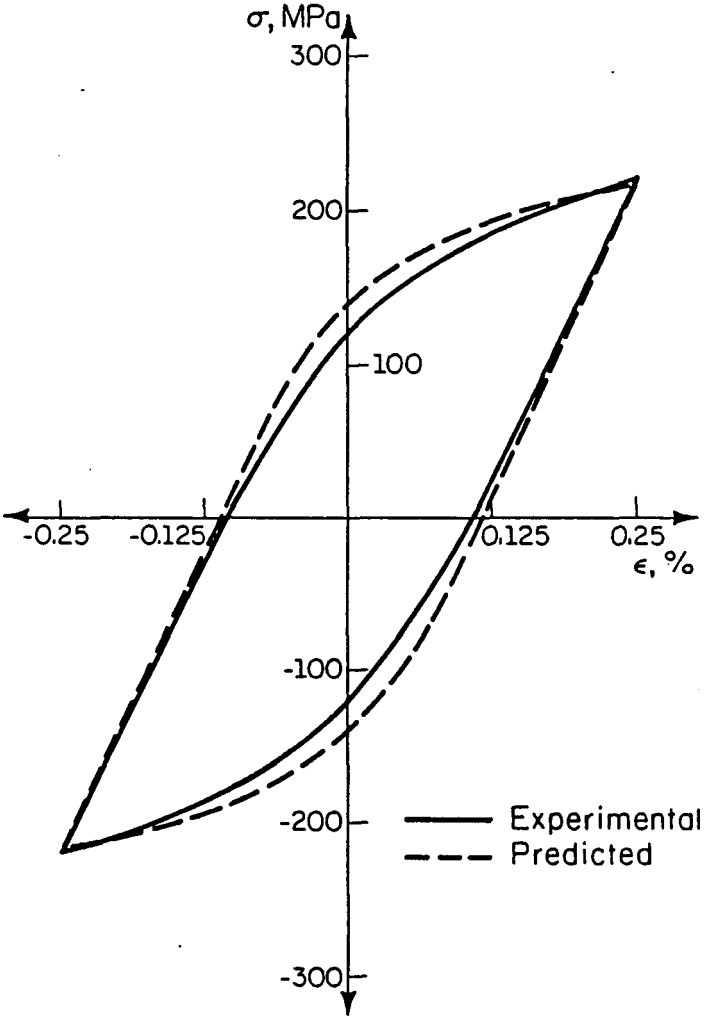

Figure 5.7c Experimental versus predicted hysteresis loops at cycle No. 2500 for a 0.5% strain range cyclic test.

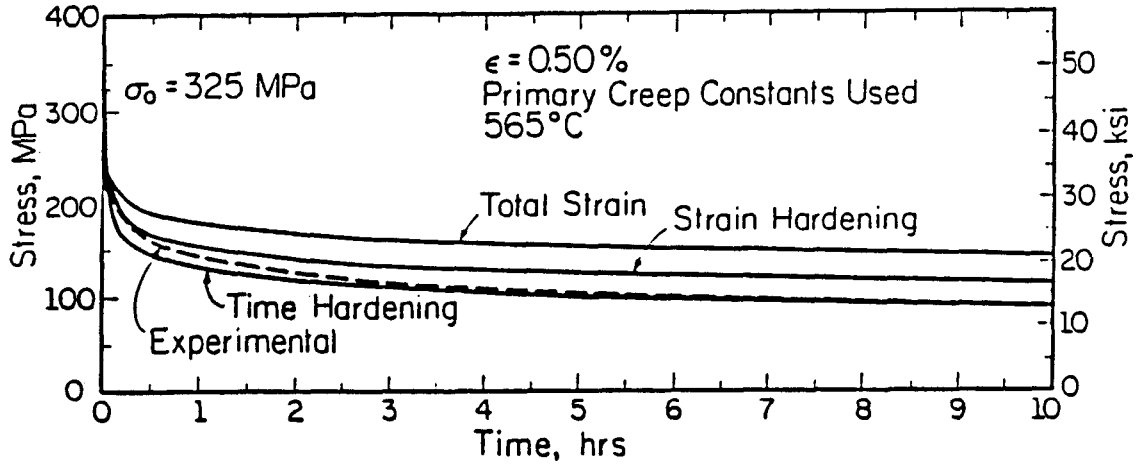

Figure 5.8a Predicted results of stress relaxation behavior using primary creep constants

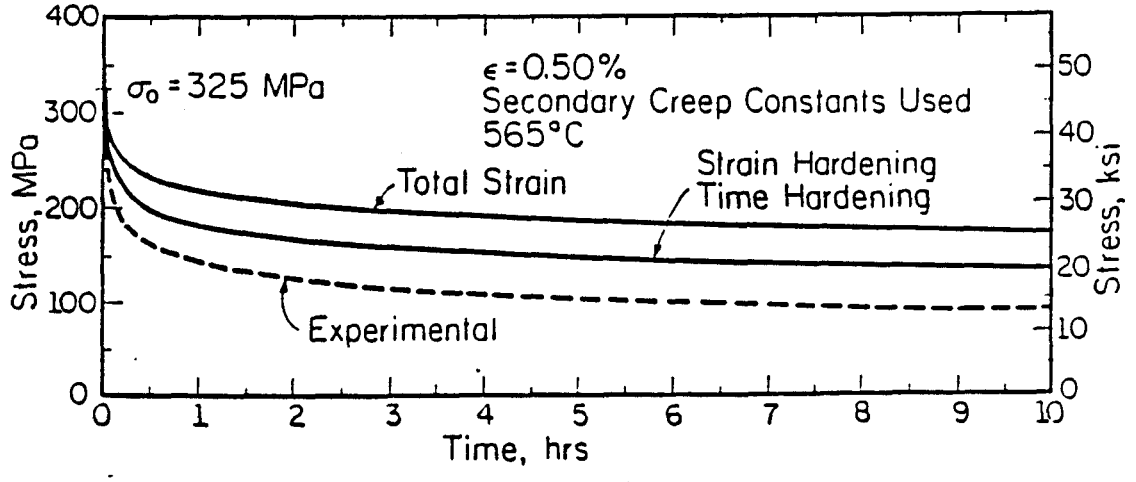

Figure 5.8b Predicted results of stress relaxation behavior using secondary creep constants.

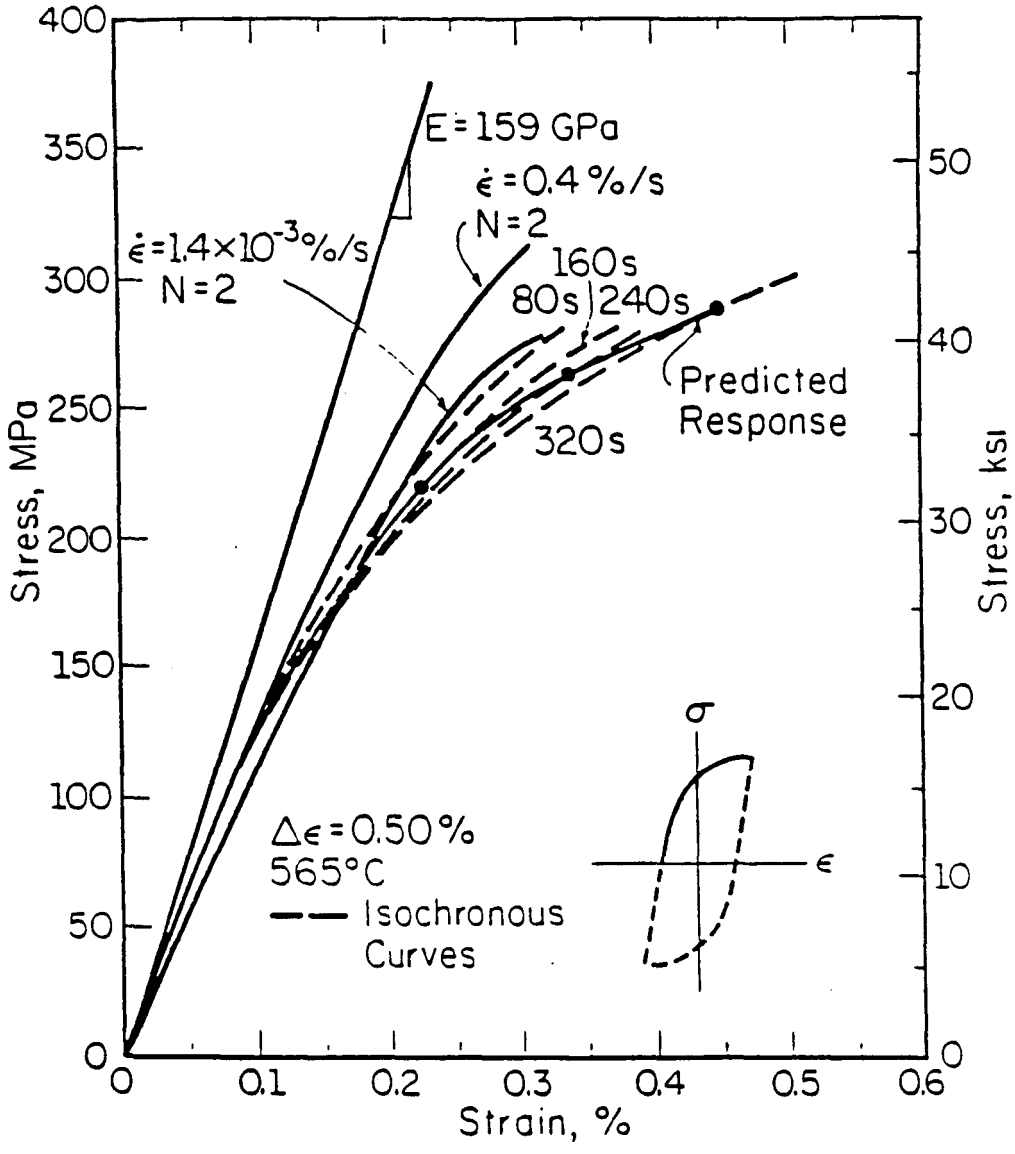

Figure 5.9a Experimental and predicted time dependent material behavior ($\Delta\varepsilon$ = 0.5%, N = 2)

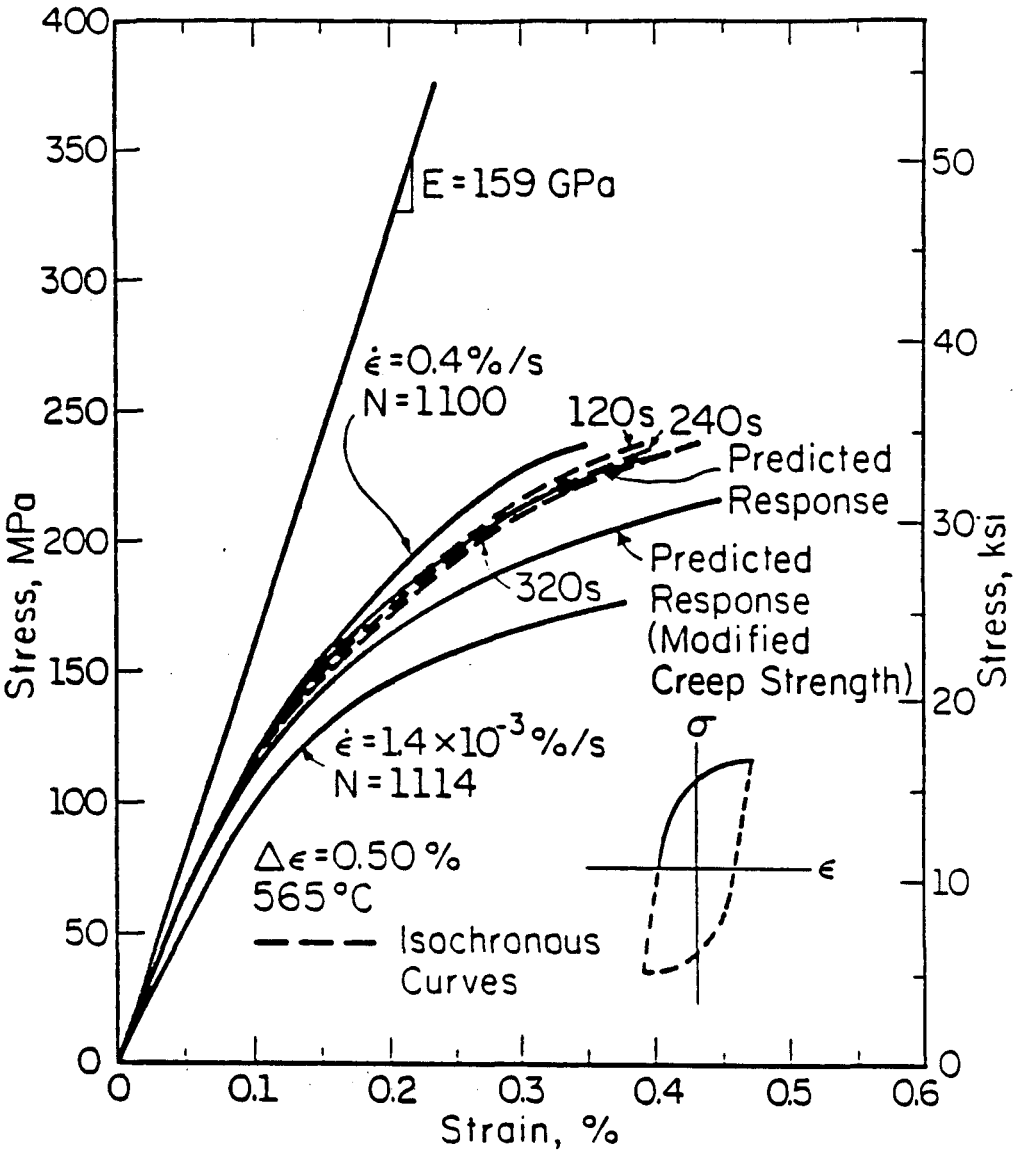

Figure 5.9b Experimental and predicted time dependent material behavior ($\Delta\varepsilon$ = 0.5%, N = 1100/1114).

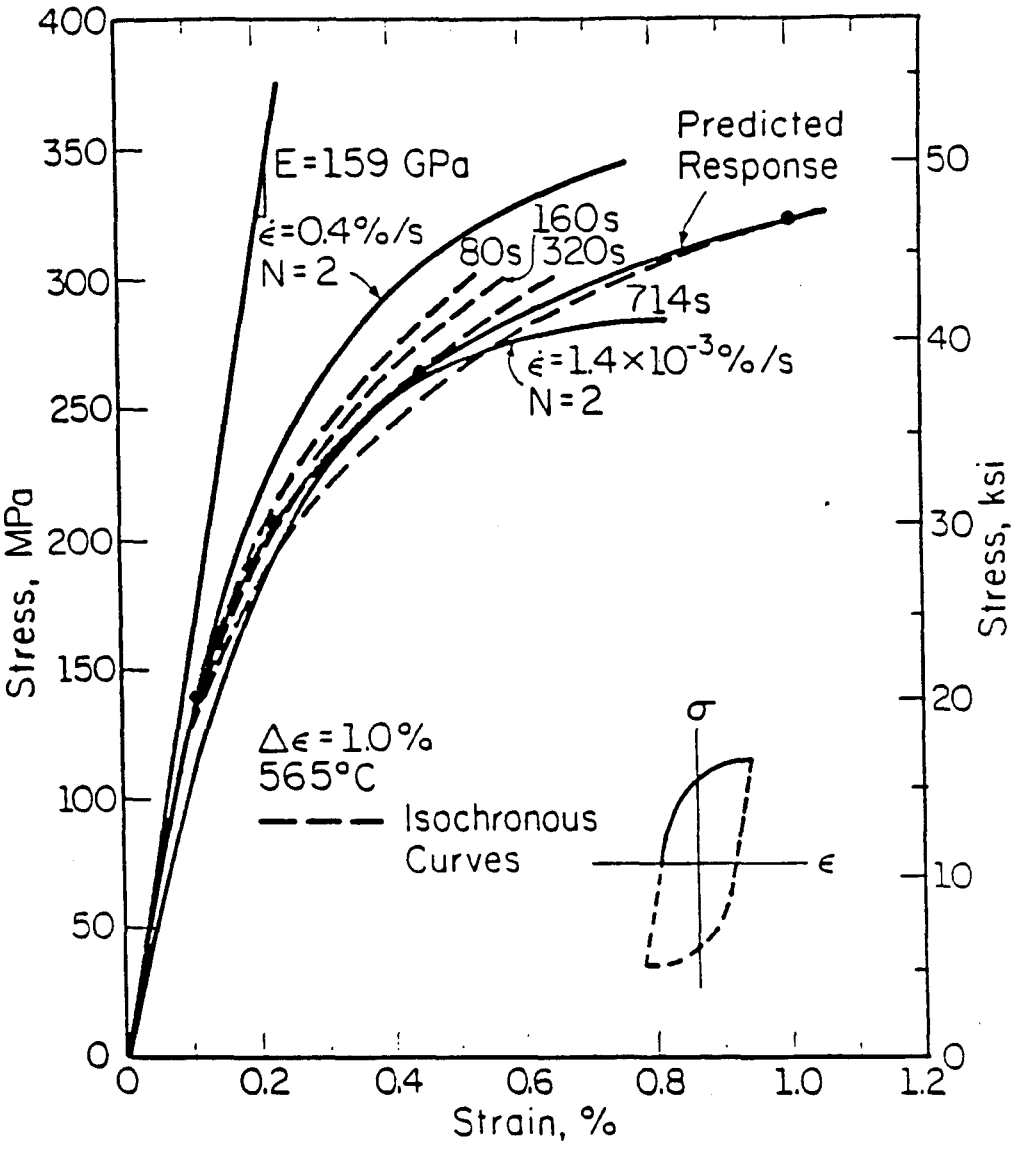

Figure 5.10a Experimental and predicted time dependent material behavior ($\Delta\varepsilon$ = 1.0%, N = 2).

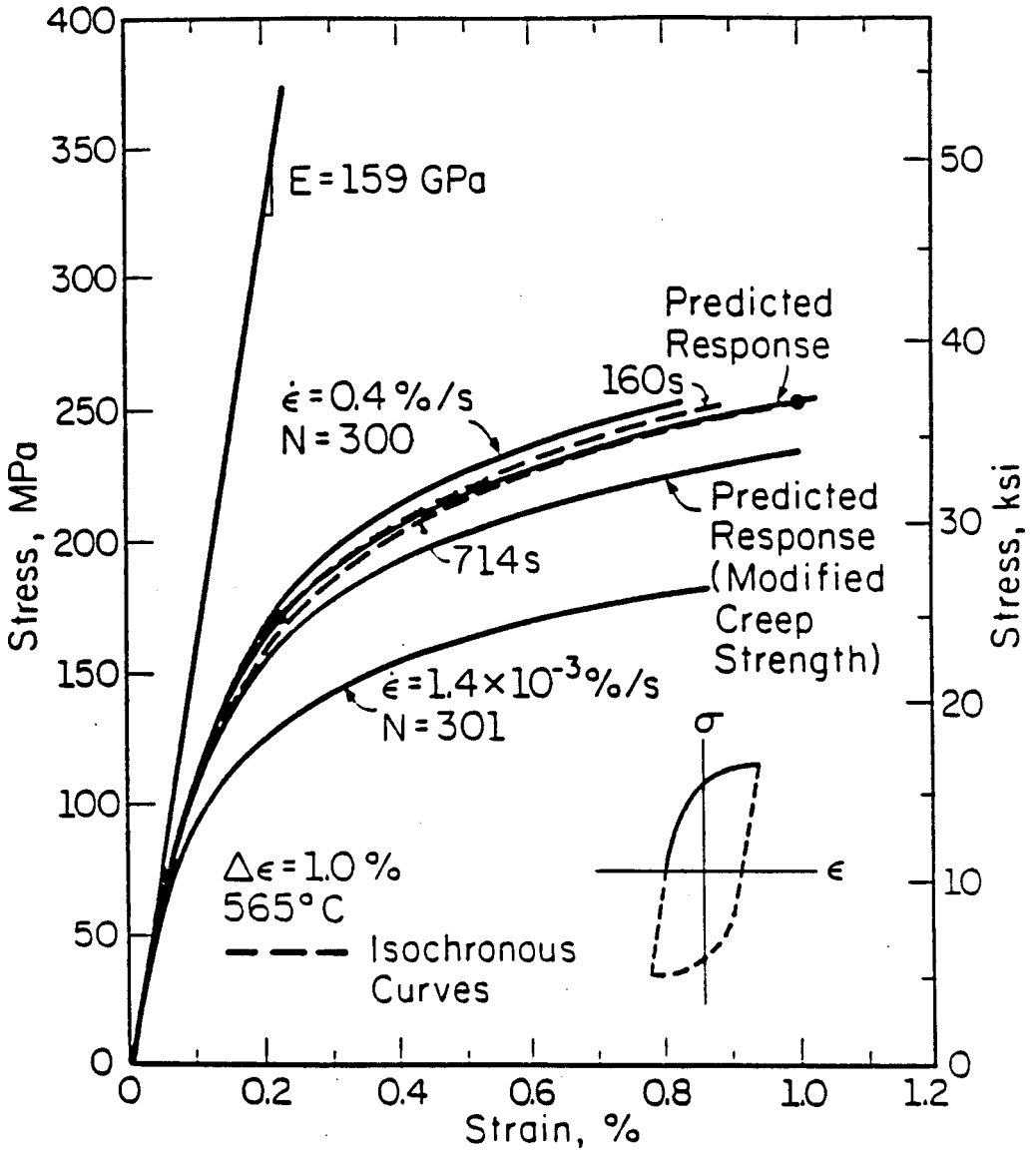

Figure 5.10b Experimental and predicted time dependent material behavior ($\Delta\varepsilon$ = 1.0%, N = 300/301).

6. FINITE ELEMENT ANALYSIS OF BRIDGMAN NOTCHED SPECIMEN

6.1 INTRODUCTION

In this chapter an analysis performed on the Bridgman notched specimen configuration using the finite element code ANSYS [6.1-6.7] is presented. The purpose of this analysis was to investigate the progression of softening in an actual component under the application of repeated load cycles and then determine the effects of this softening on the load carrying capability of the component. The Bridgman notch geometry was chosen for two reasons. Firstly, this geometry was employed in the experimental test programs discussed in [5.10]. Actual test results are therefore available for comparison to the predictions derived from this analytical work. Secondly, this geometry is fairly representative of structures which are likely to be found in service. The notch configuration produces a stress gradient in the specimen which is similar to that found at areas such as flanges and nozzles in piping systems.

The completion of finite element analyses on components composed of cyclic softening material subjected to repeated load reversals is difficult at best. The application of cyclic loads in a finite element analysis itself can lead to enormous run times, especially if one requires results reaching into the thousands or tens of thousands of cycles. In the current case the difficulty is even greater since the material response is continually changing. Most finite element programs are very inefficient when dealing with such conditions. Not only do run times become unacceptable but a large degree of user interaction is necessary to implement the desired changes in material behavior. For these reasons in the current analysis isocyclic cyclic stress-strain curves were used in an attempt to capture the cyclic characteristics of this material. By this means a series of static analyses were used to approximate the cyclic response of the structure. These isocyclic cyclic stress-strain curves were developed for six cyclic cases, ranging from the virgin material response to the material's response after 5000 cycles. This particular range of cycle values was chosen since it allows a direct comparison of experimental test results. The effect of softening on the structure at a given stress level was then investigated by examining the series of static results obtained at that stress level.

In addition to the softening phenomenon creep and fatigue mechanisms are also present in the high temperature operation of this material. For this evaluation high frequency material response data has been used. This was done in order to eliminate time dependent processes, such as creep, to allow a more unobstructed evaluation of the softening phenomenon. It is still necessary though to consider the fatigue behavior of the material. This was accomplished by the modification of the material cyclic stress-strain curves in such a manner that the strength of the material dropped to zero when the fatigue life was reached.

6.2 DEVELOPMENT AND EXECUTION OF FINITE ELEMENT PROGRAM

6.2.1 Modeling of Test Specimen Geometry

The finite element program used in this investigation was developed from a program written by Kloos [6.8,6.9] to investigate a geometrically similar structure. The finite element mesh developed is given in Fig. 6.1. The mesh itself was comprised of 148 nodes and 122 elements. The elements used were 4 noded, two-dimensional isoparametric solid elements (STIF42) having plasticity capabilities. Due to symmetry it was only necessary to model one quarter of the structure. The remainder of the structure was defined by choosing the axisymmetric option of the STIF42 element and prescribing the appropriate boundary conditions. These boundary conditions specified that no nodal displacements were allowed in the radial (x) direction along the axial (y) axis or in the axial (y) direction along the radial (x) axis. Loading was applied to the model in the form of a negative uniform pressure acting over the top surface of elements 118 to 122.

6.2.2 Material Characterization

The material data used for this evaluation was taken from smooth specimen, strain-control, fully reversed fatigue tests performed by Pejsa [6.10] and Kschinka [6.11,6.12]. These tests were performed at a strain rate of 0.4%/sec for total strain ranges of 0.30, 0.40, 0.50, 0.67, and 1.00%. The tests were conducted at a temperature of 565•C in an air environment. This particular set of test data was chosen for several reasons. Firstly, the strain ranges over which these tests have been completed are typical of the

strains which occur in the Bridgman specimen operating in the low cycle fatigue regime. Since test data for the Bridgman specimen tested under these conditions currently exists this reduces the amount of extrapolation required in comparing the results of the current analysis to actual test data. The second reason for choosing this particular data set is due to the strain rate at which the tests were performed. Since these tests were conducted at a relatively high strain rate the effects of time dependent processes should be minimal. This essentially eliminates creep effects, reducing the problem to one of examining softening and fatigue behavior alone.

From the raw data of Pejsa's and Kschinka's tests one is able to plot stress range as a function of log cycles. Such a plot is shown in Figs. 6.2a and 6.2b. From these figures one can construct isocyclic cyclic stress-strain curves by determining the stress range as a function of strain range at a given number of cycles. For example, at cycle number 1000 the stress range changes from 433 to 484 to 476 to 463 MPa as the total strain range changes from 0.30 to 0.40 to 0.50 to 0.67%. At 1.00% total strain range the specimen failed before reaching 1000 cycles. The cyclic stress-strain curves constructed by this method are shown in Fig. 6.3. Also shown in this figure is a monotonic stress-strain curve for this material [6.12].

It should be pointed out that the total stress and strain ranges indicated in Figs. 6.2a and 6.2b are actually representations of cyclic hysteresis behavior. Under the specified test conditions this material shows a high degree of symmetry in cyclic hysteresis response [15]. As a result the cyclic stress-strain values can be obtained by simply halving the total stress and strain range values. This accounts for the factor of two difference in stress and strain values found between Figs. 6.2 and 6.3.

From Fig. 6.3 one observes a significant amount of cyclic softening. For example, at 0.5% strain the cyclic strength of the material drops from the initial monotonic strength by 20 percent in the first 50 cycles of loading and by 32 percent in the first 500 cycles of loading. In addition to an overall reduction in cyclic strength these curves show that conditions can result in which the cyclic strength of the material decreases as straining increases. This behavior can result in localized instability, causing sudden structural collapse.

Using ANSYS, monotonic nonlinear material behavior can be modeled as either piece-wise linear or bilinear [6.1]. In this investigation the piece-wise linear material representation was used. Using this

method the individual segments of a stress-strain curve are defined by the specification of up to five sets of stress-strain values. During an analysis if a strain value is required which is greater than the largest strain specified the values associated with the largest strain are used. Figure 6.4 shows the piece-wise linear representations of the material cyclic stress-strain curves used in this study (shown by solid lines).

As discussed earlier, high strain rate material data was used in this evaluation in order to minimize the effects of time dependent processes, namely creep. It was still necessary though to include the effects of fatigue. To accomplish this the cyclic stress-strain curves were modified to include failure by fatigue. From strain life data one can determine the total strain range necessary to cause failure in a given number of cycles. (See Fig. 4.5.) This information was incorporated into the cyclic stress-strain behavior by requiring the stress level to drop to zero when the strain reached that value necessary to cause failure by fatigue. This modification to the cyclic stress-strain curves is indicated by the vertical dashed lines in Fig. 6.4. Due to the limitation of defining material stress-strain curves by no more than five segments slight redefinition of the material curves at strains prior to the onset of fatigue failure was necessary. These redefined portions of the material curves are also indicated by dashed lines in Fig. 6.4.

6.2.3 Applied Loading

Loading of the finite element model was specified in the form of an external negative pressure applied to the top surface of element numbers 118 to 122. This loading is the equivalent of a tensile stress applied to the end of the structure. This gross section stress (σ_g) was increased incrementally in 88 load steps to a maximum value of 137 MPa (19.8 ksi). By prescribing a large number of load steps, and decreasing the size of the load steps as the load level, and therefore the amount of plasticity, increased, the number of iterations required to converge to a solution during any given load step was kept relatively small (e.g., typically less than about 6 or 7). Furthermore, the number and size of the loads steps chosen allowed the same loading routine to be used for each of the material behavior characterizations.

The first load step applied a gross section stress of 37.2 MPa (5.4 ksi) to the component. At this load level the net section stress (σ_{nom}) was 104 MPa (15.1 ksi), resulting in completely elastic loading for each of the stress-strain curves. The load was then increased incrementally to a maximum of 137 MPa

(19.8 ksi) gross section stress (382 MPa (55.2 ksi) net section stress). This value was chosen since it causes plastic collapse of the structure for material curves N = 500, 1000, and 5000 cycles. In addition, it causes significant amounts of plasticity for material curves N = 50 and 100 cycles.

6.2.4 Execution of Finite Element Program

A listing of the completed ANSYS finite element program developed for this investigation is contained in Appendix B. As shown, the nonlinear material property data for the six softening cyclic stress-strain curves and for the three softening cyclic stress-strain curves modified for fatigue behavior are included in the program. This information is all prefixed by comment statements. When an analysis run was to be made the comment statements preceding the particular test case desired were removed. One notes that the program is currently configured to perform an analysis for the softening N = 1000 cycles test case. The nonlinear material property data was incorporated into the program in this manner in order to minimize the amount of editing necessary to perform the individual analyses, thereby reducing the likelihood of making on error in modifying the program. It also makes the program, and all the required material property data, completely self-contained, providing further convenience in completing the analyses. Once again, this was made possible since the load step input was defined such that the same loading routine could be used for all test cases.

The execution of this program was completed on the HP9000 computer system located in the Mechanical Engineering Building at the University of Illinois. Typical run times varied from just under two hours (requiring 59 iterations) for the N = 5000 cycles modified for fatigue behavior case to just over eight hours (requiring 416 iterations) for the N = 100 cycle case.

In solving plasticity problems, ANSYS utilizes the initial stress approach [6.1]. In this method a reference elastic material stiffness is defined which is used to form a constant triangularized stiffness matrix. This matrix is then used through an iterative procedure in conjunction with a changing load vector. In determining solution convergence a plasticity convergence criterion of 0.01 was used. This criterion determines that convergence of a load step has been achieved when the ratio of plastic strain increment to total elastic strain (termed plasticity ratio) is less than 0.01 for every element in the structure. In the

current analysis a maximum of 15 iterations were allowed before it was assumed that convergence could not be met and the test ended. For more detailed information regarding the solution procedure utilized by ANSYS in performing plasticity analyses one is referred to Ref. [6.5].

6.3 DISCUSSION OF RESULTS

Nine finite element analysis runs were completed in this study using the isocyclic cyclic stress-strain curves discussed in Section 6.2.2. In order to keep the amount of solution printout from these runs to a manageable size detailed output results were limited to element stress solutions at a number of carefully selected load levels. These load levels included gross section stress (σ_g) levels of 37.2, 62.1, 87.6, 105, 123, and 137 MPa (5.4, 9.0, 12.7, 15.2, 17.8, and 19.8 ksi, respectively). These corresponded to net section stress (σ_{nom}) levels of 104, 174, 245, 293, 344, and 382 MPa (15.1, 25.2, 35.5, 42.5, 49.8, and 55.4 ksi, respectively). The first of these load levels was chosen since it results in purely elastic loading for all test cases. The third, fourth, and fifth load levels (σ_g = 87.6, 105, and 123 MPa, respectively) were chosen since these values correspond to stress levels used by Kschinka [6.12] in experimental tests conducted on this specimen geometry. The second and sixth load levels (62.1 and 137 MPa, respectively) were chosen so as to bound those load levels used by Kschinka.

The detailed element stress solutions, printed out at the previously mentioned load levels, contained the following information for every element in the structure (from Refs. [6.1,6.6]).

Stress Components S_x, S_y, S_{xy}, S_z

Principal Stresses σ_1, σ_2, σ_3

Stress Intensity ($\sigma_1 - \sigma_3$)

Equivalent Stress seff = $(1/\sqrt{2})\,[(\sigma_1 - \sigma_2)^2 + (\sigma_2 - \sigma_3)^2 + (\sigma_3 - \sigma_1)^2]^{1/2}$

Elastic Strain Components ε_{ex}, ε_{ey}, ε_{exy}, ε_{ez}

Plastic Strain Components ε_{px}, ε_{py}, ε_{pxy}, ε_{pz}

Equivalent Strain ε_{peff} (strain from uniaxial stress-strain curve at σ_{eff})

Ratio of Current Stress State to Stress State on Yield Surface μ

Since the current problem is axisymmetric the stress and strain coordinate directions x, y, xy, and z refer to radial, axial, in-plane shear, and hoop values, respectively.

These stress and strain values correspond to the centroid of the element.

This detailed information provided a record of the spread of plasticity in from the root of the notch as the applied load to the structure was increased. In this study two different "yield" criteria were used to indicate the spread of plasticity. In the first case an effective plastic strain of 0.01% was used to indicate whether an element in the structure had "yielded". This particular strain level was chosen since it represents a deviation from elastic behavior. The effective 0.01% yield strength values and corresponding effective total strain values determined from the six isocyclic cyclic stress-strain curves are given in Table 6.1.

The second criterion used for measuring the spread of plasticity considers an element to have "yielded" if the effective total strain in an element exceeds the strain corresponding to the maximum obtainable effective stress. This stress level is analogous to ultimate tensile strength (σu) and so in the current discussion will be referred to as such. The effective ultimate strengths and corresponding effective total strain values obtained from the isocyclic cyclic stress-strain curves are given in Table 6.1.

The detailed element stress results for each isocyclic test case records the spread of plasticity in the structure as the load is increased. By using the collective results of all the test cases, the cyclic spread of plasticity under the application of a constant stress range can be investigated. Using the two plasticity criteria the elements at each detailed output stress level which were indicated to have yielded were recorded. Tables 6.2 and 6.3 contain a summary of these results. Each vertical column of these tables represents the cyclic progression of softening in the structure at a given stress level. A plot of these results at nominal stress levels of 245, 293, and 344 MPa are given in Figs. 6.5a, 6.5b, and 6.5c, respectively. In each of these figures, results for both the 0.01% offset yield strength and the ultimate tensile strength are given. As expected, the stress concentration at the notch root caused the elements which were located in this region to yield first. In all cases the yield zone continued to propagate as the material was cycled. This would suggest that the Bridgman notch geometry is very poor at withstanding material softening effects. This is not very surprising if one recognizes that under steady state conditions

this geometry develops a relatively uniform axial stress distribution. This means that any loss of strength at the root of the notch causes a redistribution of stress which affects the entire geometry cross-section.

In addition to the detailed element stress results provided at selected load levels the number of iterations required for convergence at each load step was also output. Furthermore, the maximum plasticity ratio value, and the element in which it occurred, was also given for each iteration. This information provides an indication of the amount of nonlinear material behavior being experienced, and therefore the relative proximity of the structure to final collapse. In this analysis a maximum of 15 iterations were allowed per load step. If convergence did not occur within these 15 iterations it was assumed that the structure had reached collapse and execution of the program was terminated. The load level at which convergence was not achieved was recorded for each of the nine test cases. These limiting net stress (σ_L) values are given in Table 6.4.

In the case of the three softening curves modified to include fatigue behavior the maximum number of iterations allowed for convergence was raised to 50. This increase was made since it was felt that additional iterations would likely be needed for convergence when the strain in an element exceeded the strain for failure by fatigue and the strength was reduced to zero. As it turned out this increase was not needed. In all cases when convergence was not met in 15 iterations it was still not met in 50 iterations. Furthermore, examination of the plasticity ratios during convergence indicated that when the first element failed by fatigue (this element was located at the root of the notch on the radial axis) the remainder of the elements along the radial (x) axis failed in succession from the root of the notch towards the central axis.

In Fig. 6.6 the limiting stresses for the three softening material curves and the three fatigue modified softening curves have been plotted against cycle number. Also shown in this figure is a 0.5% strain range softening curve [6.13]. The three softening limit stress values appear to follow this softening curve. This suggests that the isocyclic cyclic stress-strain curves provide a good representation of the softening characteristics of this material. These predictions however, missed the occurrence of failure by fatigue. As the material is continually cycled the softening curve shows a dramatic decrease in strength as the fatigue life is approached. The softening limit stresses predicted the rate of decrease in strength to

remain constant. This accelerated decrease in strength due to failure by fatigue was, however, predicted by the fatigue modified limit stresses.

Plotted in Fig. 6.6 are the results of experimental tests completed by Kschinka [6.12] on test specimens geometrically similar to the geometry evaluated here. (See Table 6.5 for further details regarding these experimental tests.) The fatigue modified softening curves accurately predict the rate of decrease in life with stress level of these results, though the actual life prediction values themselves are somewhat conservative. This conservatism can be explained by the manner in which the isocyclic cyclic stress-strain curves were modified to account for fatigue. For each cyclic curve, strength was reduced to zero when the strain for failure by fatigue in the number of cycles corresponding to the current isocyclic cyclic stress-strain curve was exceeded. This requirement assumes that all previous cycles were as damaging as the current cycle. This is simply not true. As the material is cycled it's strength decreases. For a given total strain range, the amount of plastic strain obtained in each cycle continually increases. This means that each fatigue cycle becomes increasingly more damaging. Since the fatigue life is calculated solely upon the damage in the current cycle (which is the most damaging cycle in the history) fatigue predictions will be conservative.

6.4 CONCLUSIONS

Isocyclic cyclic stress-strain curves have been used to characterize the softening behavior of this material under applied load cycles. These isocyclic material curves were used to perform an analysis on the Bridgman notch specimen geometry. Use of these curves allowed a series of monotonic loading finite element analyses to be completed which provided a reasonably accurate representation of material behavior under cyclic conditions. The predicted decrease in component load carrying capability agreed quite closely with the observed decrease in material strength with number of cycles. Modification of the isocyclic curves for fatigue behavior resulted in accurate predictions of the decrease in life with increase in applied stress level of actual experimental test results. The predicted values themselves were consistently conservative by a factor of 3.5 on life throughout the range of stress levels investigated. This

conservatism can, in part, be attributed to the manner in which fatigue behavior was incorporated into the analysis procedure.

This method appears to have great potential as a design tool. The use of a series of monotonic load cases to represent cyclic material behavior greatly reduces the amount of computational effort required in performing an analysis. The method not only accurately predicted the overall strength loss of a component during repeated cycling but provided consistently conservative estimates of final failure as well.

6.5 REFERENCES

6.1 ANSYS Engineering Analysis System User's Manual, Vol. I, Version 4.1, Swanson Analysis Systems, Inc., Houston, PA, 1983.

6.2 ANSYS Engineering Analysis System User's Manual, Vol. II, Version 4.1, Swanson Analysis Systems, Inc., Houston, PA, 1983.

6.3 ANSYS Engineering Analysis System Examples Manual, Version 4.1, Swanson Analysis Systems, Inc., Houston, PA, 1983.

6.4 ANSYS Engineering Analysis System Verification Manual, Version 4.1, Swanson Analysis Systems, Inc., Houston, PA, 1983.

6.5 ANSYS Engineering Analysis System Theoretical Manual, Version 4.1, Swanson Analysis Systems, Inc., Houston, PA, 1983.

6.6 ANSYS Engineering Analysis System User's Manual, Vol. I, Version 4.2, Swanson Analysis Systems, Inc., Houston, PA, 1985.

6.7 ANSYS Engineering Analysis System User's Manual, Vol. II, Version 4.2, Swanson Analysis Systems, Inc., Houston, PA, 1985.

6.8 Kloos, K., M.S. Independent Study Project, University of Illinois at Urbana-Champaign, IL, 1985.

6.9 Marriott, D. L., K. Kloos, and J. L. Handrock, "Approximate Analysis of Components Composed of Strain Softening Material," Properties of High-Strength Steels for High-Pressure Containments (ed., Nisbett, E. G.), MPC-27, American Society of Mechanical Engineers, NY, 1986, pp. 103-109.

6.10 Pejsa, P. N., "Elevated Temperature Low-Cycle Fatigue of Two Bainitic 2.25 Cr - 1 Mo Steels," M.S. Thesis, University of Illinois at Urbana-Champaign, IL, 1983.

6.11 Kschinka, B. A., "Creep-Fatigue-Environment Interaction in Bainitic 2.25 Cr 1 Mo Steel," M.S. Thesis, University of Illinois at Urbana-Champaign, IL, 1986.

6.12 Kschinka, B. A., unpublished test results, University of Illinois at Urbana-Champaign, IL, 1986.

6.13 Handrock, J. L., D. L. Marriott, and J. F. Stubbins, "Development of a Uniaxial Constitutive Model for a Strain Induced Softening Material," Thermal Stress, Material Deformation, and Thermo-Mechanical Fatigue (eds., Sehitoglu, H., and S. Y. Zamrik), PVP Vol. 123, American Society of Mechanical Engineers, NY, 1987, pp. 83-89.

Table 6.1 Yield and ultimate isocyclic cyclic stress-strain values.

Cyclic	Yield		Ultimate	
Number N	$\sigma_{y0.01}$ MPa	ε_y %	σ_u MPa	ε_u %
1	282	0.188	>360	>0.54
50	259	0.173	290	0.30
100	248	0.166	277	0.25
500	224	0.151	252	0.20
1000	214	0.145	241	0.20
5000	197	0.134	217	0.20

3039tables, 5

Table 6.2 Elements satisfying the 0.01% offset "yield strength(σ_y)" plasticity criterion.

Cycle Number	Applied Net Stress σ_{nom}, MPa					
N	104	174	245	293	344	382
1	None	None	1,12 13,23	1,2,12, 23,24,44	1-4,12-14, 23-26,34 44,55	1-5,12-16,
50	None	None	1,12 23	1-3,12-14, 23-26,34,44	1-5,12-16, 23-44,54, 55,66	1-7,12-20,
100	None	None	1,2,12	1-3,12-14, 23,24,44	1-6,12-17, 23-32,34, 44,55	1-9,11-44, 50-55,66,77
500	None	None	1-3,12, 13,23	1-5,12-16, 23-26,34,44	1-9,12-44, 50-55,66,77	—
1000	None	1	1-3, 12-14,23	1-5,12-17, 23-30,32, 34,44,55	—	—
5000	None	1,12	1-4,12-15, 23,24,44	1-8,12-20, 22-44,52-55, 66,77	—	—

--- Indicates collapse load exceeded.

3039tables, 6

Table 6.3 Elements satisfying the "ultimate strength (σ_u)" plasticity criterion.

Cycle Number	Applied Net Stress σ_{mon}, MPa					
N	104	174	245	293	344	382
1	None	None	None	None	None	None
50	None	None	None	1	1,2,12	1-4,12-14,23
100	None	None	None	1,2,12	1-4,12-14, 23	1-6,12-18, 23-26,30-32,44
500	None	None	1,12	1-3,12, 13,23	1-7,12-19, 23-32,34, 43,44	—
1000	None	None	1,2,12	1-4,12-14, 23,44	—	—
5000	None	None	1,2,12	1-5,12-16, 23,24,44	—	—

--- Indicates collapse load exceeded.

Table 6.4 Stress levels at no convergence.

Cycle Number N	Limit Net Stress σ_L, MPa	Effective Notch Stress σ_{eff}, MPa
1	>382	>285
50	>382	>285
100	>382	>285
500	344	257
1000	326	243
5000	301	225
500f	334	249
1000f	288	215
5000f	208	155

f appended to cycle number indicates softening curve modified for fatigue behavior.

Table 6.5 Results of experimental tests conducted on Bridgman test specimens [50].

Net Stress σ_{nom}, MPa	Effective Notch Stress σ_{eff}, MPa	Cycles to Failure N_f
244 182	8480	
292 218	3423	
341 254	1444	

All tests were fully reversed and cycled at a rate of 0.4 Hz.

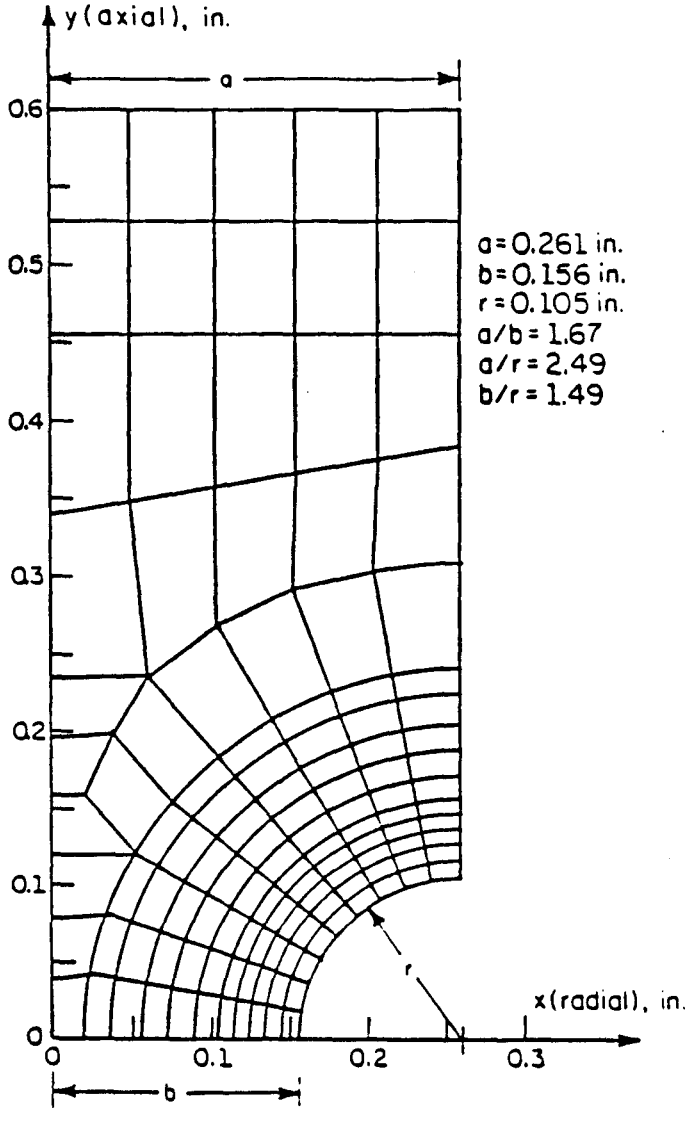

Figure 6.1a *Finite element mesh used to model the Bridgman notched specimen geometry.*

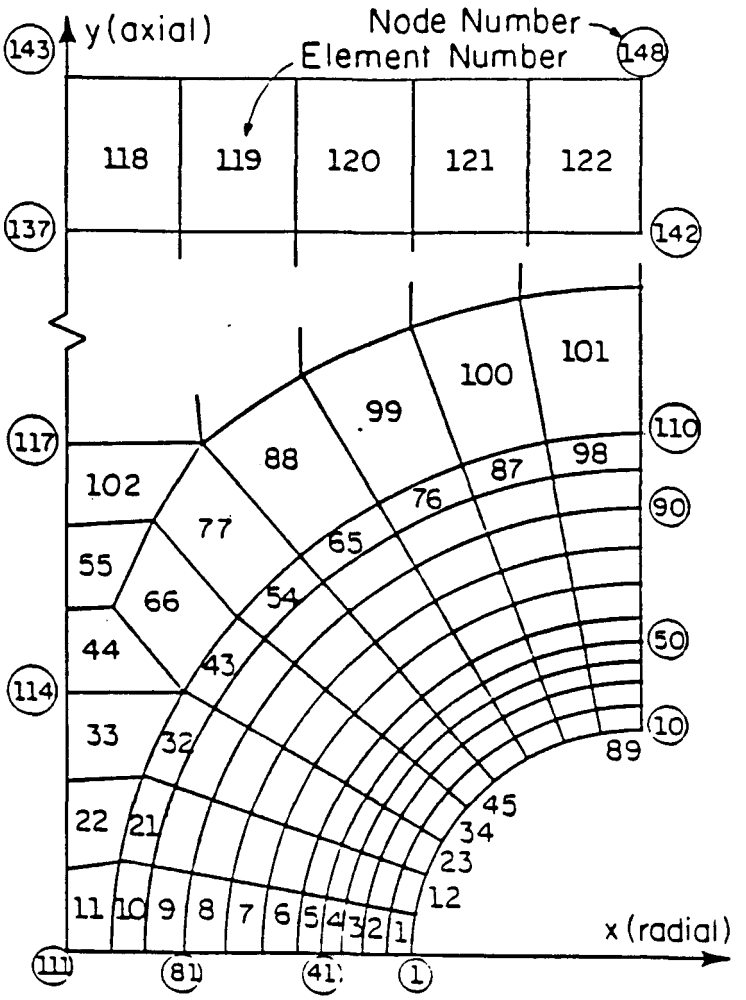

Figure 6.1b Finite element mesh used to model the Bridgman notched specimen geometry.

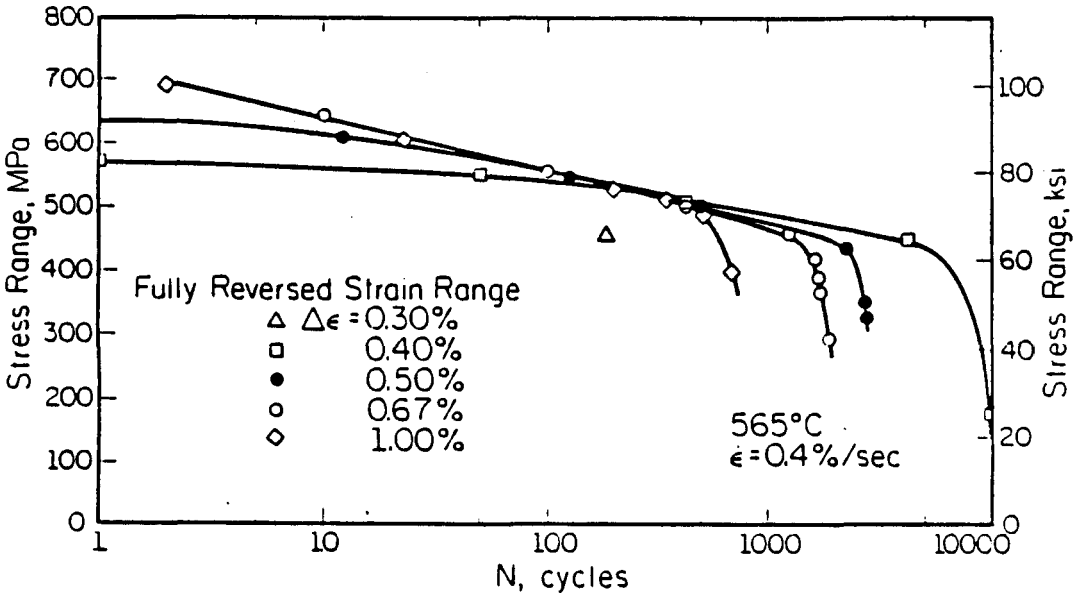

Figure 6.2a Plots of total stress range versus number of cycles for a variety of applied fully reversed constant strain ranges.

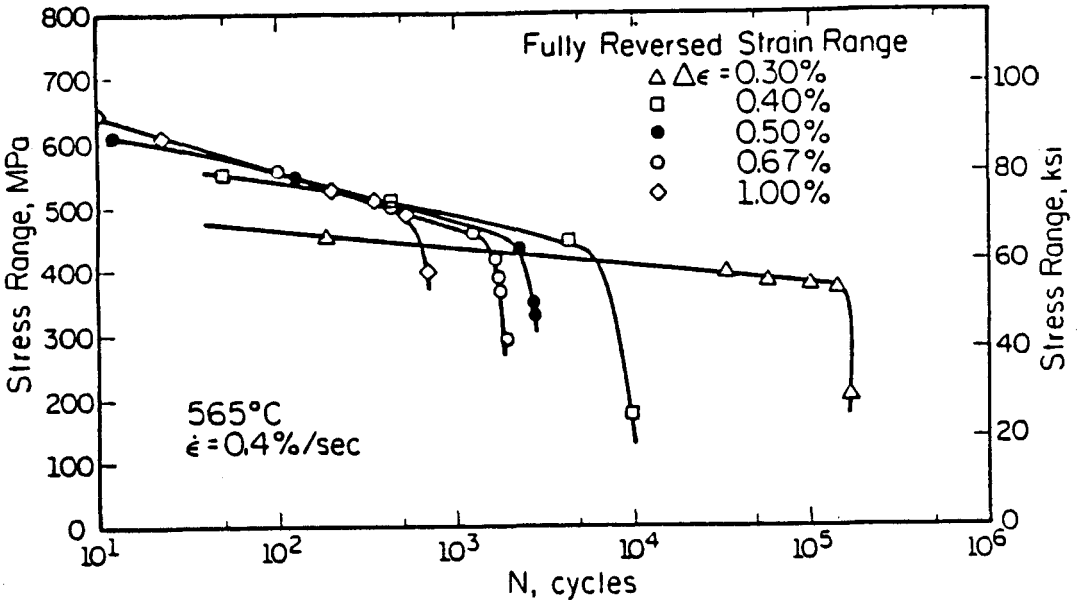

Figure 6.2b Plots of total stress range versus number of cycles for a variety of applied fully reversed constant strain ranges.

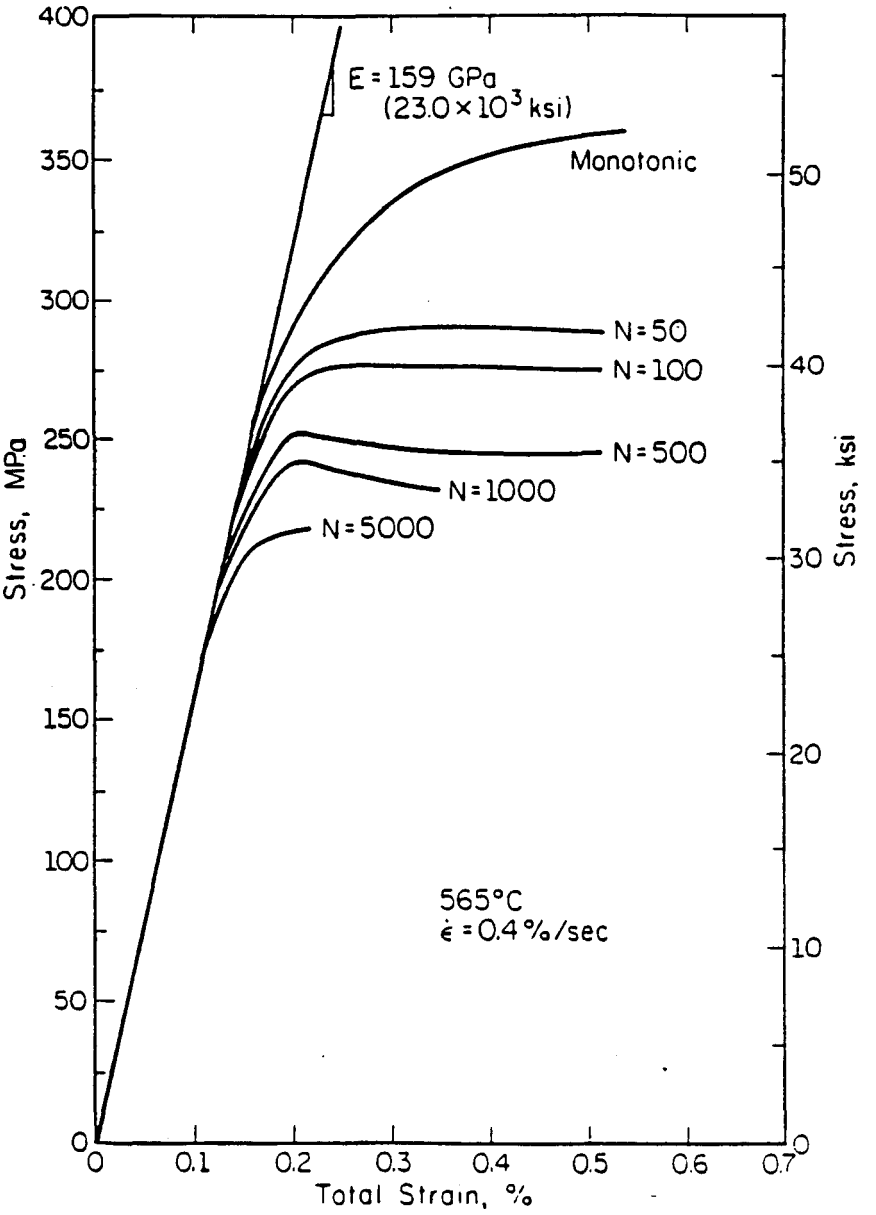

Figure 6.3 Isocyclic cyclic stress-strain curves.

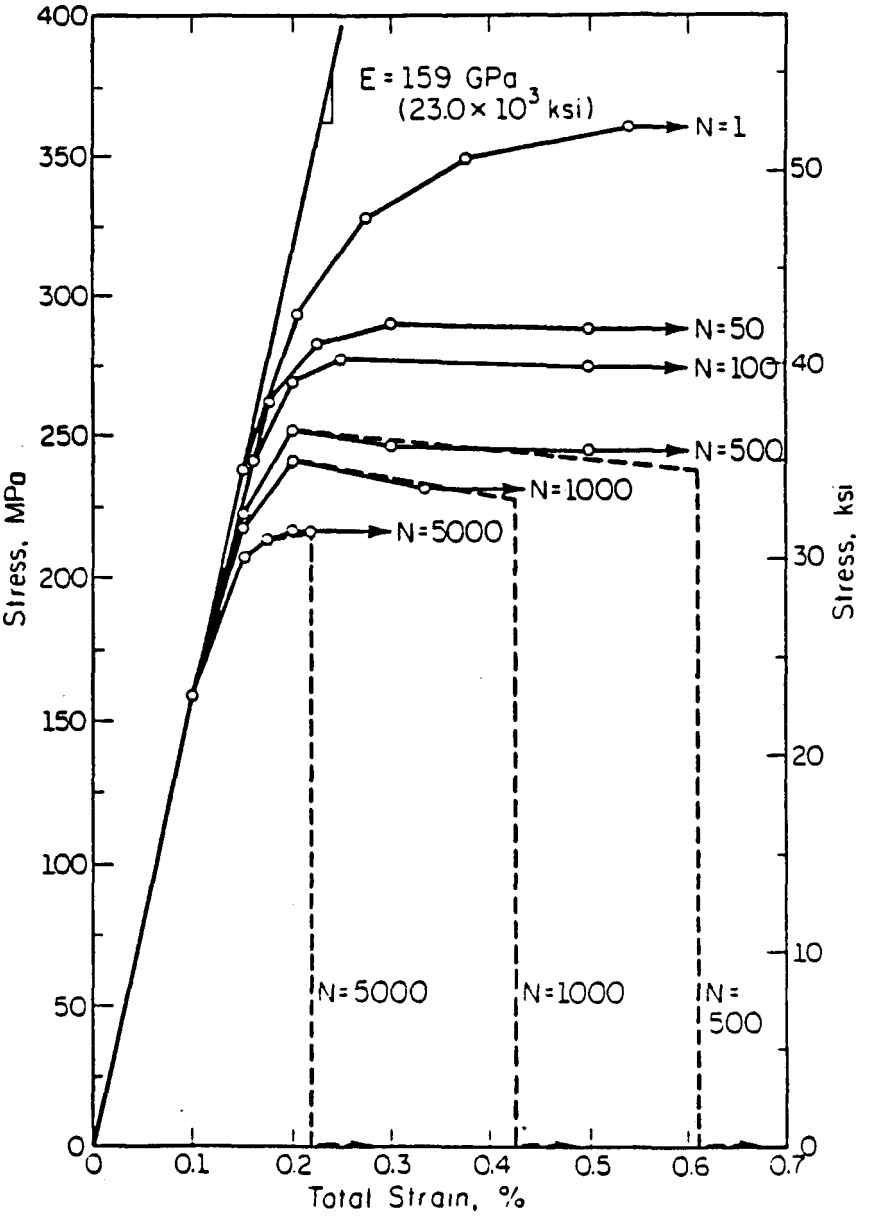

Figure 6.4 Finite element representation of isocyclic cyclic stress-strain curves.

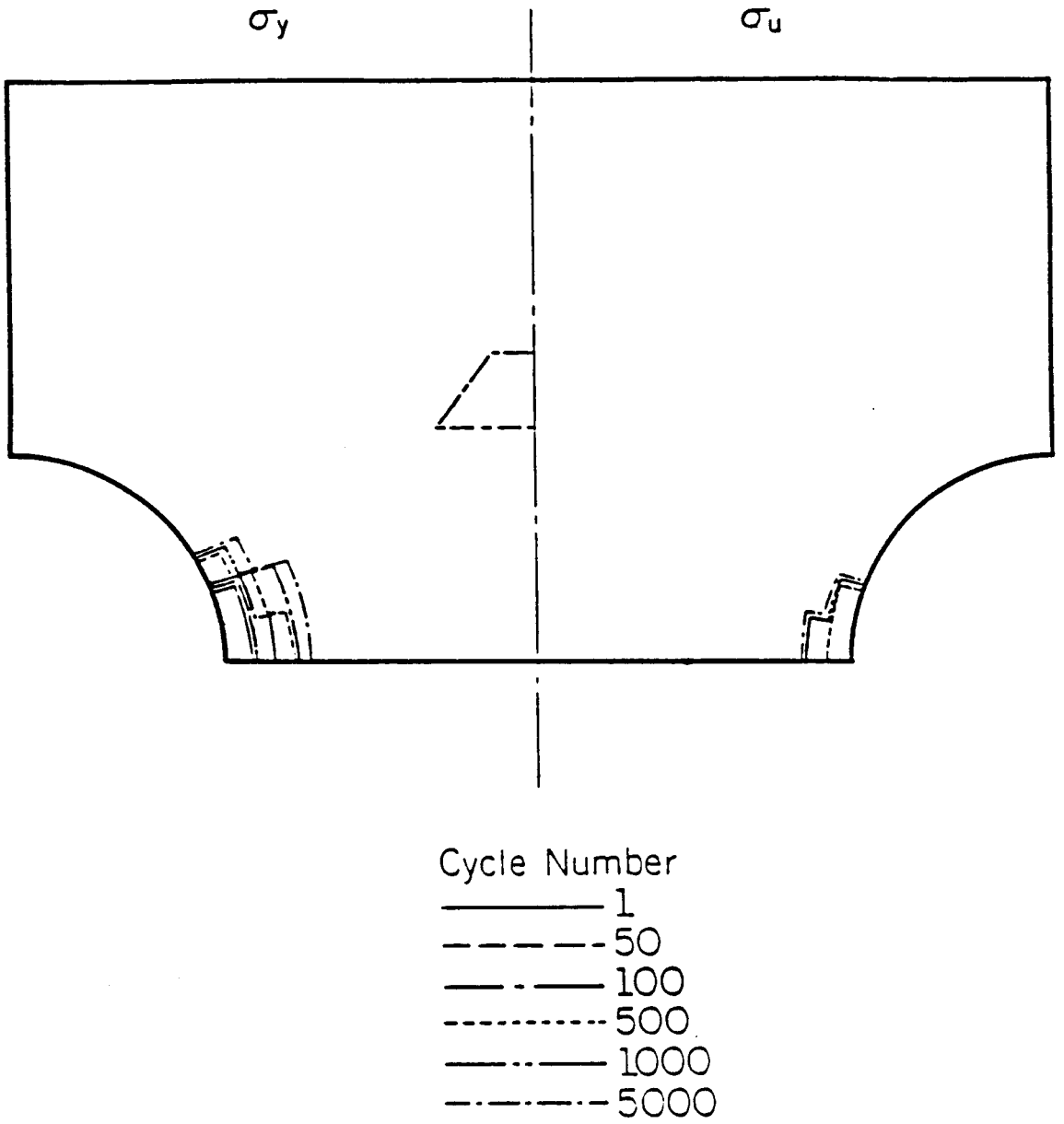

Figure 6.5a Propagation of plastic zone with applied cycles (σ_{nom} = 245 MPa).

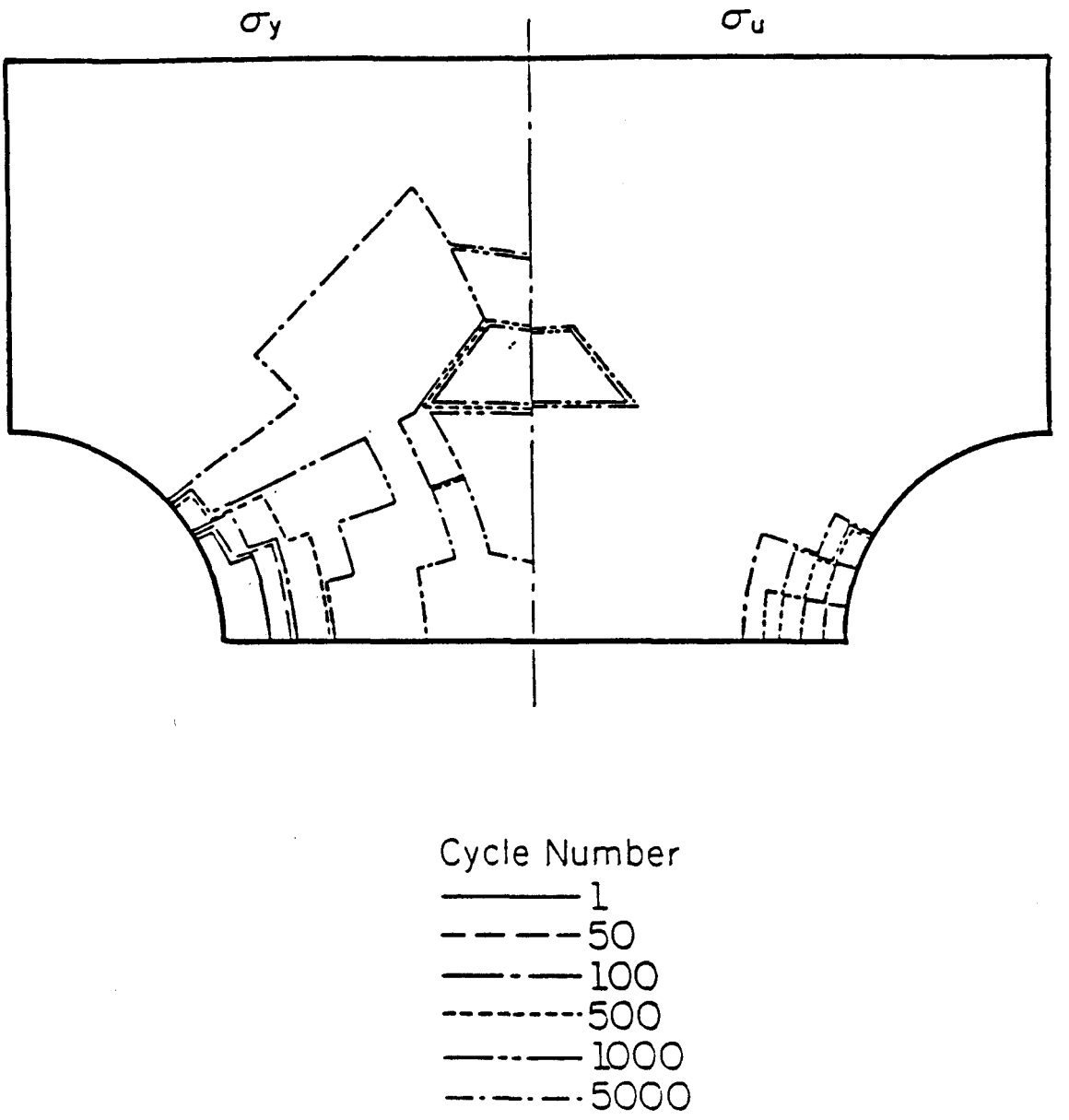

Figure 6.5b Propagation of plastic zone with applied cycles (σ_{nom} = 293 MPa)

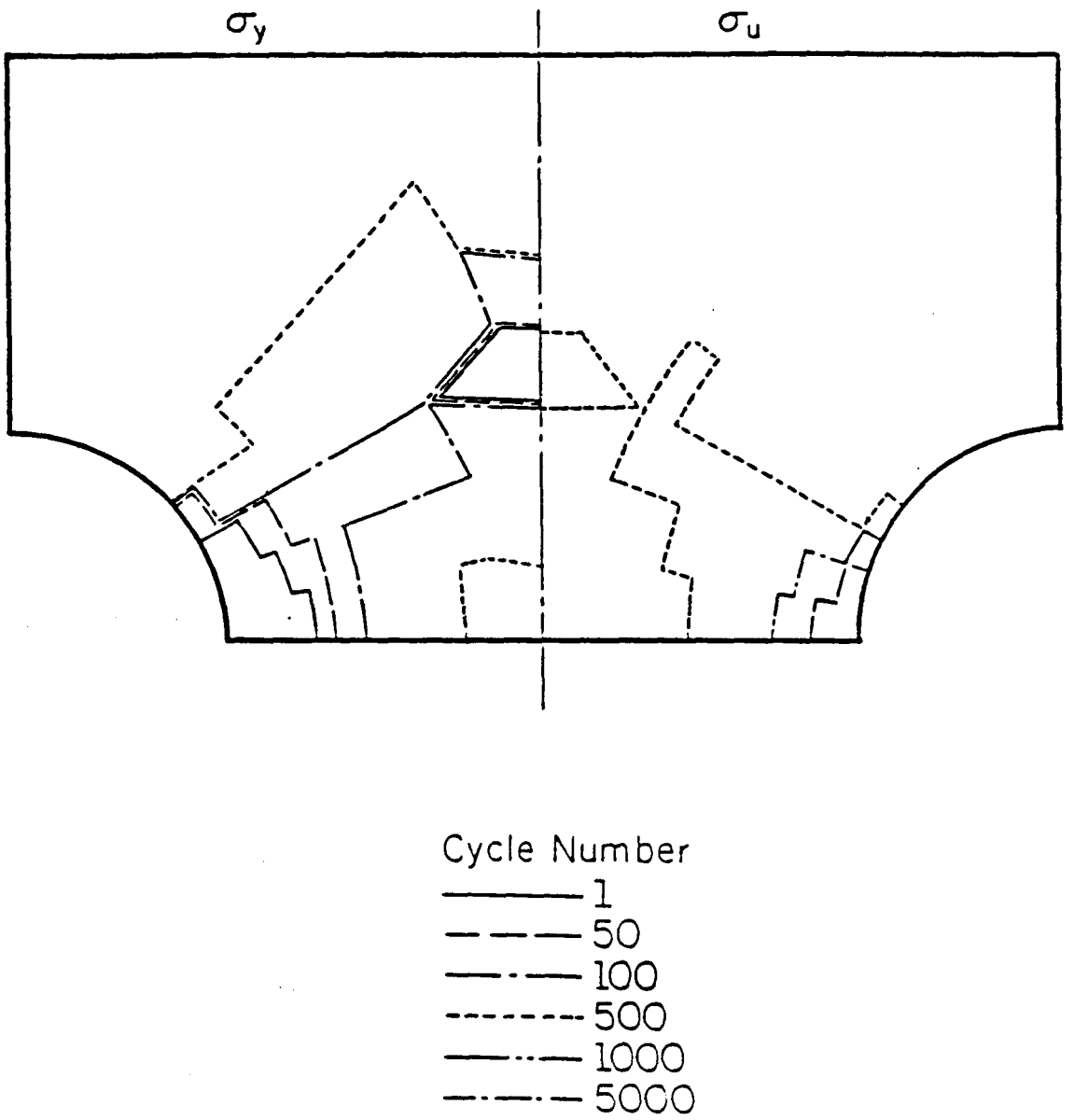

Figure 6.5c Propagation of plastic zone with applied cycles (σ_{nom} = 344 MPa).

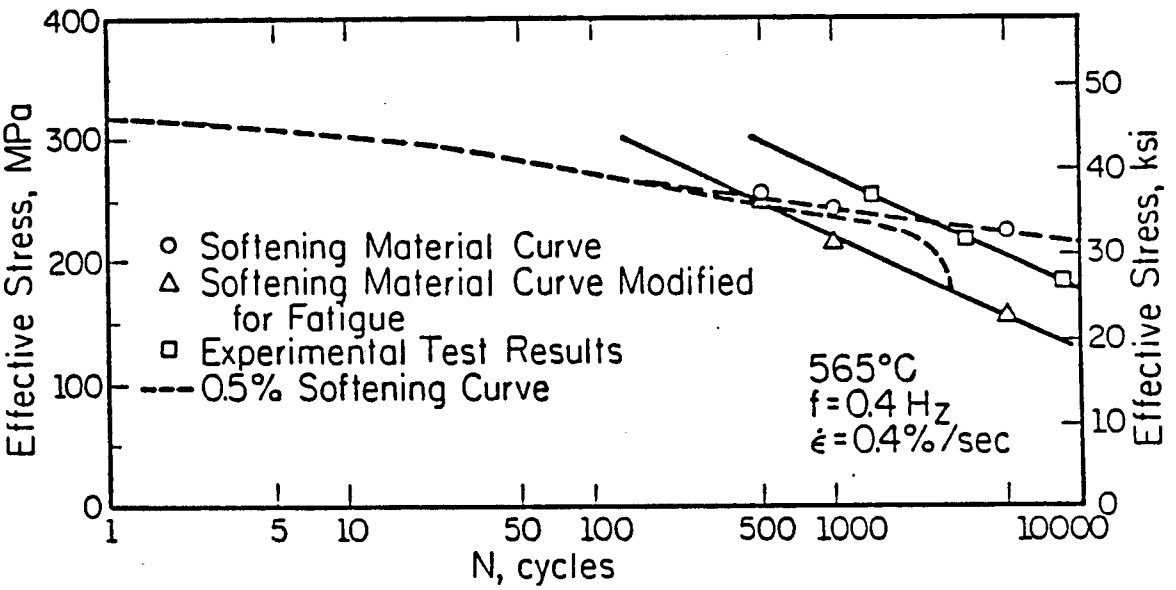

Figure 6.6 Experimental and predicted fully reversed load control test results on Bridgman notched specimens.

7. DESIGN METHODOLOGY FOR HIGH TEMPERATURE APPLICATIONS

7.1 INTRODUCTION

Cyclic softening materials create a special design problem because it is not sensible to specify universal design stresses for them, as is standard practice with other, more stable, materials. The reason is that, in some cases where cyclic deformation is not significant, design allowables based on the initial, monotonic strength are acceptable. In other instances, the initial safety margin (approximately 1.5, if the ASME Boiler and Pressure Vessel Code is being used) can be almost entirely eroded away within a few tens or hundreds of load cycles. Therefore, the selection of an allowable stress must be part of the design process itself, and must be treated as a function of the component geometry and the service conditions.

A similar problem is experienced in materials which suffer a time-related strength loss due to thermal aging. This class is of practical interest because it encompasses many of the materials used for high temperature applications, possibly including the modified stainless steel developed by Oak Ridge National Laboratory as a candidate for the next generation of very high temperature superheater and reheater tubes for fossil fuel power plants.

The metallurgical aspects of thermal overaging in this class of materials are complex, and have not yet been fully characterized. In addition, there is the question of how best to design tubing using this material, taking the aging into account without being excessively conservative.

The problem of design for thermal aging is similar to concept to that posed by stress induced cyclic softening. Aging, being temperature-dependent, does not proceed at the same rate throughout a component if the temperature varies from point-to-point. When considerable thermal gradients exist, which is more often than not, the variation could present a significant economic advantage if local aging is recognized, instead of assuming the entire component to age uniformly at the maximum rate.

A great deal still needs to be known, both qualitatively and quantitatively, before cyclic softening and aging are fully understood under all circumstances. That understanding however, is neither sufficient nor, as it turns out, entirely necessary in answering the question which still remains, i.e. how to use them efficiently. It is also necessary to identify critical performance parameters which relate to the failure of components in service, and devise practical strategies for integrating them into the design process

without causing too radical a change in the current methods of design evaluation, or making the process too complex to be practical. This is a generic design problem, which will be discussed in greater length in the next section.

7.2 DESIGN IN SOFTENING MATERIALS - PROBLEM DEFINITION

Variations in material properties while in service are not unknown. However, in the past, it has not been standard practice to take these variations into account explicitly in the design process. For instance, although the ASME Pressure Vessel and Piping Design Code [7.1] recognizes time-dependent failure mechanisms such as fatigue and creep, it does not make any specific recommendations on how to deal with time-dependent changes in the materials properties which govern these mechanisms.

There are several reasons today for which to take service-related changes in material properties into account in design.

i) Failure to do so can lead to a loss of the inherent safety margin of the component. While this is not a new problem, the degree of strength loss in these newly proposed materials can be much greater than in the past, due to the complex, thermo-mechanically produced microstructures used to optimize their high temperature strength. Consequently the normal levels of conservatism built into the design rules may not be sufficient.

ii) Service related strength loss is not necessarily uniform throughout the volume of the component and may not be equally damaging in all instances. Cyclic softening in particular may occur only in very localized regions and it might be prohibitively restrictive to assume a general loss of strength throughout the component.

iii) With greater emphasis being placed on life extension of existing plant as an economic alternative to complete replacement, it is becoming increasingly important in the design of new components to have more confident projections of the actual service life of components remaining at the end of their nominal design life.

The difficulties perceived in dealing with service related property changes in design are

i) The mechanisms of softening are not fully understood at this time.

ii) Whether understood or not, the constitutive relations needed to describe these phenomena in full are expected to be considerably more complex than the essentially linear-elastic behavior assumed in most current design.

iii) A quantum step in analytical complexity is needed in standard design procedures if complete formulations of aging and softening mechanisms are to be accommodated.

One significant change in design philosophy, which comes from considering service dependent property variations, is the fact that design allowable values can no longer be viewed as independent of the type of component being designed. If independence is assumed, in the interests of simplicity, one must assume the lowest limit on all properties. Yield strength for instance, may only be adversely affected in very localized volumes of material by cyclic softening, e.g. at the root of a sharp notch, and it is needlessly conservative to assume the fully softened state for the component as a whole.

The work described here has two objectives. The first is to determine the minimum knowledge of material behavior required to make definitive design decisions, so that is not necessary to wait indefinitely for full understanding of the material. The second is to develop a design methodology which is consistent with existing pressure vessel design practices as, for example, those mandated by the ASME Boiler and Pressure Vessel Code (the ASME Code), and with the resources, such as stress analysis programs, which might reasonably be supposed to be accessible to most engineers.

Both these objectives have been achieved, at least partly. As will be shown later, it is possible to

i) Extract the important information on cyclic softening needed in design long before the material has been tested exhaustively. More important, it is possible to decide, on the basis of very little information, whether or not it is economically worthwhile selecting a cyclic softening material in the first place. The reason is that the design decision does not depend on accurate characterization of constitutive relations, but on whether the specific application will be sensitive to cyclic softening or not.

ii) Develop a systematic design procedure which is both consistent with the ASME Code, and requires no more in the way of analytical resources than a linear elastic finite element program. In principle, the method can be implemented using a PC.

The remainder of this chapter describes some guidelines on how existing design procedures might be modified to take service dependent strength variations into account. The model adopted is the ASME Boiler and Pressure Vessel Code (for brevity referred to form here on as the "ASME Code"). The next section is a brief review of the basic ASME design procedure, defining the various stress classifications used, and how these relate to material properties. This is followed by a description of the modifications required to incorporate the effects of cycle- and time-dependent softening.

7.3 A REVIEW OF THE ASME PRESSURE VESSEL DESIGN PROCESS

The ASME Code requires any component to be evaluated systematically against four criteria [7.1].

I. Limit Load - The ability to sustain a single application of a mechanical load with an adequate margin against collapse.

II. Incremental - The ability to resist ratchetting, or incremental Collapse Collapse plastic deformation due to cyclic loading.

III. Fatigue - Resistance to initiation of a fatigue crack.

IV. Fracture - Resistance to fast fracture from an initial defect.

Only time independent, or low temperature, behavior is considered on a mandatory basis. The high temperature section of the Code exists at present merely as a guideline in the form of Code Case N47 [7.2].

Design evaluation of a pressure vessel consists of comparing various components of the stress distribution with standardized allowable stresses based on material properties. Allowable design stresses, are determined by a strict procedure, and only after rigorous testing, for a limited number of accepted materials. The discussion following this section can therefore only offer tentative guidelines on how other materials might be evaluated.

The stress limit of greatest interest in this paper is a quantity called "Sm". This is the maximum allowable static stress. It is normally calculated from the initial monotonic stress-strain behavior of the material. For simplicity sake, it will be assumed on subsequent discussion that Sm is approximately 2/3 of

Sy, the monotonic yield strength. Other factors are also involved but they do not change the basic theme of the arguments presented here.

To compare a component against the four criteria, one procedure allowed by the Code is to subdivide the stresses at critical sections into a statically equivalent "linearized" stress and a "peak" of F stress (see Fig. 7.1). The linearized stress is in static equilibrium with the normal force and bending moment on the section.

Depending on whether these imposed forces are produced by external mechanical load, or by internal compatibility constraints, such as thermal expansion or discontinuities, the resultant linearized stresses are designated Primary or Secondary, respectively. When judged to be primary, the membrane and bending components of the linearized stresses are referred to as Pm and Pb, Linearized secondary stresses are referred to as Q stresses.

7.1 PRIMARY LOAD EVALUATION

The maximum primary stresses must satisfy the following requirements

$$Pm + Pb = <1.5\ Sm$$

$$Pm = < Sm$$

This limit is called "primary" for a good reason because, if the component has an insufficient margin against collapse under a single load application, all other criteria are redundant.

7.2 INCREMENTAL COLLAPSE

The maximum range of the primary plus secondary linearized stresses, for all load transients, must not exceed 3 Sm. i.e.

$$range(Pm + Pb + Q) = <3\ Sm$$

This ensures that general cyclic yielding on any section will not exceed the yield range of approximately 2 Sy and hence will not lead to incremental plastic deformation, i.e. the component will "shakedown".

An important feature of the Code procedure is that local or "peak" stresses are ignored for the purpose of evaluating general structural deformation. The reason is that small localized regions of plastic deformation will be kinematically restrained by the surrounding bulk of elastic material. This has some significance for the treatment of materials which experience aging because if the aging phenomenon is also localized in this sense it will not affect overall structural integrity significantly.

Judging whether any stresses zone can be classed as "localized" however, is a difficult technical problem, and one which occupies a major part of this paper. As already noted, the ASME Code accepts the ad hoc device of replacing the stresses on any section by a statically equivalent linear distribution, and assumes that any excess "peak" stress to be localized. This is a commonsense rule based on experience, and it seems to work reasonably well most of the time. It is also easy to apply. However, there are other procedures available, and it is believed these offer a little more insight into the nature of displacement versus load-control which distinguishes localized from generalized inelastic deformation. One possibility is offered in this paper.

7.3 FATIGUE

The range of the total stress at a point, (Pm + Pb + Q + F), is considered for the purpose of fatigue evaluation. In the simplest case of constant amplitude fatigue, the stress amplitude, Sa, is

$$Sa = -(Pm + Pb + Q + F)max - (Pm + Pb + Q + F)min$$

In practice, because the Code is based nominally on linear elastic methods of stress analysis, Sa is frequently computed to be greater than the material yield stress, and is therefore a fictitious quantity. This is not a serious problem if inelastic behavior is constrained to a local volume because then the material will

be displacement controlled, and essentially the same strain amplitude is obtained from the linear elastic calculation as the full, but much more complicated, inelastic analysis.

To determine whether inelastic strains are indeed localized, the Code imposes a test on the range of the linearized (Pm + Pb + Q) stresses

$$\text{range } (Pm + Pb + Q) = < 3\ Sm$$

If this test is satisfied it means that the nominal membrane and bending stresses on the critical section do not exceed yield and, therefore, any inelastic deformation must be due to local stress concentrating effects.

If the test fails, it means that parts of the critical section will be losing elastic constraint due to generalized plastic deformation. A complex procedure is then invoked to calculate the resulting strain amplification, in the form of a factor, Ke, which depends on the amount by which the total stress range (Pm + Pb + Q + F) exceeds 3 Sm. Ke can be as large as 5 to 7.

7.4 FRACTURE

There is no mandatory procedure for fracture evaluation as yet. Appendix G of the Code provides a guideline which, though first introduced in 1971, is still often used today [7.1].

The Appendix G approach assumes a 1/4 thickness semi-elliptical crack at all critical sections, and calculates the elastic stress intensity factor from the linearized components of the section stress distribution, i.e. the Pm, Pb, and Q stresses. It is considered that crack growth under load control is more critical than under strain control and, for this reason, different safety factors are used for the Pm + Pb and the Q stresses, respectively.

As in the case of fatigue, corrections have to be made to the calculated stress intensity factors if the (Pm + Pb) stresses exceed the material yield stress, Sy. The strains will then be unconstrained to some degree, and a more severe condition is imposed on the assessment crack. Q stresses are not subject to

correction because they are strain controlled, and onset of plastic deformation under fixed displacement is not considered to make the situation more critical.

7.4 THE EFFECT OF SERVICE-DEPENDENT PROPERTY CHANGES ON DESIGN

It may well be that, in principle, softening effects can be dealt with by developing a full constitutive relation for the materials in question, and incorporating it in a detailed, inelastic analysis. In practice, this route is not generally viable for the following reasons.

i) A reliable constitutive model, including softening effects, has yet to be found.

ii) Detailed constitutive models, where they exist, are acceptable for evaluating existing designs, but are unsuitable for use in the conceptual design stages, where the material selection is made in the first place.

iii) Design based on detailed constitutive modeling may be costly in terms of time and resources, even when it is computationally feasible, and may not be a practical option in all industries.

iv) Detailed models require detailed input, which is seldom available in the early design stages. The batch-specific nature of material constants used in detailed material models prohibits them from being quoted in the design code.

Fortunately, the detailed route is not necessary. Cyclic- and thermal-softening are only of concern to the extent that they adversely affect one or more failure mechanisms of a component.

Regardless of the microstructural complexities of the mechanisms involved, or our current imperfect understanding of them, mechanisms involved, or our current imperfect understanding of them, the effect of softening is summarized entirely by the variations it causes in the yield stress, Sy, and the allowable ASME Code stress intensity, Sm, derived from it, through all or part of the component volume.

As can be seen from the previous section, Sm figures in every one of the failure criteria, but in different ways. It is only necessary to examine each mechanism in turn, and critically evaluate the role of Sm in each case, to determine the effect of softening. This means

a) determining whether a change in the material yield strength, Sy, is expected in any part of the component volume due to the service conditions.

b) whether this change is localized, or general to the component as a whole, and

c) the effect this change will have on each of the failure criteria used to evaluate design acceptability.

This work is concerned, in the long run, with both stress- and thermally-induced softening - synergistic combinations of the two, should any be found to exist. In this report however, the discussion will be restricted primarily to time-independent cyclic softening. This is the form of softening which has been studied longest and is the only one, so far, for which sufficient material data has been collected to quantify the design procedure with a reasonable degree of confidence. However, it is believed that the procedures developed can be extended to encompass other forms of service related softening in due occurs. Toward the end of this chapter there is some discussion on how this might be done.

From the design point-of-view cyclic softening is the more difficult problem, because both the failure criterion, Sm, and the softening phenomenon, are directly coupled to the stress history. To a first approximation, thermal softening, on the other hand, is only a function of time-at-temperature, and therefore represents a decoupled problem which is somewhat easier to deal with in component analysis.

7.4.1 A Design Rationale for Dealing with Cyclic Softening

A uniaxial specimen of cyclically softening material softens uniformly and, under load control, will fail by plastic collapse when the residual strength drops below the maximum applied load. The same is true of a complex component if the strain range throughout is of comparable magnitude, as for instance in a bar with a blunt Bridgman notch. Under these conditions, the softened strength, Sy(N), after N load cycles, is expected to govern all failure criteria and should be used instead of the initial monotonic strength, Sy, calculated from monotonic test data. The operative phrase here is "load controlled".

At the other extreme, local cyclic deformation, as might be approached at the root of a very sharp, very small notch, will cause softening under conditions of displacement control. Some failure criteria, notably fatigue, will be influenced by the increased plastic deformation, but the overall limit strength of the component will remain essentially unaffected. Assuming the fully softened state everywhere for primary

stress evaluation is needlessly conservative. If it can be established that cyclic deformation is localized, the bulk of the component will be governed by the initial monotonic strength, Sy.

The rationale proposed here avoids the need to make any complex inelastic evaluation by focussing instead on a test to determine whether the component is sensitive or otherwise to cyclic softening. Assuming for the moment that such a test is possible the design decisions which follow are relatively simple.

If softening is extensive, the softened yield strength, Sy(N), after N cycles, must be used in calculating the allowable stress intensity, Sm, under all circumstances. Here, N is a conservative estimate of the number of load cycles expected in service. The sensible conclusion in this case is likely to be not to use the material at all, unless some other factor, such as corrosion resistance, is more important than strength.

If softening is localized, the problem is more complex. Each failure mechanism must be considered separately, and the initial monotonic yield strength, Sy, or the softened value, Sy(N), may be appropriate in different situations, as described below.

I. Primary Limit Load - This is governed by the yield strength in the bulk of the component volume. By definition of localized plasticity therefore, softening will have a negligible effect. The appropriate measure of yield is the initial value, Sy.

II. Incremental Collapse - The ASME Code procedure evaluates incremental collapse by a test of the range of the linearized stress (Pm + Pb + Q) at critical points. Although it appears that the local strength is the relevant design parameter, the mechanism of incremental collapse is in fact one of generalized yielding, and the initial yield, Sy, applies once more.

III. Fatigue - Yield strength features twice in the standard ASME fatigue evaluation procedure. The first time is the "3Sm" limit to determine whether extreme fiber yielding on a section causes loss of elastic constraint. Since we are considering the case where the component has satisfied the requirement for localized softening, and this is a more severe constraint on local stress range than even the softened stress range, it would appear that the "3Sm" limit will

be automatically satisfied. This is a tentative conclusion which needs to be confirmed by further theoretical testing.

The second appearance of yield is in the Neuber correction for local plasticity. In this case it is clearly the softened state, Sy(N), that must be used.

IV. Fracture - as with fatigue, the appearance of Sy in the fracture evaluation procedure is related to a test for the loss of local elastic constraint. While further confirmation is needed, a tentative conclusion is that the problem will not arise if the component has already passed the more stringest test indicating that cyclic softening will be localized.

It is interesting that, whether softening occurs locally or extensively, neither the mechanism of cyclic softening, nor any constitutive relation describing it, enter directly into the design decisions concerned with primary load carrying capacity. Realistically, the only one time the softened state is explicitly called upon is if a Neuber-type analysis has to be done for fatigue evaluation, and even then it is only a secondary factor in the stress analysis. Usually the only design major issue will be a go/no-go decision. Does the component soften generally? Do not use softening material. Does the material soften locally? Use the initial monotonic properties. From that point onward the procedure can follow the existing ASME Code procedure virtually without modification.

The problem has been reduced to finding a criterion to discriminate between localized and extensive inelastic deformation. One possible test has been developed, and is described in the next section.

7.4.2 A Criterion for Assessment of Sensitivity to Cyclic Softening

It is assumed here that "localized plastic deformation" and "displacement controlled deformation" are synonymous. If it can be shown that cyclic softening only occurs in regions is localized and will not interfere with the primary load carrying capacity of the component.

Handrock [7.3] shows that the inelastic behavior of a component composed of cyclically softening material can be carried out approximately by constructing "iso-cyclic" cyclic stress-strain curves, and using

these curves in monotonic inelastic analysis. These iso-cyclic curves capture the material response (Fig. 7.2).

The effect of localized inelastic behavior can be represented by a Neuber like relaxation locus (Fig. 7.3). Contrary to common belief, there is no basis for assuming the universal Neuber hyperbola to represent this curve. However, it has been demonstrated by Kloos, et al. [7.4], and there is a growing body of literature on a related phenomenon called "elastic follow-up", which supports the argument, that a "relaxation locus" exists which is predominantly a function of the component geometry, and is relatively insensitive to the material constitutive relationship.

It is now possible to establish a rational test for local plastic deformation. If the relaxation locus can be found, the steepness of its slope is a direct indicator of the degree to which local conditions are loca- or displacement-controlled. If the component relaxation locus is horizontal there is, in fact, no relaxation, and local conditions are load controlled. Conversely, a vertical locus signifies displacement control, in other words, pure relaxation. For intermediate situations some stress relaxation is accompanied by positive strain accumulation in the direction of the applied stress. This is the "follow-up" phenomenon.

The choice of an objective criterion for strain control is not easy, and has not been completely resolved to date. One possible candidate is offered here.

For reasons of energy conservation, it is impossible to achieve pure strain control under fixed external loading. Some degree of follow-up must always occur. Therefore, constant strain relaxation is not a viable criterion.

An alternative is to consider whether the local strain energy density increases or decreases during stress relaxation. This criterion is approximately equivalent to the Neuber assumption that the product of stress and strain is a constant. While this is not the only possible criterion, it will be assumed here that the dividing line between load- and displacement-control is the hyperbola,

$$S_{max} \cdot e_{max} = \text{constant}$$

where S_{max} = maximum local stress

e_{max} = maximum local strain

The test of sensitivity to cyclic softening reduces to determining whether local regions of high cyclic stress will relax in a strain-controlled manner, while the remainder of the component is subjected to sufficiently low stresses that cyclic softening is not experienced. This test requires two tasks to be performed.

i) Represent the material such that cyclic softening will localized if stress relaxation is strain-controlled. This is done by selecting a fictitious stress-strain relation for the cyclic component analysis such that the "yield" stress amplitude is less than some threshold value, below which cyclic softening will not occur.

ii) Determine the component relaxation locus and compare it with the "Neuber" strain-control criterion.

As shown schematically in Fig. 7.4, the criterion for local softening is satisfied if the relaxation locus intersects the target stress state within the strain-controlled region. In this figure the dashed line represents the Neuber criterion line chosen in this study to delineate betwen load and displacement (or strain) control. Dotted lines (a), (b) and (c) represent typical relaxation curves.

(a) is a clear case which satisfies the criterion in all respects. In this case cyclic softening can be safely ignored.

(b) is a marginal case which would probably be mainly strain controlled but which does not meet the stringent conditions of the criterion presented here

(c) represents a clear case of load dominated deformation

This means that local softening was able to occur under strain control, while the stress range in the remainder of the component remained below the threshold for cyclic softening. Having performed this test it is then possible to select allowable stress intensity levels and proceed with design evaluation by following the ASME Code in the usual manner.

So far the procedure has only been described in general terms. For practical implementation, two problems need to be resolved. These are material representation and component relaxation response. The following solutions are offered for each of these problems.

I. Material Representation

From Handrock's work [7.2] an equation can be obtained relating cyclic softening to cumulative plastic deformation, (Chapter 5, Eq. (5.7)).

Handrock also found an incubation plastic strain of about 3% which must be accumulated before softening begins. Assuming 106 cycles for major load cycles, as does the ASME Code, the above equation predicts an allowable cumulative plastic strain of 3×10^{-6}% to avoid cyclic softening. For the material tested by Handrock, the allowable stress range is 221 MPa. The corresponding stress amplitude is 110.5 MPa, which is about a third of the initial, monotonic yield stress. The target stress state is shown in Fig. 7.4, superimposed on the isocyclic curves developed by Handrock.

II. Component Response

The most obvious method of determining the relaxation locus is inelastic analysis. Since the locus is essentially a function of the component, and not of the constitutive relation, any convenient nonlinear stress-strain relation can be used. For instance, Kloos et al. [7.4] used linear strain hardening with a variable hardening index. Figures 7.5a and b, derived from the results obtained by Kloos, show relaxation loci for a bar with a spherical cavity and a Bridgman notch, respectively. In the case of the spherical cavity there is a finite limit on the load exceeding first yield for localized plastic deformation. The Bridgman notch does not possess any such region. This is reflected in the fact that the Bridgman notch has been observed to soften uniformly for all cyclic loads causing peak stress ranges comparable with the yield range.

Inelastic analysis requires a high level of analytical sophistication. A desirable alternative is a procedure for computing relaxation loci, which depends only on linear elastic analysis. One such method has been found and was presented in detail by Marriott at the 1988 ASME Pressure Vessel and Piping

Conference [7.5]. It involves a succession of linear elastic finite element calculations, with the element stiffnesses adjusted in a systematic way after each run to simulate inelastic behavior. So far the method has not yet been applied directly to the softening problem, but in a closely related problem concerned with stress classification, it has been found to converse very rapidly, within three or four iterations.

3.2 Thermal Softening

If thermal softening is only a function of time-at-temperature the design problem is relatively simple. Under isothermal service conditions it is trivial. If the relation between time, temperature and residual strength is known, the procedure can be identical to the existing ASME Code with the allowable stress intensity, Sm, replaced by the time-related quantity, Sm(t,T). In Code Case N47 [7.2], there is already provision for including time dependence in the allowable stress intensity, using a quantity, Smt, which is the least of time-dependent and time-independent stress intensities.

Thermal softening is relatively simple to deal with as a design problem. Assuming that the rate of change of material property with time-at-temperature is known, the appropriate property after some designated service exposure can be used in place of the nominal, initial value. For instance, in the case of overaging affecting the strength, the effect is to have a time dependent yield strength, Sy(t), from which the Code allowable, Sm, can be calculated in the conventional way, giving a quantity, say, Sm(t).

In the simplest case of approximately steady, isothermal service conditions, this procedure would be independent of the component itself. Realistically, however, thermal aging is temperature dependent, and is therefore expected to occur at different rates in different parts of a component at high temperature, and to vary with time at any given point, because of thermal transients.

It appears that it would be conservative to assume that aging occurs uniformly, at the maximum rate. There are two potential problems associated with this route, however. The first is that aging is very temperature sensitive, and it may be unrealistically conservative to assume the entire component to age at the rate of a local hotspot. The second is that it is not clear that local softening in a relatively high strength matrix is stronger than uniform softening. Strain localization in weldments, leading to premature fatigue failure, is a case in point.

The design problem is, however, relatively easy compared with cyclic (or stress state) induced softening, since the driving force, time-at-temperature, is decoupled from the stress state. Methods are needed to deal with an inhomogeneous distribution of material properties, but this analytical problem is simpler than that of stress-induced softening. What follows in the section on design for cyclic softening therefore contains thermal softening as a special case.

The material problem associated with characterizing thermal softening for the purposes of design is not a simple one, however. To some extent thermal softening is included implicitly in the ASME Code, for those materials which experience the phenomenon, as one of many contributions to creep strength. However, as will be shown in the next section, softening does not only affect strength under steady load, as is considered in creep data. Through its effect on the yield strength it is also a significant factor in judging resistance to incremental collapse, and influences the methods of evaluating fatigue and fracture as presented by the Code, because of the corrections which have to be made to the basically elastic method of analysis used, in order to account for inelastic loss of constraint.

Explicit consideration of thermal induced aging is not therefore a major technical problem, but it is one requiring a systematic experimental program to be implemented, and a reliable, and compact means of representing the results. Given the nature of the phenomenon, it is expected that time-temperature plots of yield strength and tensile strength, based on the Larson-Miller Parameter, or one of its many competitors, is a satisfactory method of representation, but this will have to be established by further work. In addition, a practical working procedure, consistent as far as possible with existing Code practice will need to be developed for using this information for efficient design, without excessive expenditure of effort.

At the time of writing, the thermal aging design problem has not been considered in depth. However, there are close similarities between this problem and that of cyclic stress induced softening, which is considered in somewhat greater depth in the following section.

7.5 DISCUSSION OF PROPOSED DESIGN PROCEDURE

The procedure proposed here is believed to be logically sound for stress induced cyclic softening, and practical to implement in the design process.

Work still needs to be done to reduce the method for determining the relaxation locus to a more formal procedure.

Both the criterion for "local plasticity" and the definition of a threshold stress state for onset of cyclic softening used in this report are tentative at this stage. It is probable that the conventions adopted at present are conservative - and possibly overly conservative.

There is no reason other than the commonsense one for selecting the Neuber hyperbola as the boundary between local and extensive plastic deformation. At present however, no alternative can be found. Placing a limit on localized plasticity is an important generic question which impacts several important issues in component evaluation, of which local softening is only one. Others include the problem of elastic follow-up in piping systems, and the applicability of simplified methods of post yield fracture evaluation [7.5,7.6,7.7].

Definition of the threshold stress state contains two sources of conservatism. The first is a function of the simplified analysis. As shown in Fig. 7.6, it is assumed that the stress distribution in the component has a fictitious "yield stress" equal to the threshold value. In fact the correct stress distribution corresponds to the isocyclic stress/strain curve for the number of cycles of interest. This will have a higher yield stress than the threshold value, and will therefore correspond to a smaller plastic zone. It has yet to be determined whether the conservatism of the simplified approach is sufficiently accurate to justify the saving in computational effort.

The second uncertainty involved in the setting of the threshold softening stress is the actual value itself. The value used in this report was deduced by extrapolation from Handrock's results at relatively large strains and small numbers of cycles. It is likely that, long before this low limit has been reached an "endurance limit" will be reached, below which no softening occurs. More experimentation at low stress levels is needed to try to obtain this limit directly.

Although the discussion in this chapter has attempted to include both stress- and thermally-induced softening, the methods proposed here have not yet been implemented for the case thermal softening, because no material data habr been obtained so far to characterize the thermal softening phenomenon. It is expected that this information will be forthcoming as the testing of the advanced austenitic materials proceed.

7.6 REFERENCES

7.1 ASME Boiler and Pressure Vessel Design Code, Sections III and VIII, 1988.

7.2 ibid, Code Case N47-23.

7.3 Handrock, J. L., "The Effects of Strain Induced Softening on the Load Carrying Capabilty of Components," Ph.D. Thesis, University of Illinois at Urbana-Champaign, 1988.

7.4 Marriott, D. L., Kloos, K., and Handrock, J. L., "Approximate Analysis of Components Composed of Strain Softening Material," Properties of High-Strength Steels for High Pressure Components (ed. Nisbett, E. G.) MPC-27, ASME, NY, 1986, pp. 103-109.

7.5 Mariott, D. L., "Evaluation of Deformation or Load Control of Stresses under Inelastic Conditions using Elastic FEA," PVP-Vol. 136 Proc. ASME PVP Conference, Pittsburgh, June 19-23, 1988 (coord. ed. G. L. Hollinger).

7.6 Boyle, J. T., and Mitchell, J., "The Geometrical Nature of Elastic Followup" ibid.

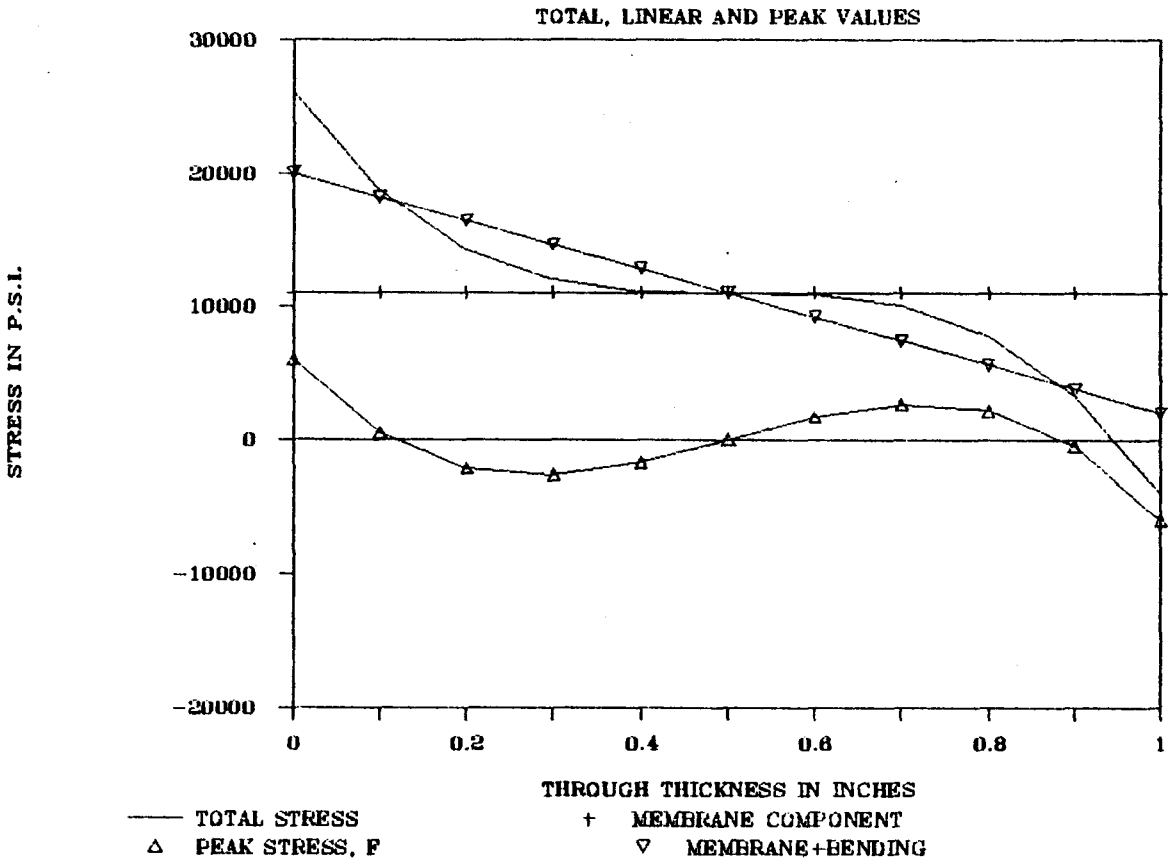

Figure 7.1 Illustration of ASME code stress categories

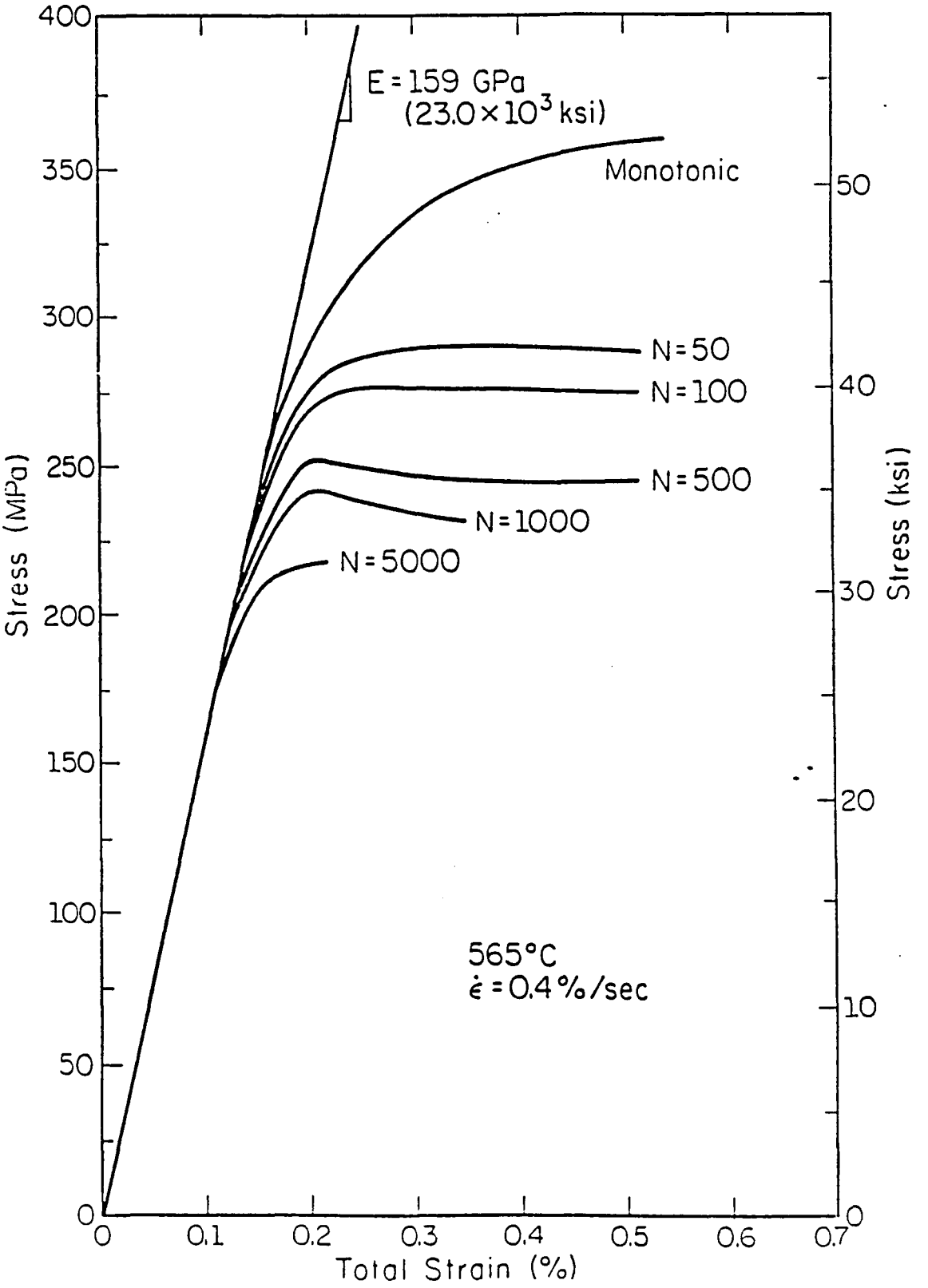

Figure 7.2 2.25 Cr 1 Mo Steel at 565°C - Isocyclic stress/strain curves

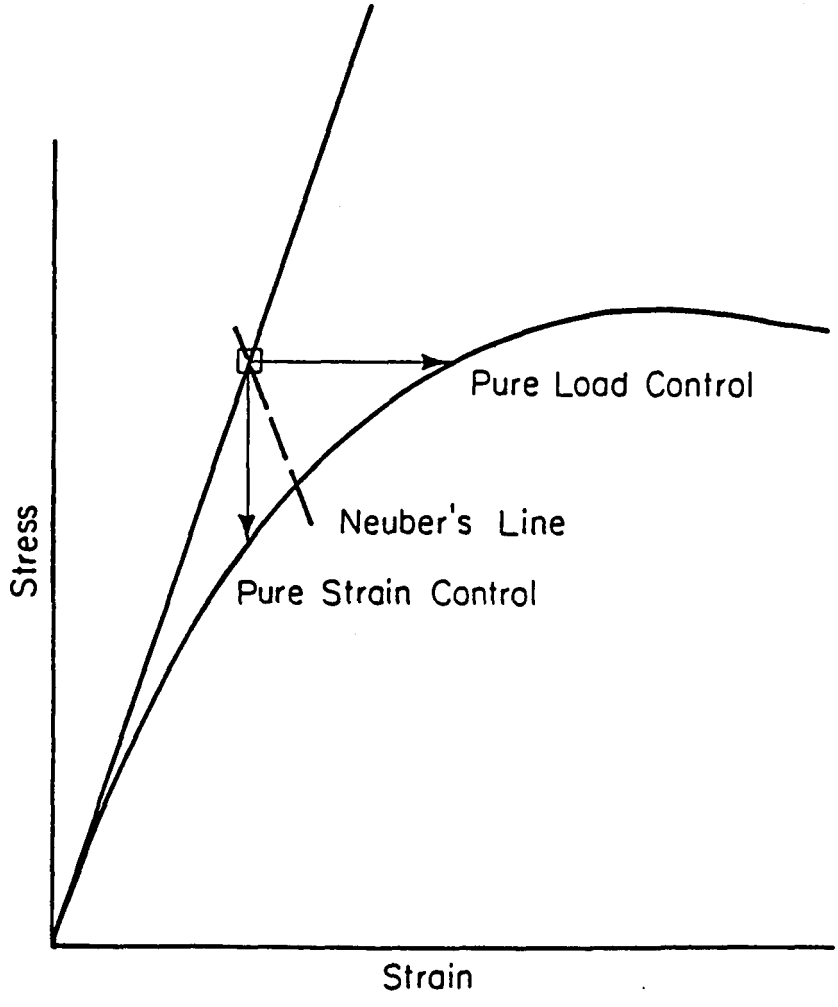

Figure 7.3 Illustration of load versus strain controlled deformation

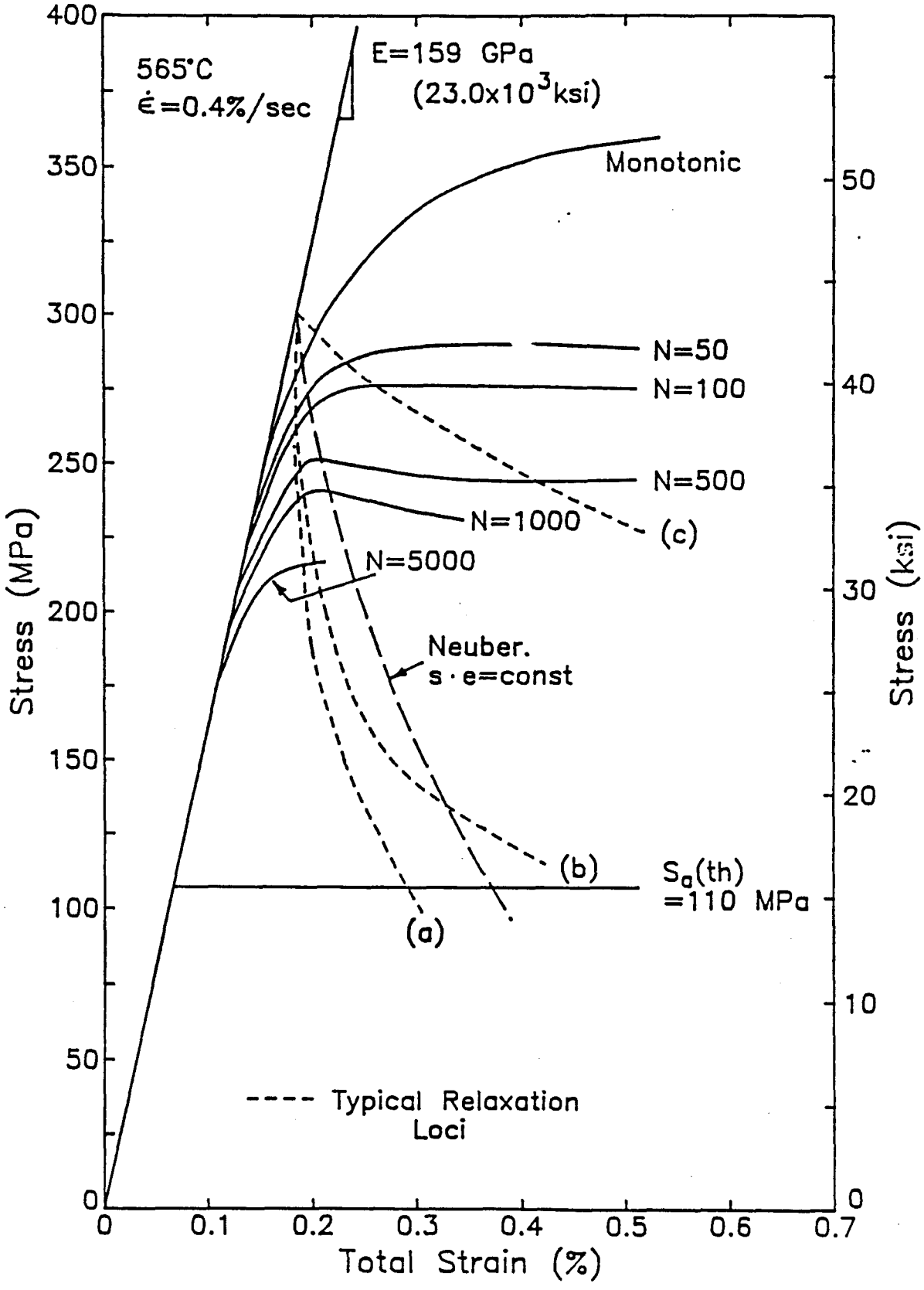

Figure 7.4 Component relaxation curve superimposed on material isocyclic curves

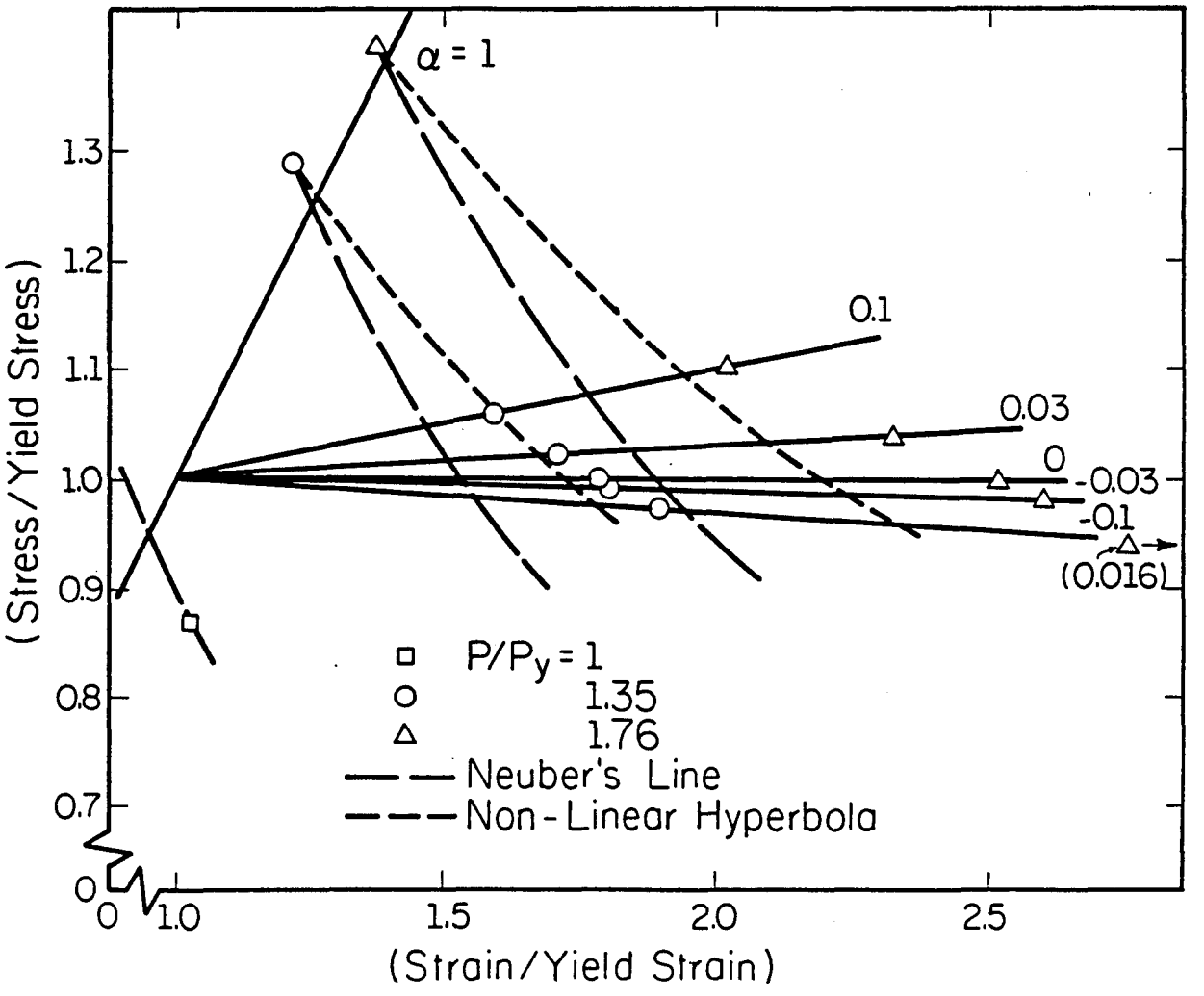

Figure 7.5a C-Notch; peak stress versus peak strain relationship

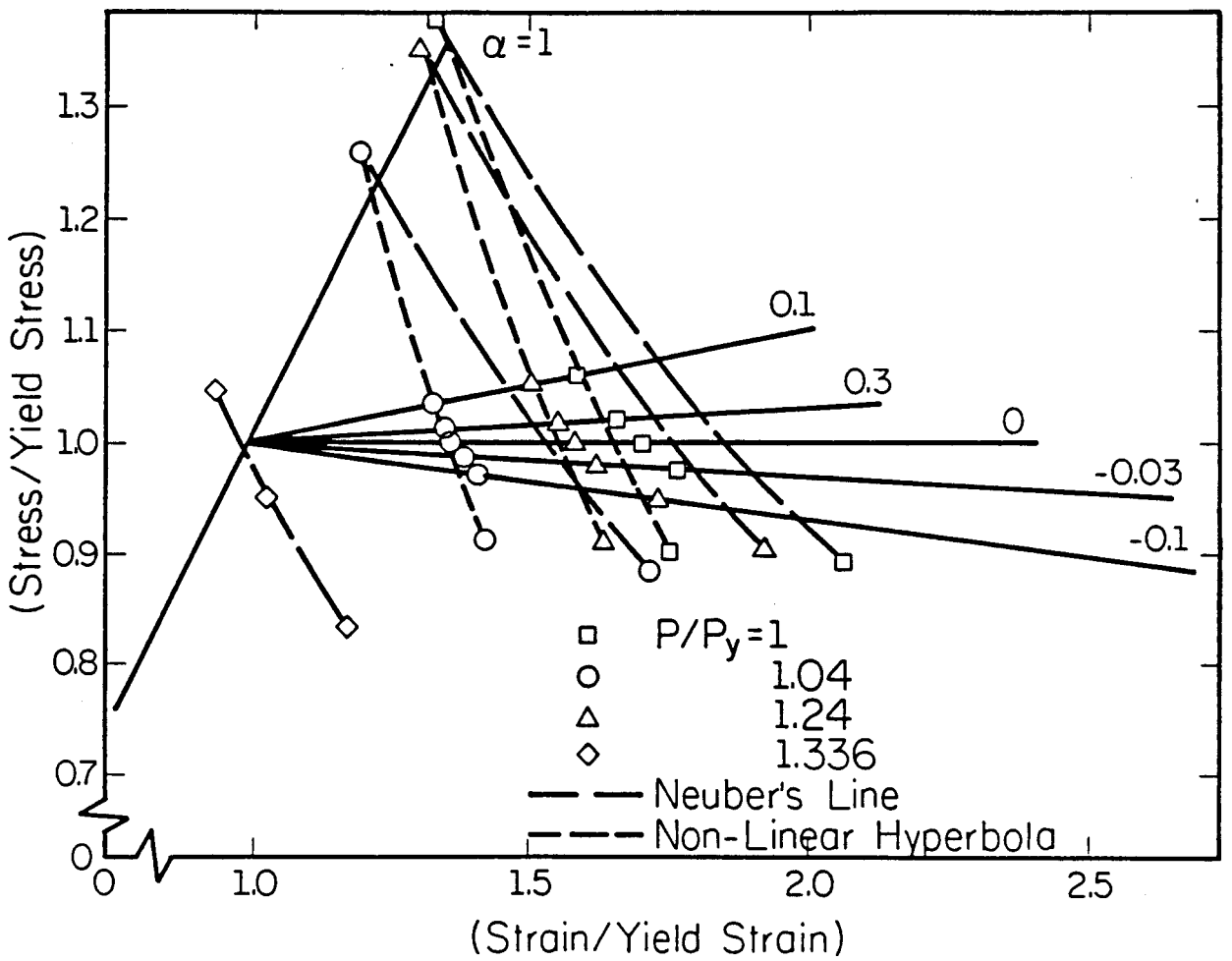

Figure 7.5b Cavity-in-Cylinder; peak stress versus peak strain relationship

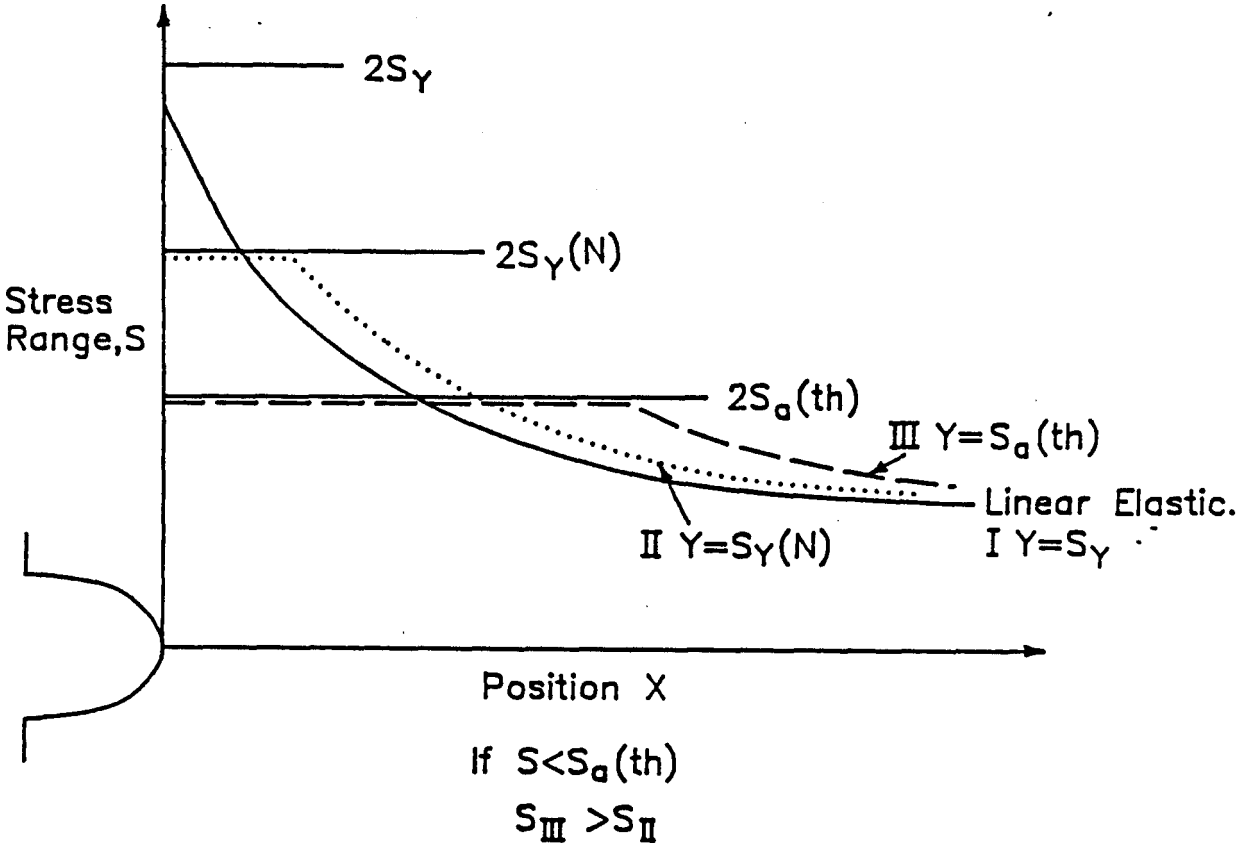

Figure 7.6 Use of fictitious yield stress to determine sensitivity ty cyclic softening

8. CONCLUSIONS AND FUTURE WORK

Specific conclusions relating to each aspect of the program are included at the end of each chapter. This chapter attempts to summarize the main conclusions and identifies needs for future work.

1. There is a significant frequency effect on the fatigue life of both the ferritic and austenitic materials for modestly low cyclic frequencies (i.e. up to 20 minutes per cycle) which still cannot be explained fully. Although the specific work has not been carried out for the 17-14 Cu Mo, the behavior of this material is in line with many studies on similar material such as 304 and 316 stainless steels. On the other hand, the hold time effect is more difficult to explain for the 2 1/4 Cr 1 Mo steel and, in fact, has not yet been successfully explained. The argument that it is an environmental effect was eliminated by performing tests in vacuum and creep damage was not observed in any of the tests carried out. All that remains at present is conjecture. One possibility which can be postulated but which is untried so far is that creep relaxation causes the stress/strain characteristic of the material at the crack tip to change from strain hardening to strain softening, resulting in strain localization and consequent amplification of the crack opening displacement.

2. The 17-14 Cu Mo steel has shown no surprising behavior in mechanical testing so far. It displays all the same qualitative characteristics of other austenitic steels. One test indicates that the thermo-mechanical treatment advocated by Maziaz can have a significant effect on creep resistance. The drastic cyclic softening observed in ferritic steel has not been found in 17-14 Cu Mo in rapid cycling fatigue tests. In fact the cyclic stress/strain loop is quite stable under these conditions. On the other hand, one test at slow strain rates indicated slight cyclic softening. It is not known at this point whether this is a real cyclic softening effect or whether it is simply a consequence of thermal aging by time-at-temperature. This needs to be the focus of future work on this material.

3. The practical issue of designing with materials which cyclically soften has been solved effectively by developing a methodology which does not require extensive knowledge of the softening phenomenon to make sensitive decisions. The basis of the approach is identifying a characteristic of component geometries known as the "relaxation locus" which is not sensitive to material constitutive behavior. The propose strategy is to ignore softening for primary design purposes if it can be demonstrated that significant cyclic softening can only occur in a localized area. A procedural test has been developed to determine when plastic deformation can be judged to be localized.

Work which emerges from this study is as follows:

1. The frequency effect observed in fatigue of 2 1/4 Cr I Mo steel needs to be resolved. It seems that this behavior may be related to the cyclic softening which occurs at the crack tip, independently of any environmental factors such as oxidation already known to exist.

2. A design related material parameter has been identified for cyclic softening. This is the "softening threshold" which must be obtained for low stress ranges and high cycles,very different conditions from those which have been investigated so far.

3. It is believed that a satisfactory design methodology has been developed to deal with cyclic softening in a practical way. This approach still needs to be validated by comparing its predictions with more detailed component analyses. Within the simplified procedure itself, some more work is needed to place the computation of the component characteristic called the "relaxation locus" on a formal basis and in particular to develop the approximate method using linear elastic FEA into a formal procedure.

4. So far the implications of thermal aging on component performance have not been investigated at all. This cannot be done until the material phenomenon of aging has been defined more precisely In principle, it is anticipated that the method already proposed for stress induced cyclic softening can be adapted to the purpose.

5. Preliminary tests on 17-14 Cu Mo suggest that all or at least most of the time-dependent changes in material of this type can be related to thermal aging, including apparent cyclic softening effects observed in low strain rate fatigue tests. A systematic program is needed to identify and characterize the effects of time-at-temperature in this class of material.

Attachment

1. ALLISON GAS TURBINE OPERATIONS, Mail Stop W-5, P.O. Box 420, Indianapolis, Indiana 46206

   P. Khandelwal

2. ARGONNE NATIONAL LABORATORY, 9700 S. Cass Avenue, Argonne, Illinois 60439

   W. A. Ellingson

3. AMERICAN WELDING SOCIETY, 550 LeJeune Road, Miami, Florida 33126

   H. G. Ziegenfuss

4. BABCOCK AND WILCOX, Fossil Power Generation Division, 20 South Van Buren Avenue, Barberton, Ohio 44203

   M. Gold

5. BATTELLE COLUMBUS LABORATORIES, 505 King Avenue, Columbus, Ohio 43201

   I. G. Wright

6. BETHLEHEM STEEL CORPORATION, Bethlehem, Pennsylvania 18016

   B. L. Bramfitt

7. CBI INDUSTRIES, 800 Jorie Blvd., Oak Brook, Illinois 60521

   W. R. Mikesell

8. CANADA CENTER FOR MINERAL AND ENERGY TECHNOLOGY, 555 Booth Street, Ottawa, Ontario, Canada K1A 0G1

   Mahee Sahoo

9. CHEVRON CORPORATION, P. O. Box 4012, Richmond, California 94804

   A. G. Imgram

10. CLIMAX MOLYBDENUM COMPANY OF MICHIGAN, P.O. Box 1568, Ann Arbor, Michigan 48106

    T. B. Cox

11. COLORADO SCHOOL OF MINES, Department of Metallurgical Engineering, Golden, Colorado 80401

    G. R. Edwards

12. CORNELL UNIVERSITY, Materials Sciences and Engineering Department, Bard Hall, Ithaca, New York 14853

Che-Yu Li

13. DOW CORNING CORPORATION, 1901 S. Saginaw Road, Midland, Michigan 48640

T. W. Fogiesong

14. EG&G IDAHO, INC., Idaho National Engineering Laboratory, P.O. Box 1625, Idaho Falls, Idaho 83415

A. D. Donaldson

15–16. ELECTRIC POWER RESEARCH INSTITUTE, 3412 Hillview Avenue, P.O. Box 10412, Palo Alto, California 94303

W. T. Bakker
J. T. Stringer

17. FOSTER WHEELER DEVELOPMENT CORPORATION, Materials Technology Department, John Blizard Research Center, 12 Peach Tree Hill Road, Livingston, New Jersey 07039

J. L. Blough

18. GAS RESEARCH INSTITUTE, 8600 West Bryn Mawr Avenue, Chicago, Illinois 60631

H. S. Meyer

19. GIBBS & HILL ENGINEERING-DRAVO, 11 Penn Plaza, New York, New York 10001

T. A. Flynn

20. KENTUCKY CENTER FOR ENERGY RESEARCH, Iron Works Pike, P.O. Box 13015, Lexington, Kentucky 40512

V. K. Sethi

21. KENNAMETAL, INC., Philip McKenna Laboratory, 1011 Old Salem Road, P. O. Box 639, Greensburg, Pennsylvania 15601

B. North

22. LUKENS STEEL COMPANY, R&D Center, Coatesville, Pennsylvania 19320

J. A. Gulya

23. THE MATERIALS PROPERTIES COUNCIL, INC., United Engineering Center, 345 E. Forty-Seventh Street, New York, New York 10017

M. Prager

24. MOBIL RESEARCH AND DEVELOPMENT CORPORATION, P. O. Box 1026, Princeton, New Jersey 08540

R. C. Searles

25. NASA-LEWIS RESEARCH CENTER, Lewis Library, MS 60-3, 21000 Brookpark Road, Cleveland, Ohio 44135

K. Grasse

26. NATIONAL BUREAU OF STANDARDS, Materials Building, Gaithersburg, Maryland 20899

S. J. Dapkunas

27. NATIONAL MATERIALS ADVISORY BOARD, National Research Council, 2101 Constitution Avenue, Washington, DC 20418

K. M. Zwilsky

28–39. OAK RIDGE NATIONAL LABORATORY, P.O. Box X, Oak Ridge, Tennessee 37831

R. A. Bradley
P. T. Carlson
W. N. Drewery, Jr. (8)
R. R. Judkins
R. W. Swindeman

40. OFFICE OF NAVAL RESEARCH, Code 431, 800 N. Quincy Street, Arlington, Virginia 22217

S. G. Fishman

41. SHELL DEVELOPMENT COMPANY, P.O. Box 1380, Houston, Texas 77001

L. W. R. Dicks

42. THE TORRINGTON COMPANY, Research Department, 59 Field Street, Corrington, Connecticut 06790

W. J. Chmura

43. UNITED TECHNOLOGIES RESEARCH CENTER, East Hartford, Connecticut 06108

K. M. Prewo

44. UNIVERSITY OF CALIFORNIA AT BERKELEY, Department of Materials Science and Mineral Engineering, Berkeley, California 94720

E. R. Parker

45. UNIVERSITY OF ILLINOIS, Department of Mechanical and Industrial Engineering, 1206 West Green Street, Urbana, Illinois 61801

D. L. Marriott

46. UNIVERSITY OF SOUTHERN CALIFORNIA, Department of Materials Science, Los Angeles, California 90089

J. A. Todd

47. UNIVERSITY OF TENNESSEE, Department of Chemical and Metallurgical Engineering, Knoxville, Tennessee 37916

C. D. Lundin

48. UNIVERSITY OF WASHINGTON, Department of Materials Science and Engineering, Roberts Hall, FB-10, Seattle, Washington 98195

J. Mueller

49. DEPARTMENT OF THE ARMY, Army Materials and Mechanics Research Center, Watertown, Massachusetts 02172

D. R. Messier

50-52. DOE, MORGANTOWN ENERGY TECHNOLOGY CENTER, P.O. Box 880, Morgantown, West Virginia 26505

D. Dubis
M. Ghate
J. S. Wilson

53. DOE, OFFICE OF FOSSIL ENERGY, Washington, DC 20545

J. P. Carr
K. N. Frye
F. M. Glaser

54. DOE, OFFICE OF BASIC ENERGY SCIENCES, Materials Sciences Division, Washington, DC 20545

F. V. Nolfi, Jr.

55. DOE, ENERGY CONVERSION & UTILIZATION TECHNOLOGIES DIVISION, Route Symbol CE-142, Forrestal Building, Washington, DC 20585

J. J. Eberhardt

56. DOE, OFFICE OF VEHICLE AND ENGINE R&D, Route Symbol CE-131, Forrestal Building, Washington, DC 20585

R. B. Schulz

57. DOE, OAK RIDGE OPERATIONS OFFICE, P.O. Box E, Oak Ridge, Tennessee 37831

E. E. Hoffman

58. DOE, PITTSBURGH ENERGY TECHNOLOGY CENTER, P.O. Box 10940, Pittsburgh, Pennsylvania 15236

S. W. Chun